

# **Bose-Einstein condensates in $\mathcal{PT}$ -symmetric potentials**

Von der Fakultät Mathematik und Physik der Universität Stuttgart  
zur Erlangung der Würde eines Doktors der Naturwissenschaften  
(Dr. rer. nat.) genehmigte Abhandlung

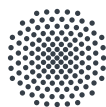
Vorgelegt von

**Daniel Haag**

aus Schwäbisch Hall

Hauptberichter: Prof. Dr. Günter Wunner  
Mitberichter: Prof. Dr. Johannes Roth

Tag der mündlichen Prüfung: 09. Februar 2017



**Universität Stuttgart**

1. Institut für Theoretische Physik

**2017**



# Inhaltsangabe

Durch die experimentellen Realisierung hat die  $\mathcal{PT}$ -Symmetrie in den letzten Jahren, auch über rein theoretische Konzepte hinausgehend, an Bedeutung gewonnen. Gerade in der Optik zeigt sich, dass neben erfolgversprechenden mathematischen Konzepten auch Anwendungen in der experimentellen Forschung möglich sind. Diese Arbeit untersucht den Einfluss  $\mathcal{PT}$ -symmetrischer komplexer Potentiale in der Mean-Field-Beschreibung ultrakalter Gase, in die Teilchen ein- oder ausgekoppelt werden. Dazu werden neben numerischen Methoden auch analytische Verfahren angewandt.

Solange die Eigenwerte und Eigenfunktionen eines Systems kontinuierlich auf den Teilchenaustausch reagieren, kann die  $\mathcal{PT}$ -Symmetrie stets für einen schwachen ausgeglichenen Teilchenverlust und -gewinn erhalten bleiben. Durch genaue Abschätzungen dieser Eigenwertänderungen ist es darüber hinaus möglich, den  $\mathcal{PT}$ -Bruch oder sein Ausbleiben vorherzusagen. Insbesondere hoch angeregte Zustände, die für die Stabilität des Systems große Bedeutung haben, numerisch aber schwer zugänglich sind, können so analytisch untersucht werden. Die Arbeit testet solche idealen Abschätzungen durch numerische Rechnungen und untersucht, inwieweit die Wechselwirkung zwischen den Teilchen die Ergebnisse verändert.

Damit können im zweiten Teil der Arbeit numerische Verfahren verwendet werden, um die physikalischen Eigenschaften verschiedener  $\mathcal{PT}$ -symmetrischer Systeme zu untersuchen. Besonders geeignet für eine experimentelle Realisierung ist die  $\mathcal{PT}$ -symmetrische Doppelmulde. Diese ist nicht nur besonders stabil unter experimentellen Bedingungen und kleinen Störungen, sondern ermöglicht die Beobachtung  $\mathcal{PT}$ -symmetrischer Effekte sogar bei starken Veränderungen. Die Arbeit schenkt einem Fall dabei besondere Aufmerksamkeit: Wie verhält sich der Teilchenstrom durch die beiden Mulden, wenn die Barriere durch einen zweiten Kanal umgangen werden kann? Es zeigt sich, dass der Strom nicht nur nicht wesentlich ansteigen muss, sondern je nach Geometrie gänzlich unterdrückt werden kann.

Zuletzt wird das Verfahren auf rotierende Bose-Einstein-Kondensate angewandt. Hier stellt sich die Frage, in wie weit ein Vortex oder mehrere Vortices, also Wirbel, den Teilchentransport durch das Kondensat behindern. Tatsächlich lässt sich zeigen, dass ein Vortex den Teilchenstrom nicht behindert, sondern sogar durch asymmetrische Verschiebungen zu ihm beiträgt.



# Abstract

$\mathcal{PT}$  symmetry, alongside its applications and possible realizations, has established itself as a hot topic in recent years. Next to its possible impact on the fundamental nature of quantum physics, it has proved to be useful in the research on open systems of all kind. While  $\mathcal{PT}$  physics has already been very successful in the field of optics, this thesis presents numerical calculations that show how  $\mathcal{PT}$  symmetry can be applied to the mean-field theory of ultra-cold gases, where particles are added and removed coherently from a Bose-Einstein condensate.

As long as the eigenvalues of a system are continuous functions with respect to such an exchange rate of particles,  $\mathcal{PT}$  symmetry is preserved for weak perturbations. Therefore, a prediction of these changes for high excitation numbers is incredibly valuable to ensure stable stationary realizations. Not only does the present work test such rigorous estimates with regard to their validity, it also goes beyond analytically accessible regimes and presents numerical estimations for the nonlinear description of interacting particles.

With this in mind, only low excited states have to be considered when studying non-trivial modifications to the  $\mathcal{PT}$ -symmetric double-well potential. Not only do the results at hand show that this simplest implementation of  $\mathcal{PT}$ -symmetric concepts is extremely stable with respect to experimental inaccuracies, but such modifications give rise to possible applications. Weakening the barrier inside the double well by introducing another particle channel from the gain to the loss well has a non-trivial effect on the net transport: In general, the net current does not profit from this modification, specific configurations even allow its complete suppression.

Further, not only static systems, but rotating condensates are considered. It is shown, that the net particle transport is not only possible in the presence of the rotation; the vortices in the rotating wave functions even generate the necessary current by moving in such a way that their circular current adds to the net current.



# Contents

<b>Inhaltsangabe</b>	<b>iii</b>
<b>Abstract</b>	<b>v</b>
<b>1. Introduction</b>	<b>1</b>
1.1. Motivation . . . . .	1
1.2. Outline . . . . .	2
<b>2. Bose-Einstein condensates with gain and loss</b>	<b>5</b>
2.1. Bose-Einstein condensation . . . . .	5
2.1.1. Mean-field description . . . . .	5
2.1.2. Dimensionless units . . . . .	8
2.2. $\mathcal{PT}$ symmetry . . . . .	9
2.2.1. Linear $\mathcal{PT}$ -symmetric systems . . . . .	10
2.2.2. Nonlinear $\mathcal{PT}$ -symmetric systems . . . . .	11
2.2.3. Pseudo-Hermitian Operators . . . . .	13
2.3. Imaginary potentials in the mean-field description . . . . .	13
2.3.1. Master equation . . . . .	14
2.3.2. Particle loss in a single mode . . . . .	15
2.3.3. Particle gain in a single mode . . . . .	16
2.3.4. Balanced gain and loss and experimental realizations . . . . .	17
<b>3. Numerical methods</b>	<b>19</b>
3.1. One-dimensional integration method . . . . .	19
3.2. Finite element method . . . . .	20
3.3. Bicomplex numbers . . . . .	24
3.4. B-Splines . . . . .	26
3.5. Multi-mode approximation . . . . .	28
<b>4. The <math>\mathcal{PT}</math>-symmetric double well</b>	<b>29</b>
4.1. Linear two-mode system . . . . .	29
4.2. Nonlinear two-mode system . . . . .	30
4.3. Time-dependency of non-stationary solutions . . . . .	32
4.4. Spatially extended double well . . . . .	34

<b>5. Existence of real spectra</b>	<b>37</b>
5.1. Perturbation theory . . . . .	37
5.2. Riesz basis and general estimates . . . . .	39
5.3. Numerical test of estimates for singular perturbations . . . . .	41
5.3.1. Properties of the $\mathcal{PT}$ -symmetric harmonic trap . . . . .	41
5.3.2. Eigenvalue spectra . . . . .	43
5.3.3. Eigenvalue shifts . . . . .	47
<b>6. <math>\mathcal{PT}</math>-symmetric currents in modified double wells</b>	<b>51</b>
6.1. Three-mode approximation . . . . .	51
6.1.1. Linear matrix model . . . . .	53
6.1.2. Nonlinear three-mode approximation . . . . .	56
6.2. Extended double well with side channel . . . . .	59
6.3. Asymmetries in the particle flux . . . . .	63
<b>7. Rotating condensates in <math>\mathcal{PT}</math>-symmetric potentials</b>	<b>69</b>
7.1. Introduction to rotating systems . . . . .	69
7.1.1. Vortices in coherent wave functions . . . . .	69
7.1.2. Rotating coordinate frame . . . . .	70
7.2. Two-dimensional calculations . . . . .	72
7.2.1. Numerical solutions without gain and loss . . . . .	73
7.2.2. Numerical solutions including gain and loss . . . . .	77
7.3. Three-dimensional calculations . . . . .	82
<b>8. Summary and Outlook</b>	<b>89</b>
<b>A. Additional analysis of the two-dimensional rotating system</b>	<b>93</b>
<b>Bibliography</b>	<b>97</b>
<b>Zusammenfassung in deutscher Sprache</b>	<b>105</b>
<b>Curriculum Vitae</b>	<b>113</b>
<b>Danksagung</b>	<b>115</b>

# 1. Introduction

## 1.1. Motivation

From the first discovery of real eigenvalues in a non-Hermitian  $\mathcal{PT}$ -symmetric Hamiltonian by Bender and Boettcher in 1998 [1] a lot of work was put in replacing the original concept of Hermitian quantum mechanics with the more general condition of  $\mathcal{PT}$  symmetry [2–4]. However, quickly the quest for a first experimental realization of a  $\mathcal{PT}$ -symmetric physical system started. In the course of this search the attention shifted to optical systems, where the symmetry is accomplished by an complex refraction index that in the equations effectively models a gain and loss of the field strength [5–9].

Indeed the first realizations succeeded in two coupled optical waveguides. In an early experiment two different absorption strengths were used to create a virtual gain in the wave guide with weaker loss [10], and in a second realization one guide was actively pumped to amplify the field strength [11]. Thus, while the original concepts of  $\mathcal{PT}$  symmetry focused on fundamental changes on the nature of quantum mechanics, its first applications lie in an effective mean-field description, again attracting new theoretical and experimental efforts [12–15]. An even simpler approach to a realization lies in purely electronic frameworks [16, 17].

With the success in these other mean-field systems in mind, suggesting Bose-Einstein condensates as a new realization [6] is quite comprehensible. In this many-particle system, the in- and out-coupling acts directly on the particle density, increasing or decreasing the number of particles. Numerical calculations in spatially extended potentials confirm that condensates are in principle able to provide all the effects known from linear optical realizations [18–22]. Proposals for an experimental realization in analogy with two optical waveguides have been made. They include embedding a double-well system in a longer chain of wells with time-dependent coupling parameters [23], and the description of two separate condensates exchanging their particles [24].

These realizations establish  $\mathcal{PT}$  symmetry in a closed, Hermitian quantum system. However, the concepts of  $\mathcal{PT}$  symmetry also hold for a particle exchange with an environment. The first application of such systems with balanced gain and loss that comes to mind is the promising application of an atom laser [25]. To realize a stable source of coherent atoms for the study of a *continuous* atom laser, particles

have to be coupled in and out of the condensate coherently. Both approaches have already been realized experimentally, by an out-scattering electron beam [26] and by letting atoms fall into the condensate from a second reservoir condensate [27]. This permits the realization of an open double well where most interesting many-particle effects were recently found predicting a periodic collapse and revival of the condensed phase [28–30].

Even though, compared with optical experiments, the laborious implementation of particle gain and loss in Bose-Einstein condensates makes an experimental realization quite difficult, this opens a new fundamental area of research. It is therefore particularly important to ensure the stability of the double-well realization and investigate how it can be influenced by deliberate modifications. However, next to the obvious motivation of proving that the principles of  $\mathcal{PT}$  symmetry hold for ultracold atomic gases, the applications in the aforementioned atom laser, and the realization of new many-particle effects, it is desirable to propose applications and effects native to the Bose-Einstein condensation. A striking example is the observation of vortices in rotating or shaken condensates [31, 32]. With such studies, one leaves the extensively studied double well behind to search for new  $\mathcal{PT}$ -symmetric systems.

## 1.2. Outline

Due to the timeliness of the results presented in this thesis, most parts were published beforehand, references to these publications are given below.

Starting with a short introduction to the system at hand,  $\mathcal{PT}$  symmetry in Bose-Einstein condensates is presented in Chap. 2. To motivate the equations solved in this work, the mean-field approximation of the quantum mechanical description of Bose-Einstein condensates is introduced in Sec. 2.1. Using, amongst other concepts, a master equation introduced by Dast et al. [28] the following sections discuss the relevance and physical interpretation of complex potentials and  $\mathcal{PT}$  symmetry in the mean-field description of Bose-Einstein condensates [21]. Numerical methods such as the finite-element method published in [33] are provided in Chap. 3. A simple double well is discussed in Chap. 4 to summarize results from previous works [20–22, 34] and presenting some of them, employing the potentials and numerical methods used throughout the rest of the thesis.

Next, the basis for all further realizations is provided by Chap. 5 where perturbation theory is used to provide insight into the  $\mathcal{PT}$  symmetry breaking of degenerate states [35]. Over and above this it will be shown how nonlinear interactions modify the impact  $\mathcal{PT}$ -symmetric potentials have on the spectrum when rigorous estimates by Mityagin [36] are tested in Sec. 5.3 [37].

Following up this general considerations, the double well is modified in Chap. 6. To test its versatility as a basis system for deliberate variations a third well is

added in Sec. 6.1 [35]. By considering asymmetric trappings in extended potentials (Sec. 6.2 [33]) and asymmetric gain and loss contributions (Sec. 6.3) the stability of the two-well system in experimental realizations is verified.

Before drawing a conclusion in Chap. 8, a last example in the form of a rotating Bose-Einstein condensate is considered in Chap. 7. After introducing the reader to vortices and rotating condensates, two distinct configurations are studied.  $\mathcal{PT}$ -symmetric currents are stimulated inside the rotating plane, providing a two-dimensional system in Sec. 7.2, or alongside the vortex center in a complete three-dimensional calculation in Sec. 7.3.



## 2. Bose-Einstein condensates with gain and loss

### 2.1. Bose-Einstein condensation

One of the most fundamental implications of the quantum nature of particles is the existence of a discrete phase space. After Satyendra Nath Bose used this phenomenon to derive Planck's law [38] for photons in 1924, a generalization by Albert Einstein provided the first quantum theory of the ideal Bose gas. If the temperature is close to zero, Einstein discussed, an increasing number of particles degenerate as they all reside in the same phase-space cell of the volume  $h^3$  [39, 40]. Due to purely statistical properties of indistinguishable bosons this leads to a phase transition at a critical temperature  $T_c$ .

This effect, where a majority of the particles are occupying the ground state is called Bose-Einstein condensation and was first realized by Anderson et al. [41, 42] in an atomic gas of rubidium, 71 years after its prediction. Due to the early theoretical prediction a wide range of effects and properties of Bose-Einstein condensates could be studied in the years after the first realization. Today there is a broad field of applications of such condensates in fundamental research, covering everything from the simulation of condensed matter in optical lattices over the study of rotating ultracold gases to transitions between fermionic superfluids and Bose-Einstein condensates [43].

This section briefly presents the transition from a many particle Schrödinger equation to the mean-field description of the common ground state, which will be studied throughout the thesis.

#### 2.1.1. Mean-field description

Following the approach used in the extensive review by Dalfovo et al. [44] the mean-field description is derived by employing Einstein's original concept that most particles are in the same single-particle state. If  $N$  particles have the same single-particle wave function  $\psi(\mathbf{r})$ , the state can be written as

$$\frac{1}{\sqrt{N!}} (\hat{a}^\dagger)^N |0\rangle = |N\rangle, \quad (2.1)$$

## 2. Bose-Einstein condensates with gain and loss

---

where the bosonic creation operator  $\hat{a}^\dagger$  creates a particle in the single-particle state  $\psi$ . Further addition or removal of one particle,

$$\begin{aligned}\hat{a}^\dagger|N\rangle &= \sqrt{N+1}|N+1\rangle, \\ \hat{a}|N\rangle &= \sqrt{N}|N-1\rangle,\end{aligned}\tag{2.2}$$

leads to states that only differ by their particle number. Even for large particle numbers  $N \rightarrow \infty$  these states are still orthogonal vectors in their Hilbert space. However, these states eventually become physically indistinguishable in the sense that the expectation values of finite-particle operators become equal. In a purely physical sense, one can then assume

$$|N\rangle \approx |N \pm 1\rangle \quad \Rightarrow \quad \hat{a}^\dagger \approx \hat{a} \approx \sqrt{N}.\tag{2.3}$$

This result can now be used to simplify the many-particle picture.

The Hamiltonian in second quantization reads

$$\begin{aligned}\hat{H} &= \int d^3\mathbf{r} \hat{\Psi}^\dagger(\mathbf{r}) \left[ -\frac{\hbar^2}{2m} \Delta + V_{\text{ext}}(\mathbf{r}) \right] \hat{\Psi}(\mathbf{r}) \\ &+ \frac{1}{2} \int d^3\mathbf{r} d^3\mathbf{r}' \hat{\Psi}^\dagger(\mathbf{r}) \hat{\Psi}^\dagger(\mathbf{r}') V(\mathbf{r} - \mathbf{r}') \hat{\Psi}(\mathbf{r}') \hat{\Psi}(\mathbf{r}),\end{aligned}\tag{2.4}$$

where  $V(\mathbf{r} - \mathbf{r}')$  is the interaction potential between two particles and  $\hat{\Psi}(\mathbf{r})$  is the field operator that annihilates a bosonic particle at position  $\mathbf{r}$ . This field operator can be written in a new basis that contains the primarily occupied state  $\psi$ ,

$$\hat{\Psi}(\mathbf{r}) = \psi(\mathbf{r}) \hat{a} + \sum_i \chi_i(\mathbf{r}) \hat{a}_i.\tag{2.5}$$

The time-dependence of this operator is given by the Heisenberg equation of motion,

$$\begin{aligned}i\hbar \frac{\partial}{\partial t} \hat{\Psi}(\mathbf{r}, t) &= \left[ \hat{\Psi}(\mathbf{r}, t), \hat{H} \right] \\ &= \left[ -\frac{\hbar^2}{2m} \Delta + V_{\text{ext}}(\mathbf{r}) + \int d^3\mathbf{r}' \hat{\Psi}^\dagger(\mathbf{r}', t) V(\mathbf{r} - \mathbf{r}') \hat{\Psi}(\mathbf{r}', t) \right] \hat{\Psi}(\mathbf{r}, t).\end{aligned}\tag{2.6}$$

Now the aforementioned transition from the annihilation operator of a highly occupied wave function to a complex number,  $\hat{a} \rightarrow \sqrt{N}$ , can be used. The result is called the Bogoliubov prescription for the formulation of a mean-field theory. The field operator then reads

$$\hat{\Psi}(\mathbf{r}, t) = \sqrt{N} \psi(\mathbf{r}, t) + \delta \hat{\Psi}(\mathbf{r}, t),\tag{2.7}$$

where any deviations from of a perfect condensate are found in the operator  $\delta\hat{\Psi}(\mathbf{r}, t)$ . The normalized function  $\psi(\mathbf{r}, t)$  is called the wave function of the condensate.

By inserting this mean-field approximation of the field operator into Eq. (2.6) and neglecting all deviations  $\delta\hat{\Psi}(\mathbf{r}, t)$  one obtains the time-dependent Gross-Pitaevskii equation [45, 46],

$$\left[ -\frac{\hbar^2}{2m}\Delta + V_{\text{ext}}(\mathbf{r}) + \int d^3\mathbf{r}' V(\mathbf{r} - \mathbf{r}') N |\psi(\mathbf{r}', t)|^2 \right] \psi(\mathbf{r}, t) = i\hbar \frac{\partial}{\partial t} \psi(\mathbf{r}, t). \quad (2.8)$$

For temperatures considerably lower than the critical temperature of the condensate the Gross-Pitaevskii equation is known to provide very accurate results; it is only in the vicinity of dynamic instabilities, where the description has some limitations [47, 48].

The integro-differential Gross-Pitaevskii equation can be solved for various interaction potentials  $V$ . However in this thesis only isotropic short-range interactions, like the van der Waals interaction or repulsive interactions resulting from Pauli's exclusion principle, are studied. Such interactions only affect the system when particles get close to each other. Thus, if one is only interested in cold and dilute gases such as atomic Bose-Einstein condensates, they only act in rare particle-particle scattering processes. Due to the low temperature, and consequently the low momentum of the atoms, and the isotropic nature of the force, the s-wave scattering dominates the process. As long as the solely defining value of such a scattering process, the scattering length, does not change, the specific shape of the interaction potential is irrelevant.

The interaction potential assumes the simplest form in case of the contact interaction  $V(\mathbf{r} - \mathbf{r}') = 4\pi\hbar^2 a/m \delta(\mathbf{r} - \mathbf{r}')$ , where  $a$  is the scattering length. Note that this potential must in general be regularized if the wave function is allowed to contain a singularity. The Gross-Pitaevskii equation with contact interaction reads

$$\left[ -\frac{\hbar^2}{2m}\Delta + V_{\text{ext}}(\mathbf{r}) + \frac{4\pi\hbar^2 Na}{m} |\psi(\mathbf{r}', t)|^2 \right] \psi(\mathbf{r}, t) = i\hbar \frac{\partial}{\partial t} \psi(\mathbf{r}, t), \quad (2.9)$$

while stationary states

$$\psi(\mathbf{r}, t) = \psi(\mathbf{r}) e^{-i\mu t/\hbar}, \quad (2.10)$$

with the chemical potential  $\mu$  are defined by the time-independent equation

$$\left[ -\frac{\hbar^2}{2m}\Delta + V_{\text{ext}}(\mathbf{r}) + \frac{4\pi\hbar^2 Na}{m} |\psi(\mathbf{r}')|^2 \right] \psi(\mathbf{r}) = \mu\psi(\mathbf{r}). \quad (2.11)$$

This equation resembles the Schrödinger equation with the important difference that a nonlinearity occurs. To emphasize the analogy, the chemical potential  $\mu$  is called an eigenvalue and the corresponding wave function is called an eigenstate.

The energy of the corresponding many-particle state is defined as the expectation value of the Hamiltonian (2.4). The energy per particle is called the mean-field

## 2. Bose-Einstein condensates with gain and loss

---

energy,  $E_{\text{MF}}$ . For considerably strong nonlinearities, the chemical potential and the mean-field Energy differ strongly. Since the ground state minimizes the total energy, and therefore the mean-field energy, the chemical potential is unable to indicate if a given stationary state acts as the system's ground state.

The existence of the nonlinear term also has another crucial effect, the stationary states and the spectrum do no longer define the dynamical properties of the system. An investigation of the full dynamical properties therefore requires extensive effort. If one is only interested in the stability of stationary states, it can be examined solving a linear system of equations called the Bogoliubov-de Gennes equations,

$$\frac{\hbar^2}{2m} \Delta u(\mathbf{r}) = (V(\mathbf{r}) - \mu - \omega + 2g |\psi_0(\mathbf{r})|^2) u(\mathbf{r}) + g\psi_0^2(\mathbf{r})v(\mathbf{r}), \quad (2.12a)$$

$$\frac{\hbar^2}{2m} \Delta v(\mathbf{r}) = (V^*(\mathbf{r}) - \mu^* + \omega + 2g |\psi_0(\mathbf{r})|^2) v(\mathbf{r}) + g\psi_0^{*2}(\mathbf{r})u(\mathbf{r}), \quad (2.12b)$$

with  $g = 4\pi\hbar^2 Na/m$ . These equations are easily recovered expanding the Gross-Pitaevskii equation to linear terms with respect to the perturbation

$$\delta\psi(\mathbf{r}) = u(\mathbf{r}) \exp(-i\omega t/\hbar) + v^*(\mathbf{r}) \exp(i\omega^* t/\hbar). \quad (2.13)$$

Apparently, the perturbed state oscillates around the stationary state with the frequency  $\text{Re}\omega$ . If  $\omega$  is purely real, the state is assumed to be stable, while any positive imaginary contribution  $\text{Im}\omega > 0$  leads to an exponential growth rendering the state unstable.

### 2.1.2. Dimensionless units

For numerical calculations it is beneficial if all variables and parameters have the same order of magnitude. Therefore, a dimensionless formulation of all studied equations is needed. One should emphasize that such a formulation also simplifies the application of numerical calculations to a wider range of experimental systems. To do so, an initially arbitrary distances  $l_0$  is introduced. A new energy scale,  $E_0 = \hbar^2/(2ml_0^2)$ , is chosen such that all physical constants in the kinetic part of the Gross-Pitaevskii equation vanish. To remove Planck's constant  $\hbar$  from the left side of the time-dependent equation (2.9), the appropriate timescale for all dynamical considerations is chosen to be  $t_0 = \hbar/E_0$ . For the sake of simplicity of the notation from this point on, every parameter and value is given in the appropriate dimensionless value even though the same variable is used. This yields the dimensionless Gross-Pitaevskii equation,

$$[-\Delta + V(\mathbf{r}) + 8\pi Na|\psi(\mathbf{r})|^2] \psi(\mathbf{r}) = \mu\psi(\mathbf{r}), \quad (2.14)$$

and the Bogoliubov-de Gennes equations read

$$\Delta u(\mathbf{r}) = (V(\mathbf{r}) - \mu - \omega + 16\pi Na |\psi_0(\mathbf{r})|^2) u(\mathbf{r}) + 8\pi Na \psi_0^2(\mathbf{r}) v(\mathbf{r}), \quad (2.15a)$$

$$\Delta v(\mathbf{r}) = (V^*(\mathbf{r}) - \mu^* + \omega + 16\pi Na |\psi_0(\mathbf{r})|^2) v(\mathbf{r}) + 8\pi Na \psi_0^{*2}(\mathbf{r}) u(\mathbf{r}). \quad (2.15b)$$

All spatially extended potentials in this thesis contain the harmonic oscillator. The rescaled isotropic case of such a trapping potential,  $(m/2) \omega_{\text{SI}}^2 r_{\text{SI}}^2$ , where the subscript SI marks the values in the unscaled unit system, e.g. the International System of Units, takes the form

$$V_{\text{osci}} = \frac{1}{4} \omega^2 r^2, \quad \omega = \frac{\omega_{\text{SI}}}{\omega_0} = \frac{\omega_{\text{SI}} \hbar}{E_0} = \frac{2m\omega_{\text{SI}} l_0^2}{\hbar}. \quad (2.16)$$

Obviously, due to the arbitrary length scale  $l_0$ , the dimensionless trap frequency is adjustable at will. Without loss of generality the choice  $\omega = 1$  is used in this section, to compare the numerical values used in the Gross-Pitaevskii equation to experimental data.

Anderson et al. used a radial trapping frequency of about  $\omega_{\text{SI}} = 267 \text{ s}^{-1}$  [41]. The length scale then reads

$$l_0 = \sqrt{\frac{\hbar}{2m\omega_{\text{SI}}}} \approx 1.67 \mu\text{m}. \quad (2.17)$$

When the first condensate arose, 20 000 particles populated the trap, while a pure condensate was reached at 2000 particles [41]. With a scattering length of about 100 times the Bohr radius [49, 50] the nonlinearity parameter covers the range,

$$6 \lesssim Na \lesssim 60. \quad (2.18)$$

One has to keep in mind, that by taking advantage of Feshbach resonances the scattering length can be changed, increasing the feasible range of nonlinear strengths by some orders of magnitude [51, 52].

## 2.2. $\mathcal{PT}$ symmetry

In quantum mechanics physical observables are represented by operators whose eigenvalues are the only possible outcomes of a measurement. Dirac argues that since these observables are supposed to be real an equivalent condition should be formulated for the corresponding operators [53]. Motivated by the strong connection between the adjunction of an operator and the complex conjugation of a complex number, one requires these operators to be self-adjoint. This condition is nowadays commonly known as one of fundamental axioms of quantum mechanics.

Irrespective of the success of these axioms, the self-adjointness is not necessary to ensure real eigenvalues. In 1998, Bender and Boettcher [1] discussed a quantum

system with a complex potential,  $\hat{H} = \hat{p}^2/(2m) + m^2 x^2 - (ix)^N$ . Even though this Hamiltonian is non-Hermitian, they found an entirely real eigenvalue spectrum in some ranges of  $N$ . The property which was proposed to be responsible for this behavior is the  $\mathcal{PT}$  symmetry [54] of the system.  $\mathcal{PT}$  symmetry has the quite charming property that the operators involved are purely physical in contrast to the mathematical condition of Hermiticity. This fact motivated a wide range of fundamental research evaluating whether  $\mathcal{PT}$  symmetry can completely replace the condition of Hermiticity [2].

### 2.2.1. Linear $\mathcal{PT}$ -symmetric systems

A linear system is called  $\mathcal{PT}$  symmetric if its Hamiltonian commutes with the combined action of the parity and time reversal operator  $[\hat{H}, \mathcal{PT}] = 0$ . With  $\hat{H} = \hat{p}^2/2m + V(\hat{r})$  and the operators  $\mathcal{P} : \hat{r} \rightarrow -\hat{r}, \hat{p} \rightarrow -\hat{p}$  and  $\mathcal{T} : \hat{p} \rightarrow -\hat{p}, i \rightarrow -i$  one gains the necessary condition

$$V(\hat{r}) = V^*(-\hat{r}), \quad (2.19)$$

i.e., the real part of the potential must be symmetric and the imaginary part antisymmetric. Linear  $\mathcal{PT}$ -symmetric systems have the following properties [55]:

If  $\psi$  is an eigenstate of the Hamiltonian  $\hat{H}$  with the energy eigenvalue  $E$ , the state  $\mathcal{PT}\psi$  is also an eigenstate with the complex conjugate energy eigenvalue  $E^*$ . Consequently, if  $\psi$  is in addition an eigenstate of the operator  $\mathcal{PT}$ , i.e.  $\mathcal{PT}\psi = \lambda\psi$ , then the corresponding energy eigenvalue  $E = E^*$  is real. Also the inverse statement holds, the eigenspace to a real eigenvalue can always be constructed out of  $\mathcal{PT}$ -symmetric states.

With these two properties the following important conclusion can be derived. If and only if all eigenstates of the Hamiltonian can be written as eigenstates of the  $\mathcal{PT}$  operator, the spectrum is entirely real. One refers to this case as unbroken  $\mathcal{PT}$  symmetry, otherwise the  $\mathcal{PT}$  symmetry is broken. The importance of unbroken symmetry in linear systems is obvious: A complex energy  $E$  leads to the time-dependency  $|\psi(t)|^2 \propto \exp(2 \text{Im } E t/\hbar)$ . Not only can a state only be truly stationary if  $\text{Im } E = 0$ , but if any state is  $\mathcal{PT}$ -broken, every remaining stationary state is unstable.

Since  $\mathcal{PTPT} = 1$  holds, the eigenvalue of the parity-time-reflection must be of norm one,  $\lambda = \exp(i\chi)$  and can be changed by applying a global phase,

$$\mathcal{PT}e^{i\phi}\psi = e^{-i\phi}\mathcal{PT}\psi = e^{-i\phi}e^{i\chi}\psi = \underbrace{e^{i(\chi-2\phi)}}_{e^{i\chi'}}e^{i\phi}\psi. \quad (2.20)$$

The case  $\lambda = 1$  is called exact  $\mathcal{PT}$  symmetry, and refers to the case in which the imaginary part of the wave function is antisymmetric and the real part is symmetric.

### 2.2.2. Nonlinear $\mathcal{PT}$ -symmetric systems

To translate the condition of  $\mathcal{PT}$  symmetry to nonlinear systems, the simple commutator relation,  $[\hat{H}, \mathcal{PT}] = 0$ , must be expanded to incorporate a Gross-Pitaevskii-like equation,

$$\hat{H}_{\text{lin}}\psi + \hat{f}(\psi)\psi = i\hbar\frac{\partial}{\partial t}\psi, \quad (2.21)$$

where  $\hat{H}_{\text{lin}} = -\hat{p}^2/2m + V(\hat{r})$  and  $\hat{f}(\psi)$  is a general nonlinear part. Since the global phase of a wave function should not possess any physical relevance, this discussion is restricted to nonlinearities which are invariant under the application of such a phase,

$$\hat{f}(e^{i\chi}\psi) = \hat{f}(\psi), \quad \chi \in \mathbb{R}. \quad (2.22)$$

Furthermore, this condition ensures that a stationary state which has an oscillating global phase can exist which is evidently mandatory for the discussion of  $\mathcal{PT}$ -symmetric states. For nonlinear systems one replaces the commutator relation of linear  $\mathcal{PT}$ -symmetric systems with

$$\mathcal{PT} \left[ \left( \hat{H}_{\text{lin}} + \hat{f}(\psi) \right) \psi \right] \stackrel{!}{=} \left[ \hat{H}_{\text{lin}} + \hat{f}(\mathcal{PT}\psi) \right] \mathcal{PT}\psi. \quad (2.23)$$

It will be shown, that this condition suffices to regain the properties of linear  $\mathcal{PT}$  symmetry. If the linear part  $\hat{H}_{\text{lin}}$  is  $\mathcal{PT}$  symmetric, Eq. (2.23) is reduced to a simple condition for the nonlinear part  $\hat{f}(\psi)$ ,

$$\mathcal{PT}\hat{f}(\psi) = \hat{f}(\mathcal{PT}\psi)\mathcal{PT}. \quad (2.24)$$

This work concentrates mainly on the properties of stationary states. Therefore one has to look at the time-independent nonlinear Schrödinger equation,

$$\hat{H}_{\text{lin}}\psi + \hat{f}(\psi)\psi = \mu\psi. \quad (2.25)$$

In the Gross-Pitaevskii equation the eigenvalue  $\mu$  is identified as the chemical potential. Application of the  $\mathcal{PT}$  operator leads to

$$\hat{H}_{\text{lin}}\mathcal{PT}\psi + \hat{f}(\mathcal{PT}\psi)\mathcal{PT}\psi = \mu^*\mathcal{PT}\psi, \quad (2.26)$$

where Eq. (2.24) and  $[\hat{H}_{\text{lin}}, \mathcal{PT}] = 0$  were used. Equations (2.25) and (2.26) show immediately that the energy eigenvalues  $\mu$  occur in complex conjugate pairs with the eigenstates  $\psi$  and  $\mathcal{PT}\psi$ , respectively. Also the most striking property of  $\mathcal{PT}$  symmetry, namely the concurrence of  $\mathcal{PT}$ -symmetric states and real eigenvalues, is true for such nonlinear systems. This can be seen by evaluating Eq. (2.26) for  $\mathcal{PT}$ -symmetric states  $\mathcal{PT}\psi = \exp(i\varphi)\psi$ ,

$$\hat{H}_{\text{lin}}\psi + \hat{f}(e^{i\varphi}\psi)\psi = \mu^*\psi. \quad (2.27)$$

## 2. Bose-Einstein condensates with gain and loss

---

As stated in Eq. (2.22) only phase independent nonlinearities are considered, and thus for  $\mathcal{PT}$ -symmetric states the energy eigenvalue must be real  $\mu = \mu^*$ .

Again this proof works also in the inverse direction. For non-degenerate real eigenvalues Eqs. (2.25) and (2.26) demand that the eigenfunction is  $\mathcal{PT}$  symmetric because  $\psi$  and  $\mathcal{PT}\psi$  fulfill the same eigenvalue equation. However if a real eigenvalue is degenerate, it is in general not possible to choose  $\mathcal{PT}$ -symmetric eigenstates because the superposition principle is only valid in linear systems.

The results can be summarized as follows. In nonlinear systems with non-degenerate eigenspectra of type (2.21) with a  $\mathcal{PT}$ -symmetric linear part and a nonlinear part which fulfills the conditions (2.22) and (2.24)

- the eigenvalues are either real or occur in complex conjugate pairs,
- the eigenvalues are real if and only if the eigenstate itself is  $\mathcal{PT}$ -symmetric,
- if  $\psi$  is eigenstate to  $\mu$  then  $\mathcal{PT}\psi$  is eigenstate to  $\mu^*$ .

Another condition can be found for the case that the nonlinear part assumes the form of a complex function in position space,  $\hat{f}(\psi) \rightarrow f(\psi, \mathbf{r})$ . For a given  $\mathcal{PT}$ -symmetric wave function  $\mathcal{PT}\psi = e^{i\varphi}\psi$  such a nonlinearity ensures that

$$f^*(\psi, -\mathbf{r}) = \mathcal{PT}f(\psi, \mathbf{r}) \stackrel{(2.24)}{=} f(\mathcal{PT}\psi, \mathbf{r}) \stackrel{(2.22)}{=} f(\psi, \mathbf{r}) \quad (2.28)$$

holds, i.e., the real part of  $f$  is symmetric and the imaginary part is antisymmetric. Since for a given state  $\psi$  the nonlinearity has to be seen as a contribution to the potential  $V$ , this view closes the circle to linear  $\mathcal{PT}$  symmetry.

These general considerations are now applied to the special case of the Gross-Pitaevskii nonlinearity,

$$f(\psi, \mathbf{r}) = \int d^3\mathbf{r}' V(\mathbf{r}, \mathbf{r}') |\psi(\mathbf{r}')|^2. \quad (2.29)$$

Because the wave function only appears as a square modulus, the nonlinearity is not changed by an arbitrary phase and thus condition (2.22) is always fulfilled independently of the interaction type. The second condition (2.24) carries over to a condition for the interaction potential,

$$\int d^3\mathbf{r}' V^*(-\mathbf{r}, \mathbf{r}') |\psi(\mathbf{r}')|^2 = \int d^3\mathbf{r}' V(\mathbf{r}, \mathbf{r}') |\psi^*(-\mathbf{r}')|^2, \\ V(\mathbf{r}, \mathbf{r}') = V^*(-\mathbf{r}, -\mathbf{r}'), \quad (2.30)$$

by simply renaming  $\mathbf{r} \rightarrow -\mathbf{r}$  on both sides and substitution of  $\mathbf{r}' \rightarrow -\mathbf{r}'$  in the right integral. The most common interaction potentials, namely the contact, monopolar and dipolar interaction, fulfill this requirement and therefore are possible candidates for  $\mathcal{PT}$ -symmetric Bose-Einstein condensates.

### 2.2.3. Pseudo-Hermitian Operators

By now it is well understood how  $\mathcal{PT}$ -symmetric operators relate to their self-adjoint counterparts. In position space  $\hat{p}^\dagger = \hat{p}^*$  and therefore  $\hat{H}^\dagger = \hat{H}^*$  holds. The  $\mathcal{PT}$ -symmetry condition then transfers to

$$\hat{H} = \mathcal{PT}\hat{H}\mathcal{PT} = \mathcal{PTT}\hat{H}^*\mathcal{TPT} = \mathcal{P}\hat{H}^\dagger\mathcal{P}, \quad (2.31)$$

which means that  $\hat{H}$  is pseudo-Hermitian with respect to  $\mathcal{P}$ , i.e., it behaves Hermitian for the modified scalar product,

$$\langle \psi_i | \psi_j \rangle_{\mathcal{P}} = \langle \psi_i | \mathcal{P}\psi_j \rangle. \quad (2.32)$$

It can be shown [56–58] that every pseudo-Hermitian operator is indeed  $\mathcal{OT}$  symmetric where  $\mathcal{O}$  is a unitary and Hermitian operator, i.e., it behaves like the parity operator  $\mathcal{P}$ . Unfortunately the corresponding modified scalar product is not able to define a norm for the Hilbert space, since it is not positive definite.

Starting from the original formulation of Hermitian quantum mechanics, using pseudo-Hermiticity as a generalization of the original concept seems obvious. Unsurprisingly this possibility encouraged a wide range of work regarding such a generalization [3, 4]. However, in the present thesis using  $\mathcal{PT}$ -symmetric potentials in the Gross-Pitaevskii equation does not require a fundamental generalization of quantum mechanics but has a clear physical interpretation, which will be presented in the next section.

## 2.3. Imaginary potentials in the mean-field description

Since every linear operator can be split into a Hermitian and an anti-Hermitian part, a non-Hermitian operator can be seen as a Hermitian operator disturbed by an anti-Hermitian operator. In position space, such operators can be constructed by adding a purely imaginary part to the potential,  $V(\mathbf{r}) = V_{\text{R}}(\mathbf{r}) + iV_{\text{I}}(\mathbf{r})$ .

While the real part contributes to the energy, the influence of the imaginary part is not directly obvious. To understand this term, one can turn to the continuity equation that takes the following form,

$$\frac{\partial}{\partial t} |\psi(\mathbf{r}, t)|^2 = \text{div } \mathbf{j}(\mathbf{r}, t) + 2 |\psi(\mathbf{r}, t)|^2 V_{\text{I}}(\mathbf{r}), \quad (2.33)$$

with the probability current density  $\mathbf{j}(\mathbf{r}) = (2i)^{-1} (\psi^*(\mathbf{r})\nabla\psi(\mathbf{r}) - \psi(\mathbf{r})\nabla\psi^*(\mathbf{r}))$ . The imaginary part appears as an additional source term. Positive imaginary parts increase the modulus square of the wave function locally whereas negative imaginary parts introduce a decay.

Since the Gross-Pitaevskii equation is nonlinear, in the mean-field description the norm of the wave function changes the physics of the system. The interaction

term  $8\pi Na|\psi(\mathbf{r}, t)|^2$  is strengthened for high absolute values and weakened by low values of the wave function as if the particle number were varied. Therefore, the modulus square can be reinterpreted as a local particle density  $n(\mathbf{r}, t) = N|\psi(\mathbf{r}, t)|^2$  and the norm denotes the particle number relative to  $N$ . The imaginary potential then becomes a source or sink of particles. Indeed this technique is nearly as old as the first condensate realizations and has been used, for example, to describe feeding from a particle cloud or the decay resulting from three-body interactions [59].

### 2.3.1. Master equation

Imaginary potentials lead to an effective particle exchange in the mean-field description. The question, however, remains how the physical many-particle state behaves due to this in- and out-coupling. Furthermore, the mean-field description only holds in very special circumstances, i.e., it is only valid if and only if a majority of particles are condensed to the same ground state. To answer these questions, a many-particle description has to be studied. One important technique for such a description is the quantum master equation in Lindblad form [60]. It determines the dynamics of a system which is coupled to a reservoir that does not change due to this coupling, it has no memory. After a partial trace over the reservoir part of the Hilbert space any coherent dynamics of the reservoir is removed from the formalism. Instead the effects of the coupling results in the appearance of classical probabilities and the system is described by the density matrix  $\hat{\rho}$ .

To study the physical interpretation of the in-coupling and out-coupling separately, the exact spatial distribution of the condensate can be neglected. Instead, all particles are supposed to be and stay in the same single-particle state from which particles are either removed or added coherently. Due to the superselection rule for massive particles [61, 62], superpositions of different particle numbers are not permitted. Thus, any coherent state is completely defined by its particle number in the Fock state  $|n\rangle$ . A classical distribution between different particle numbers is characterized by the density matrix,

$$\rho(t) = \sum_{i=0}^{\infty} P_n(t) |n\rangle \langle n| \quad (2.34)$$

with the classical probabilities  $P_n$  that  $n$  particles are found in the system at time  $t$ . Exact solutions of the dynamics described by the master equation with particle gain or loss in this simplest possible many-particle system can then provide the basis for a solid interpretation.

### 2.3.2. Particle loss in a single mode

The master equation in Lindblad form with particle loss,

$$\frac{d}{dt}\hat{\rho} = -\gamma \left( \hat{a}^\dagger \hat{a} \hat{\rho} + \hat{\rho} \hat{a}^\dagger \hat{a} - 2\hat{a} \hat{\rho} \hat{a}^\dagger \right), \quad (2.35)$$

allows a rigorous derivation of the mean-field limit with imaginary potentials [28, 63],

$$i\frac{\partial}{\partial t}\psi = -i\gamma\psi. \quad (2.36)$$

The mean-field solution of this equation is trivial,  $\psi(t) = \psi_0 \exp(-\gamma t)$ , and leads to a decay of the particle number,

$$N(t) = N_0 |\psi(t)|^2 = N_0 e^{-2\gamma t}. \quad (2.37)$$

To interpret this mean-field solution beyond the average number of particles, the original original master equation has to be discussed. Inserting the ansatz (2.34) into Eq. (2.35) yields the equations of motion for the particle number probabilities,

$$\frac{d}{dt}P_n(t) = 2\gamma((n+1)P_{n+1} - nP_n). \quad (2.38)$$

For the case of an exact initial number of  $N$  particles the solution of this equation can be derived using clear physical arguments.

The bosons in the condensate are not distinguishable. The probability that a single particle is lost from the condensate must therefore be the same for all particles. Since the total particle number decreases as defined by Eq. (2.37) the probability for every single particle to be found inside the condensate should drop in exactly the same way,  $P_{\text{in}} = \exp(-2\gamma t)$ . The combined probability that  $n$  particles are still inside the condensate then corresponds to a binomial distribution that out of  $N$  experiments,  $n$  successes were made,

$$P_{n,N}(t) = \binom{N}{n} P_{\text{in}}^n(t) (1 - P_{\text{in}}(t))^{N-n}. \quad (2.39)$$

This is indeed the solution of Eq. (2.38) with the initial values  $P_n(0) = 0, \forall n \neq N$ ,  $P_N(0) = 1$  as can be easily checked. Thus, the predictions for the total particle number are the same for the master equation and the mean-field theory.

One has to emphasize that this formulation of particle decay is very general. It covers many scenarios where single particles are independently and separately removed from the condensate. The fundamental condition is, that system and reservoir are separable and all prior correlations between out-coupled particles vanish. It does not only hold for a weak coupling to an empty reservoir [64], where it was compared with exact many-particle calculations, but also covers other stochastic processes of particle removal such as the important case of particle out-scattering by a laser or particle beam [26].

### 2.3.3. Particle gain in a single mode

In a similar manner as in the case of particle loss, gain in one well can be described by the following master equation,

$$\frac{d}{dt}\hat{\rho} = -\gamma \left( \hat{a}\hat{a}^\dagger\hat{\rho} + \hat{\rho}\hat{a}\hat{a}^\dagger - 2\hat{a}^\dagger\hat{\rho}\hat{a} \right), \quad (2.40)$$

and the same mean-field transition is possible [28],

$$i\frac{\partial}{\partial t}\psi = +i\gamma\psi. \quad (2.41)$$

This time, however, the particle number predicted by the mean-field description,

$$N(t) = N_0|\psi(t)|^2 = N_0e^{2\gamma t}, \quad (2.42)$$

differs from the many-particle description for low particle numbers. The equation of motion for the expectation value of the particle number operator  $\hat{n}$  reads

$$\frac{d}{dt}\langle\hat{n}\rangle = 2\gamma(\langle\hat{n}\rangle + 1), \quad (2.43)$$

and implements an inhomogeneity that allows (physically correct) particles to be coupled into the condensate even if no initial particle density is found. For high particle numbers, i.e., in the mean-field limit discussed in this thesis, the effect can be neglected, however, it is crucial in calculations with low particle numbers [28].

To gain a deeper understanding of the stochastic properties of the process, an analytic solution can be given that solves the equations of motion,

$$\frac{d}{dt}P_n(t) = 2\gamma(nP_{n-1} - (n+1)P_n). \quad (2.44)$$

Unlike the case of the loss contributions before, the solution to this equation cannot be deduced purely by exploiting physical assumptions. The special case of  $P_n(0) = 0, \forall n \neq N, P_N(0) = 1$  leads to the result

$$P_{N+n,N}(t) = \binom{N+n}{n} P_{\text{in}}^n(t) (1 - P_{\text{in}}(t))^{N+1}. \quad (2.45)$$

Inserting this ansatz in the equation of motion (2.44) results in the probability  $P_{\text{in}}(t) = 1 - \exp(-2\gamma t)$ .

Although this result is as concise as the one found for the loss case, its physical interpretation is much more concealed. Since not only the original but also all newly in-coupled particles are able to stimulate the gain contribution, a uniform probability  $P_{\text{in}}$  for every one of these in-coupling processes cannot be formulated. However, the structure and meaning of the probability distribution (2.45) can be

made conceivable using another stochastic experiment. Consider the following setup where the probability of success for each trial, e.g., a dice throw, is  $P_{\text{in}}$ . The number of initial trials is  $N + 1$ . In a physical sense, this corresponds to the spontaneous injection into the system and the  $N$  original particles, which stimulate further in-coupling. For every success, one additional trial must be conducted that can lead to another success and so on.  $P_{N+n,N}$  represents the probability that after finishing all trials,  $n$  successes have been made. This was possible due to  $N + n$  free trials generating the successes and one additional fail that breaks the chain. This is exactly the distribution given in Eq. 2.45.

### 2.3.4. Balanced gain and loss and experimental realizations

$\mathcal{PT}$ -symmetric systems provide equally strong negative and positive imaginary parts (c.f. Eq. (2.19)) which can lead to a system with balanced gain and loss of particles. Since these must at least be described by a two-mode, or two-well, system analytic solutions stop being handy. While the mean-field approach is still analytically solvable and will be discussed in Chap. 4, the master equation can only be evaluated by approximations or numerically exact methods.

Such studies have revealed very promising effects [28–30]. Not only was it possible to show that for reasonable timescales and typical particle numbers in Bose-Einstein condensates, the mean-field approximation provides very good results. Moreover, the evaluation of the corrections to the mean-field case showed particular new effects like the periodic collapse and revival of the condensed phase.

The significance of such systems and the results presented in the aforementioned publications can be illustrated in the light of possible experimental realizations. Not only is a reasonable balance of in- and out-coupling and the consequent conservation of the particle number mandatory to ensure a reasonable lifetime to study the microscopic processes. The existence of a coherent condensate mode is crucial for many physical applications. A prominent example of a system in which the particle coherence and the balancing of particle exchanges is important is the continuous atom laser [25]. The particle in-coupling necessary for this balance was already realized by Robins et al. [27]. To achieve the necessary continuity, the source condensate that feeds the atom laser has to be replenished using particles from a second condensate located above the condensate of interest. By an excitation into a non-trapped electron state, some atoms are released from this upper condensate and start to fall downwards. Using another electronic transition, the atoms are slowed down absorbing a photon and, stimulated by the neighboring atoms, emit into the lasing source mode. If condensate feeding and lasing are not realized at the same spatial coordinates, a  $\mathcal{PT}$ -symmetric system is studied.

One fact must be emphasized. Even though the simple Lindblad master equations above provide a possible microscopic realization for imaginary potentials, there is no physical reason to assume that they are unique. Indeed, all mean-field

## 2. Bose-Einstein condensates with gain and loss

---

predictions of the  $\mathcal{PT}$ -symmetric double well can be modeled reasonably well in larger closed quantum systems.

To this end, two proposals have been made. The first considers two separate condensates. The loss of particles in the first condensate is used as the source of the second condensate's particle gain and vice versa [24]. The particles are therefore transferred between two condensates. Another realization needs only one condensate but is realized not in two but in a chain of at least four wells. By carefully tuning the time-dependent coupling between the wells, the two middle wells behave exactly as expected from a  $\mathcal{PT}$ -symmetric double well [23]. However, the first realization, using two coupled condensates, leaves the microscopic transfer process completely open, while the second realization inside a chain needs permanent time-dependent parameter adjustments.

## 3. Numerical methods

Although, as seen in Chap. 2, compared to the full many-particle system the mean-field theory is an enormous approximation, the resulting nonlinear, nonlocal partial differential equation is still quite tough. Even though this work deals with apparently simple local interactions, an analytic solution is only possible in some special cases. For most results one therefore must rely on numerical calculations, for which the methods used are introduced in this chapter.

### 3.1. One-dimensional integration method

For one-dimensional systems the Gross-Pitaevskii equation is an ordinary differential equation of second order. Therefore the unique solution is completely defined by its value and its first derivative at any single point. Thus, together with the possibly complex chemical potential  $\mu$ , there are three complex parameters defining a wave function that complies with the Gross-Pitaevskii equation.

However, a physical wave function has to be normalized, i.e., it has to decline for  $x \rightarrow \pm\infty$  exponentially. To handle this boundary condition, one introduces a finite boundary at which the wave function vanishes numerically,  $\psi(\pm x_{\max}) = 0$ . A definite norm of one and a specific phase together provide two additional real conditions to fulfill. Altogether there are six real parameters to fulfill an equal number of conditions via a root search.

The Gross-Pitaevskii equation is nonlinear. Therefore the normalization to unity is vital to achieve comparable solutions for different strengths of the nonlinearity. The choice of the exact phase condition on the other hand is completely arbitrary. One common choice is to set  $\text{Im } \psi(0) = 0$ , which enforces the imaginary part of the wave function to be antisymmetric. In case of a  $\mathcal{PT}$ -symmetric wave function it renders the function exact  $\mathcal{PT}$  symmetric. However, for completely antisymmetric wave functions this condition is always fulfilled and therefore insufficient to define a unique solution. Since the open quantum systems discussed in this thesis almost always include a current over the whole wave function, nodes are extremely rare in one dimensional systems, and exact  $\mathcal{PT}$  symmetry remains a suitable condition.

For each set of parameters, the wave function is integrated outwards, the conditions are checked and the parameters varied using an implementation of the Powell-Hybrid method [65] similar to the FORTRAN packet MINPACK [66]. The general approach is sketched in Fig. 3.1.

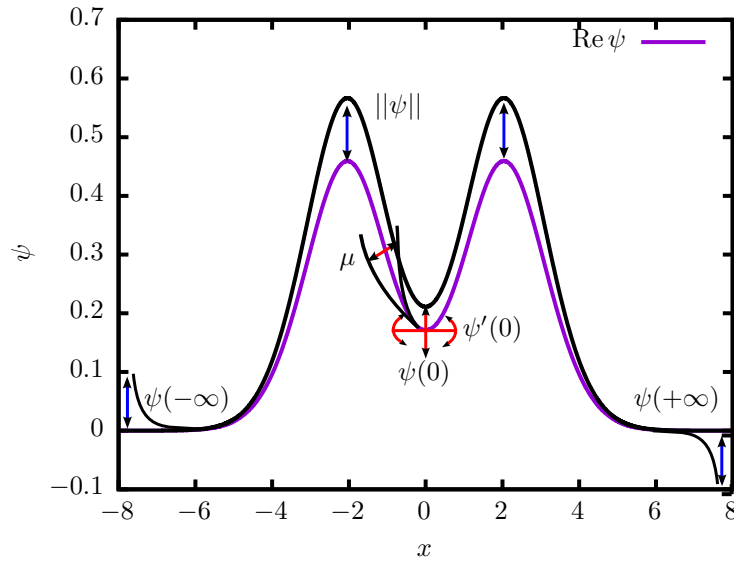


Figure 3.1.: Real part of a wave function of a double-well ground state as an example for the nonlinear root search. The function value and slope at  $x = 0$  are chosen directly while the curvature can be affected by changing the chemical potential (red arrows). The boundary values and the norm of the function change accordingly (blue arrows).

This method is the easiest approach to obtain numerically exact solutions, it enables one to implement delta potentials by a jump in the wave function's slope, and it is cheap enough in terms of computational cost. However it is only applicable in one-dimensional problems.

## 3.2. Finite element method

Another way to achieve numerically accurate solutions for an arbitrary potential is to approximate the wave function by a finite dimensional basis. The specific basis used for this method does not have a major influence on the numerical procedure. If the basis consists of spatially separated functions defined in spatially confined volume elements, the method is called the finite-element method. The weak formulation discussed in this section builds the mathematical background of all such methods independently of the basis choice.

All solutions to the Gross-Pitaevskii equation are assumed to be well approximated by a linear combination of a given set of real basis functions,

$$\psi(\mathbf{r}) = \sum_{j=1}^D c_j \phi_j(\mathbf{r}), \quad (3.1)$$

where the complex nature of the wave function  $\psi$  is accounted for by complex coefficients  $c_j$ . However, since the approximation is not perfect, it does not solve the equation exactly,

$$\sum_{j=1}^D (-\Delta + V + 8\pi Na|\psi|^2 - \mu) \phi_j c_j \neq 0. \quad (3.2)$$

To retrieve a closed expression, the left hand side of this equation is projected on each of the basis functions, restricting the solution to be correct only in the subspace spanned by the functions  $\{\phi_j\}$ . The result is called the weak formulation of the Gross-Pitaevskii equation,

$$\sum_{j=1}^D \left[ \underbrace{\int \nabla \phi_j \nabla \phi_i + (V + 8\pi Na|\psi|^2) \phi_j \phi_i \, d^n \mathbf{r}}_{K_{ij}} c_j - \mu \underbrace{\int \phi_j \phi_i \, d^n \mathbf{r}}_{M_{ij}} c_j \right] = 0. \quad (3.3)$$

The matrix  $K$  describes the potential, the particle-particle interaction and kinetic contributions, while the mass matrix  $M$  describes the overlap of the possibly non-orthogonal basis functions. For every solution  $c_j$  of this equation, the error, given by the function (3.2), must be orthogonal to the space  $\{\phi_j\}$ , and therefore small by requirement.

In the linear case  $Na = 0$ , Eq. (3.3) can be reduced to the linear eigenvalue problem

$$Kc = \mu Mc, \quad (3.4)$$

which can be solved by various generalized eigenvalue solvers. It should be emphasized at this point that, since the matrix is non-Hermitian, the eigenvalues will be complex in general.

For  $Na \neq 0$  the  $K$ -matrix depends on the modulus squared of the wave function, and thus on the basis coefficients  $c_j$ . Therefore a nonlinear system of equations has to be solved. In contrast to the generalized eigenvalue problem the solution of the system of nonlinear equations needs to be normalized,

$$\int |\psi|^2 \, d^n \mathbf{r} = c^\dagger M c = 1. \quad (3.5)$$

The global phase of the solution is still free. While it would, in principle, be possible to use this freedom to reduce the dimension of the problem by setting  $\text{Im } c_j = 0$ , this approach can lead to an ill-defined problem if the coefficient vanishes,  $c_j = 0$ . Therefore an arbitrary linear combination of the imaginary parts,

$$\sum_{j=1}^D b_j \text{Im } c_j = 0, \quad (3.6)$$

### 3. Numerical methods

---

with the weights  $b_j$  is used. Again the weights have to be chosen in such a way that the root search is well defined in most cases. Randomly chosen weights were found to be very effective avoiding ill defined systems of equations. Please note that this is indeed only necessary for non-Hermitian problems. For any Hermitian system,  $\mu$  would be a real number, effectively reducing the number of unknown real parameters by one.

To solve the nonlinear system of equations one uses derivative-based methods such as the Newton method, and to avoid time consuming numerical calculations the required Jacobian is derived analytically. This gives rise to another complication: the modulus squared is not differentiable. However, this problem can be circumvented by rephrasing the  $D$  complex functions from Eq. (3.3) as  $2D$  real functions. Additionally the  $D$  basis coefficients  $c_j$  and the chemical potential have to be split into real parameters. With the conditions given in Eqs. (3.5) and (3.6) the nonlinear system of equations is  $2D + 2$ -dimensional matching the number of parameters. The parameter vector for the root search is then given by

$$\mathbf{a}^T = (\text{Re } \mathbf{c}^T \quad \text{Im } \mathbf{c}^T \quad \text{Re } \mu \quad \text{Im } \mu), \quad (3.7)$$

and the functions

$$\mathbf{f}(\mathbf{a}) = \begin{pmatrix} \text{Re}((K(\mathbf{c}) - \mu M)\mathbf{c}) \\ \text{Im}((K(\mathbf{c}) - \mu M)\mathbf{c}) \\ \mathbf{c}^{T*} M \mathbf{c} - 1 \\ \sum b_j \text{Im } c_j \end{pmatrix} \quad (3.8)$$

are differentiable with respect to each parameter.

Now the Jacobian  $J_{ij} = \partial f_i / \partial a_j$  can be written in closed form,

$$J = \begin{pmatrix} S^{11} & S^{12} & -M \text{Re } \mathbf{c} & -M \text{Im } \mathbf{c} \\ S^{21} & S^{22} & -M \text{Im } \mathbf{c} & +M \text{Re } \mathbf{c} \\ 2(M \text{Re } \mathbf{c})^T & 2(M \text{Im } \mathbf{c})^T & 0 & 0 \\ \mathbf{0}^T & \mathbf{b}^T & 0 & 0 \end{pmatrix}, \quad (3.9)$$

with the  $D \times D$ -dimensional submatrices

$$S_{ij}^{11} = \text{Re } K + \text{Re } \mu M + \int 16\pi N a \phi_i \phi_j (\text{Re } \psi)^2 d^n \mathbf{r}, \quad (3.10a)$$

$$S_{ij}^{12} = -\text{Im } K - \text{Im } \mu M + \int 16\pi N a \phi_i \phi_j \text{Re } \psi \text{Im } \psi d^n \mathbf{r}, \quad (3.10b)$$

$$S_{ij}^{21} = \text{Im } K + \text{Im } \mu M + \int 16\pi N a \phi_i \phi_j \text{Re } \psi \text{Im } \psi d^n \mathbf{r}, \quad (3.10c)$$

$$S_{ij}^{22} = \text{Re } K + \text{Re } \mu M + \int 16\pi N a \phi_i \phi_j (\text{Im } \psi)^2 d^n \mathbf{r}. \quad (3.10d)$$

Since the matrices  $K$  and  $M$  are known from the evaluation of the functions  $f$ , only the new integrals in the submatrices  $S$  have to be calculated to determine the Jacobian.

The non-Hermiticity of the problem provides only minor changes to the finite element method. Firstly, since the chemical potential in general can be complex, the dimension of the problem increases by one. Secondly, it has the consequence that the wave functions can almost never be chosen real, instead each coefficient is complex consisting of a real and imaginary part. Altogether compared to the solution of the Gross-Pitaevskii equation with a real potential, the dimension of the problem increases by a factor of two.

While in the linear case this method can be used to calculate multiple solutions without any initial guess, the nonlinear solver needs initial values that lie very close to the correct solution. There are multiple ways to provide these values, two of which are used in this thesis: On the one hand, it often suffices to calculate linear solutions and pursue them for increasing nonlinear strengths. On the other hand, one can randomly create wave functions with specific symmetries and properties in a numerically cheap system, i.e., in one or two spatial dimensions. The product states from these different stationary states can provide a good approximation to the correct wave functions in three dimensions. After finding the initial values, the method is able to follow branches of solutions from one set of parameters to another.

The stability of the stationary states can be determined using the Bogoliubov-de Gennes equations. In in weak formulation they read

$$\sum_{j=1}^D \left[ \underbrace{\int \nabla \phi_j \nabla \phi_i + (V + 16\pi Na |\psi_0|^2) \phi_j \phi_i d^n \mathbf{r}}_{K'_{ij}} u_j + \underbrace{\int 8\pi Na \psi_0^2 \phi_j \phi_i d^n \mathbf{r}}_{N_{ij}} v_j - (\mu + \omega) \underbrace{\int \phi_j \phi_i d^n \mathbf{r}}_{M_{ij}} u_j \right] = 0, \quad (3.11a)$$

$$\sum_{j=1}^D \left[ \underbrace{\int \nabla \phi_j \nabla \phi_i + (V^* + 16\pi Na |\psi_0|^2) \phi_j \phi_i d^n \mathbf{r}}_{K'^*_{ij}} v_j + \underbrace{\int 8\pi Na \psi_0^{*2} \phi_j \phi_i d^n \mathbf{r}}_{N'^*_{ij}} u_j - (\mu^* - \omega) \underbrace{\int \phi_j \phi_i d^n \mathbf{r}}_{M_{ij}} v_j \right] = 0, \quad (3.11b)$$

where the mass matrix  $M$  appears unchanged, while the matrix  $K'$  assumes a doubled interaction strength compared to the matrix  $K$  and is evaluated for the wave function  $\psi_0$ , for which the stability is to be tested. The coupling between the

two parts  $u$  and  $v$  of the perturbation is done by the nonlinear matrix  $N$ , which is again evaluated for the function  $\psi_0$ . Using these matrices, the equations are simplified,

$$\begin{pmatrix} (K' - \mu M) & N \\ -N^* & -(K' - \mu M)^* \end{pmatrix} \begin{pmatrix} \mathbf{u} \\ \mathbf{v} \end{pmatrix} = \omega \begin{pmatrix} M & 0 \\ 0 & M \end{pmatrix} \begin{pmatrix} \mathbf{u} \\ \mathbf{v} \end{pmatrix}, \quad (3.12)$$

to a generalized eigenvalue problem of dimension  $2D$ .

Finally, one can assume that even non-stationary states can be described by the finite basis, i.e., states that lie inside the subspace spanned by the basis at  $t = 0$  will do so for a long time. If this is the case, the same approximation as before can be made for the time-dependent calculation. The time-dependent Gross-Pitaevskii equation then reads

$$K(\mathbf{c})\mathbf{c} = iM\dot{\mathbf{c}}. \quad (3.13)$$

### 3.3. Bicomplex numbers

In the finite-element method, one has to take care of the non-analyticity of the Gross-Pitaevskii equation. The modulus square nonlinearity not only interferes with any numerical root search, but is also responsible for the occurrence of bifurcation scenarios where the number of stationary states changes. From a numerical point of view, it is therefore of great importance to find a reliable way to deal with this difficulty. In this work this is done using bicomplex numbers, commutative hypercomplex numbers that build a ring [67, 68]. It should be emphasized that the following method raises the numerical cost and introduces new fundamental difficulties. It is therefore only used in the case of a low-dimensional basis.

In the context of the finite-element method in the last section, the non-analyticity was avoided by rewriting every complex equation into two real equations featuring the real and imaginary part. This yields real differentiable equations that can be extended to the complex number space by rendering both, real and imaginary part, complex themselves. To achieve this, the new complex units  $j$  and  $k = ij$  are introduced,

$$\text{Re } z = z^1 + jz^j, \quad \text{Im } z = z^i + jz^k. \quad (3.14)$$

One bicomplex number therefore has four degrees of freedom. By introducing a useful basis for all further calculations,

$$z = \underbrace{(z_+^1 + jz_+^j)}_{e_+} \frac{1+k}{2} + \underbrace{(z_-^1 + jz_-^j)}_{e_-} \frac{1-k}{2}, \quad (3.15)$$

all elementary operations can be transferred one to one to the components  $z_+$  and  $z_-$ . The modulus square in bicomplex numbers then takes the form

$$zz^* = z_+z_-, \quad (3.16)$$

which shows plainly how a bicomplex description renders the complex number and its conjugate independent. For complex numbers, i.e.  $z^j = z^k = 0$ ,  $z_+ = z_-^*$  holds.

With the bicomplex expansion of the wave function,  $\psi(\mathbf{r}) = \psi_+(\mathbf{r})e_+ + \psi_-(\mathbf{r})e_-$ , the appropriate finite-element matrix

$$K_{ij} = \int \nabla \phi_j \nabla \phi_i + (V + 8\pi Na\psi_+\psi_-) \phi_j \phi_i d^n \mathbf{r}, \quad (3.17)$$

and the familiar mass matrix, the Gross-Pitaevskii equation reads

$$\mathbf{f}_0 = \begin{pmatrix} K(\mathbf{c}_+, \mathbf{c}_-) & 0 \\ 0 & K(\mathbf{c}_+, \mathbf{c}_-) \end{pmatrix} \begin{pmatrix} \mathbf{c}_+ \\ \mathbf{c}_- \end{pmatrix} = \begin{pmatrix} \mu_+ M & 0 \\ 0 & \mu_- M \end{pmatrix} \begin{pmatrix} \mathbf{c}_+ \\ \mathbf{c}_- \end{pmatrix}. \quad (3.18)$$

Again, these equations are coupled by the nonlinearity present in the matrix  $K$ . Together with a normalization condition and a fixation of the phase, both of which are now complex conditions, the bicomplex equations

$$\begin{pmatrix} \mathbf{f}_0 \\ \mathbf{c}_-^T M \mathbf{c}_+ - 1 \\ \sum b_n (c_+^n - c_-^n) \end{pmatrix} = 0 \quad (3.19)$$

have to be solved. This can be done straightforwardly since every function is now complex differentiable, and therefore the Jacobian

$$J = \begin{pmatrix} S^{++} & S^{+-} & -M\mathbf{c}_+ & 0 \\ S^{-+} & S^{--} & 0 & -M\mathbf{c}_- \\ \mathbf{c}_-^T M & (M\mathbf{c}_+)^T & 0 & 0 \\ \mathbf{b}^T & -\mathbf{b}^T & 0 & 0 \end{pmatrix} \quad (3.20)$$

with

$$S_{ij}^{++} = K_{ij} - \mu_+ M + \int 8\pi Na\psi_+\psi_-\phi_j\phi_i d^n \mathbf{r}, \quad (3.21a)$$

$$S_{ij}^{--} = K_{ij} - \mu_- M + \int 8\pi Na\psi_+\psi_-\phi_j\phi_i d^n \mathbf{r}, \quad (3.21b)$$

$$S_{ij}^{+-} = \int 8\pi Na\psi_+^2 \phi_j\phi_i d^n \mathbf{r}, \quad (3.21c)$$

$$S_{ij}^{-+} = \int 8\pi Na\psi_-^2 \phi_j\phi_i d^n \mathbf{r} \quad (3.21d)$$

can be easily derived.

There is one fundamental challenge involved in this method. If one of the two bicomplex components vanishes, i.e.  $c_\pm = 0$ , a normalization is no longer possible. This becomes obvious looking at the trivial case  $Na = 0$ . Since the two components

are independent in this limit, the possible solutions for  $c_{\pm}$  are the solutions of the linear Schrödinger equation or zero. However, if one is aware of such limitations, this method proves extremely powerful for systems with few basis functions, e.g. the multi-mode approximation discussed in Sec. 3.5.

Every solution is present in this representation for all parameters for which the normalization condition from Eq. (3.19) assumes a finite value. Therefore the only possible disturbance lies in the appearance of bifurcations, at which multiple solutions become equal and therefore indistinguishable. For numerically cheap systems this last difficulty can be overcome by a simple modification. Instead of solving the original problem, a randomized bicomplex matrix, which is of the same dimension and scaled by a parameter  $\lambda$ , is added to the Hamiltonian. Now one can systematically search for all solutions within a given range of energies, including the linear solutions calculated by a generalized eigenvalue solver. If a complete set is found, every parameter configuration of the system can be reached in two simple steps. Firstly, the perturbed system is used to follow its branch of solutions to the parameter set of interest. Secondly, one tunes the scaling  $\lambda$  down to zero. If the resulting state is complex, i.e.,  $c_+ = c_-$  holds, the common finite-element method can be used to calculate the stability eigenvalues. Due to the randomized perturbation, not only the possibility of a vanishing norm condition is suppressed, but also the risk that bifurcations are encountered can be neglected.

## 3.4. B-Splines

Now that the principles of the weak formulation and the solution recipes for nonlinear systems have been clarified, one has to decide which basis functions to use. Since the wave functions for a continuous potential will be quite smooth, an ansatz of locally defined polynomials should yield reasonable solutions. In this thesis a basis of B-Splines is employed, which, for example, already has been used very successfully in the calculation of atomic spectra in strong magnetic fields [69].

The numerical calculation is done using de Boor's algorithm [70], in which every spatial dimension is discretized by  $n_i$  vertices constructing  $n_i - 1$  elements, in which the splines are used to interpolate the wave function. The B-Spline functions are defined recursively,

$$B_j^o(x) = \frac{x - s_j}{s_{j+o} - s_j} B_j^{o-1}(x) + \frac{s_{j+o+1} - x}{s_{j+o+1} - s_{j+1}} B_{j+1}^{o-1}(x), \quad (3.22a)$$

$$B_j^0(x) = \begin{cases} 1, & \text{if } x \in [s_j, s_{j+1}), \\ 0, & \text{otherwise,} \end{cases} \quad (3.22b)$$

where the  $s_j$  denote the spatial positions of the vertices and  $B_j^o$  denotes the B-Spline of  $o$ -th order starting from the  $j$ -th vertex. A B-Spline of  $o$ -th order has a

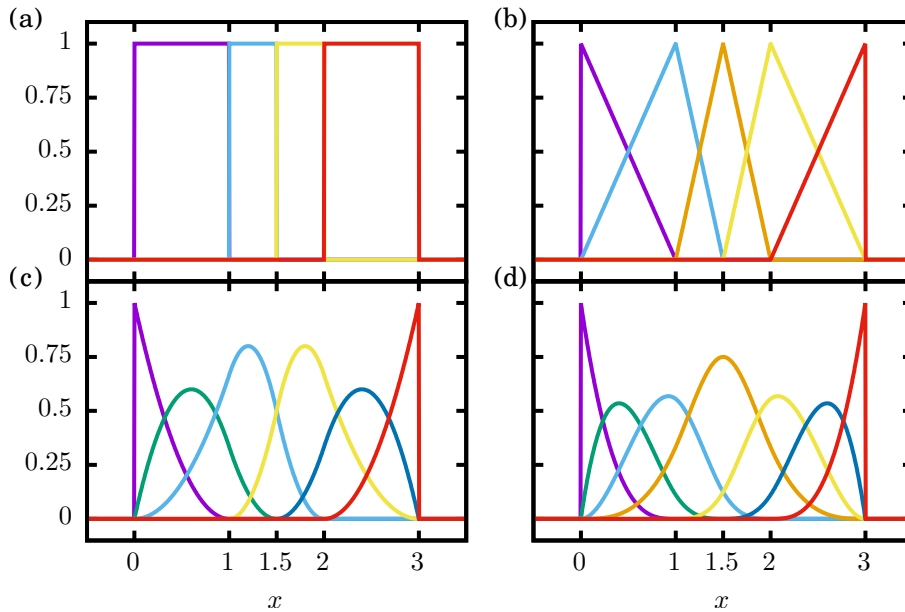


Figure 3.2.: A complete B-Spline basis for five vertices at  $x = \{0, 1, 1.5, 2, 3\}$  of zeroth (a), first (b), second (c), and third (d) order. The support of the B-Spline functions increases with ascending order leading to an overlap between more and more basis functions. Only the first and the last functions contribute to the boundary value, and thus are responsible for fulfilling the boundary conditions.

support of  $n + 1$  adjacent elements. This algorithm only provides one spline in the first and last element, respectively. To improve the quality of this basis in these elements, the first and last vertex are used  $o + 1$  times when evaluating the formulae (3.22). This leads to a basis with exactly  $o + 1$  spline functions per element and increases the dimension of the basis to  $n_i - 1 + o$ . An example of B-Splines up to the second order over five vertices is shown in Fig. 3.2.

If one can assume that the wave functions vanish in the region outside the space covered by the grid, boundary conditions can be taken into account. This eliminates the two outermost basis functions, thus reducing the dimension to a total of  $d_i = n_i + o - 3$ . At last, the basis for higher-dimensional systems is created by a product ansatz of the one-dimensional basis functions. For three dimensions this reads  $\phi_{j(n,m,l)}(x_0, x_1, x_2) = B_n^o(x_0)B_m^o(x_1)B_l^o(x_2)$ . The full basis is then  $D = d_0d_1d_2$ - dimensional.

### 3.5. Multi-mode approximation

The finite-element method with B-Splines leads to excellent results for arbitrary potentials. But what if a small finite number of basis states is already able to capture most effects of the considered system? Using a B-Spline basis to approximate these basis states is then no longer reasonable. Instead a weak formulation of the Gross-Pitaevskii equation in these system-dependent modes is in order.

A system with  $M$  wells is considered, in which every well supports at least one bound state when regarded separately. The energetically lowest state of the  $i$ -th well is called  $\phi_i(\mathbf{r})$ , where the wave functions of every pair of these states only have an overlap in a very small region. These wave functions are considered to keep their shape even when system parameters or the interaction strength between condensate particles are changed. If this holds true, the complete mean-field wave function can be given by

$$\psi(\mathbf{r}) = \sum_{j=1}^M \psi_j \phi_j(\mathbf{r}), \quad (3.23)$$

provided only energies below the first excitations inside the separate wells are assumed. The weak formulation in this basis,

$$\sum_{j=1}^M \left[ \underbrace{\int \nabla \phi_j \nabla \phi_i + V \phi_j \phi_i \, d^3 \mathbf{r}}_{H_{ij}} + \underbrace{\int 8\pi N a |\psi|^2 \phi_j \phi_i \, d^3 \mathbf{r}}_{U \delta_{ij}} - \mu \underbrace{\int \phi_j \phi_i \, d^3 \mathbf{r}}_{M_{ij} = \delta_{ij}} \right] \psi_j = 0, \quad (3.24)$$

assumes a much easier form than for the general case. Since the wave functions do not overlap much, the mass matrix is chosen diagonal. For normalized wave functions it even turns into the identity. This is even more true for the nonlinear contribution. Its strength is given by the dimensionless scaled parameter  $U$ . The complete linear part including the kinetic and the potential part of the Gross-Pitaevskii equation enters the matrix  $H$ . The final form therefore reads

$$\sum_{j=1}^M \left[ H_{ij} + U \delta_{ij} |\psi_j|^2 - \mu \delta_{ij} \right] \psi_j = 0. \quad (3.25)$$

Commonly the matrix  $H$  is not calculated numerically for a given extended potential but defined ad hoc to provide an easily interpretable Hamiltonian. The diagonal elements are found to correspond to the on-site energy of the bound state in each well, while the off-diagonal elements act as a coupling between different wells, i.e., the overlap between two basis functions. For the numerical technique used to solve this equation and the corresponding Bogoliubov-de Gennes equations, the reader is referred to the finite-element method in complex and bicomplex spaces in Secs. 3.2 and 3.3.

## 4. The $\mathcal{PT}$ -symmetric double well

Using the methods given in Chap. 3 one can turn to the simplest realization of a realistic  $\mathcal{PT}$ -symmetric system, the double well. As the double-well plays a major role in this thesis, its properties and relevant effects, shown in numerous works in various approximations and numerically exact calculations [18, 20, 34], are recapitulated. As will be seen in the comparison drawn in Sec. 4.4, analytic results of the two-mode approximation already provide most characteristics of the complete spatially extended  $\mathcal{PT}$ -symmetric double well.

### 4.1. Linear two-mode system

Consider two spatially separated wells, both of which do provide an individual bound ground state. If these states do not overlap too strongly, the two-mode approximation from Sec. 3.5 can be used. The Hamiltonian of this system,

$$H = \begin{pmatrix} i\gamma & -1 \\ -1 & -i\gamma \end{pmatrix}, \quad (4.1)$$

describes the most general case of a  $\mathcal{PT}$ -symmetric two-mode system. In the second well, particles are removed from the condensate, while the particles in the first well stimulate an influx.

The eigenvalues of the linear, i.e., non-interacting, system,

$$\mu = \pm \sqrt{1 - \gamma^2}, \quad (4.2)$$

are real up to the threshold  $\gamma_c = 1$ . Both eigenvalues correspond to real stable stationary solutions; the number of particles stays the same even though there is a continuous in- and out-coupling. This property is the major reason, why  $\mathcal{PT}$ -symmetric systems are investigated in atomic physics. Since both eigenstates can be chosen exactly  $\mathcal{PT}$  symmetric,

$$\psi_{g/e} = \frac{1}{\sqrt{2}} \begin{pmatrix} e^{-i\delta_{g/e}/2} \\ e^{+i\delta_{g/e}/2} \end{pmatrix}, \quad (4.3)$$

the ground and first excited state are fully defined by their phase difference,

$$\delta_g = \arcsin(\gamma), \quad (4.4a)$$

$$\delta_e = \pi - \arcsin(\gamma). \quad (4.4b)$$

#### 4. The $\mathcal{PT}$ -symmetric double well

---

It is apparent that both states become more and more alike for growing parameters  $\gamma$ . At the critical parameter  $\gamma_c = 1$  both eigenstates coalesce, and thus the Hamiltonian is no longer diagonalizable. Its Jordan normal form reads

$$J = \begin{pmatrix} 0 & 1 \\ 0 & 0 \end{pmatrix}. \quad (4.5)$$

If such a Jordan block is found for a specific choice of physical parameters, this point is called an exceptional point and corresponds to a branch point, at which solutions to the system of equations merge and split up [71]. In the present case of a two-dimensional Jordan block the exceptional point is of second order and called EP2 [72]. Please note that this nomenclature is applicable even if the matrix describes the system only locally in the vicinity of the exceptional point.

After the exceptional point, the eigenvalues are complex conjugates of each other and stay complex for all parameters  $\gamma > 1$ . The  $\mathcal{PT}$ -symmetry that is omnipresent in the Hamiltonian is spontaneously broken. The eigenstates in this regime provide an asymmetric distribution of the probability or particle density between the two wells. One well is more strongly occupied by the factor  $(\gamma + \sqrt{\gamma^2 - 1})^2$ . In optical experimental realizations, this marks the transition between bidirectional and unidirectional wave guides. Active, i.e., pumped, optical materials in this regime can exhibit interesting effects such as unidirectional invisibility, either with focus on suppressed reflections [13, 14] or the absence of resonances [15].

## 4.2. Nonlinear two-mode system

As shown in Chap. 2 the concept of  $\mathcal{PT}$ -symmetric systems can be applied to the nonlinear mean-field theory of Bose-Einstein condensates. The corresponding Gross-Pitaevskii equation,

$$\mu \begin{pmatrix} \psi_1 \\ \psi_2 \end{pmatrix} = \begin{pmatrix} U|\psi_1|^2 + i\gamma & -1 \\ -1 & U|\psi_2|^2 - i\gamma \end{pmatrix} \begin{pmatrix} \psi_1 \\ \psi_2 \end{pmatrix}, \quad (4.6)$$

differs only slightly from a form given by Graefe [34], in which the nonlinear part is rescaled to be independent of the total norm of the state. This is due to a different interpretation of the imaginary potentials in many-particle systems and need not be discussed in any more detail. However, the stationary states given in that reference hold true even for the present system, simply because they are already normalized.

The eigenvalues, adapted to the scales and parameters used in this thesis, read

$$\mu = \begin{cases} U/2 \pm \sqrt{1 - \gamma^2} & \gamma < 1, \\ U \pm i\gamma \sqrt{1 - ((U/2)^2 + \gamma^2)^{-1}} & (U/2)^2 + \gamma^2 > 1, \end{cases} \quad (4.7)$$

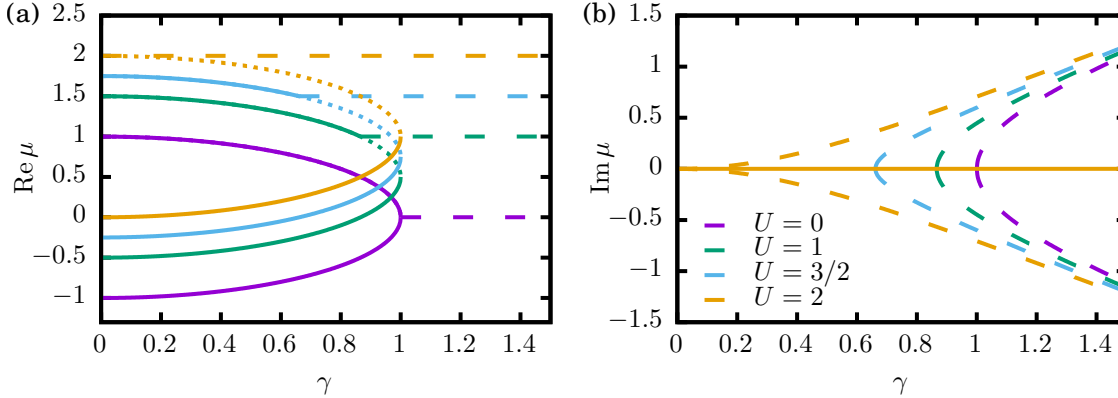


Figure 4.1.: Real (a) and imaginary (b) parts of the eigenvalues of the  $\mathcal{PT}$ -symmetric double well over the strength of particle in- and out-coupling  $\gamma$  for different values of the nonlinearity  $U$ . The eigenvalues of  $\mathcal{PT}$ -symmetric states (solid, dotted) do not change in shape with increasing interaction strengths, but are shifted to higher energies. Stable states are depicted by solid lines, unstable states are shown as dotted lines. Eigenvalues of  $\mathcal{PT}$ -broken states (dashed), however, are shifted more strongly upwards, still bifurcating at a branch point from the symmetric branches up to  $U = 2$ , above which they exist for all parameters  $\gamma$ .

while the corresponding wave functions for the  $\mathcal{PT}$ -symmetric case (real eigenvalues) are the same as in the linear case discussed before. The eigenvalues for different nonlinearities are shown in Fig. 4.1. Apparently, the strength of the nonlinearity, i.e., the interaction strength, provides a shift of the real part of the eigenvalues. The  $\mathcal{PT}$ -symmetric states are shifted by the value  $U/2$  while the broken states rise even higher by  $U$ . This provides a first important result. For  $U = 0$  the broken states emerge at exactly the same point at which the symmetric states vanish. This changes for  $U > 0$ . Due to the stronger shift, rather than branching directly from this exceptional point, broken states now bifurcate from the excited  $\mathcal{PT}$ -symmetric state at the coupling strength  $\gamma = \sqrt{1 - (U/2)^2}$ . For  $U > 2$  this bifurcation also vanishes and the broken states exist for all values of  $\gamma$ . The symmetric states still disappear at  $\gamma = 1$  in a so-called tangent bifurcation. Since no state is found on the other side of this point, the denomination as an exceptional point is no longer valid. It has been shown that the analytic continuation of the Gross-Pitaevskii equation using bicomplex numbers as introduced in Sec. 3.3 generates new solutions that reinstate the exceptional behavior of this point [21].

In all cases two stationary states with real eigenvalues are found that exist up to  $\gamma = 1$ . For a physical realization, however, it is of utmost importance that these states are stable under any small perturbation. Such an investigation of the stability is done using the Bogoliubov-de Gennes equations (2.15). The results are also shown in Fig. 4.1, where solid lines depict eigenvalues of stable states and dotted lines represent unstable states. It is visible that the excited state becomes unstable the moment the  $\mathcal{PT}$ -broken states bifurcate. This is not only the common behavior of the so called pitchfork bifurcation, but also, as will be shown in the last section, the first difference between the presented two-mode model and the calculations of spatially extended potentials.

### 4.3. Time-dependency of non-stationary solutions

Another elegant property of the two-mode system is that even for non-Hermitian potentials, where the state's norm can grow or decay, each state can be defined by three real parameters,

$$\psi(R, \phi, \theta) = R \begin{pmatrix} \cos(\theta/2)e^{-i\phi/2} \\ \sin(\theta/2)e^{+i\phi/2} \end{pmatrix}. \quad (4.8)$$

Using the norm  $R$  of the state as the radius, and the two angles  $\theta \in [0, \pi]$  and  $\phi \in [0, 2\pi)$  as spherical coordinates, every state  $\psi$  is represented as a point in the three-dimensional real space. This so-called Bloch-sphere representation is commonly used for the case  $R = 1$ . In this configuration it was used by Graefe et al. [73] studying the dynamics of the  $\mathcal{PT}$ -symmetric Bose-Hubbard dimer, for which  $R = 1$  could be chosen for every possible configuration. Since the norm of the wave function has an important impact on the dynamics of the system discussed here, this restriction is no longer possible.

The double well is an ideal candidate to study the exact dynamics of a  $\mathcal{PT}$ -symmetric system. A comparison with Eq. (4.3) shows that  $\mathcal{PT}$ -symmetric states lie on the great circle with  $\theta = \pi/2$ . Integrating the time-dependent Gross-Pitaevskii equation in two-mode approximation (3.13) using a fourth-order Runge-Kutta method yields trajectories in the real space spanned by the tuple  $(R, \phi, \theta)$ . Figure 4.2 shows such trajectories for different parameters  $\gamma$  and  $U$ . The trajectories start on the coordinates  $R(t=0) = 1$  and  $\theta(t=0) = \pi/2$ , i.e., as  $\mathcal{PT}$ -symmetric states on the Bloch sphere, and differ only in their phase difference  $\phi$ . Due to the orientation of the Bloch sphere, where the  $z$ -axis is pointing to the left, this corresponds to a meridian through both stationary states. Small values of  $z$ , i.e., states that are occupying the right well, are therefore depicted by points of the right side, and vice versa.

Three important parameter ranges can be distinguished. The first range is represented by Fig. 4.2(b) where every trajectory is closed and both states are

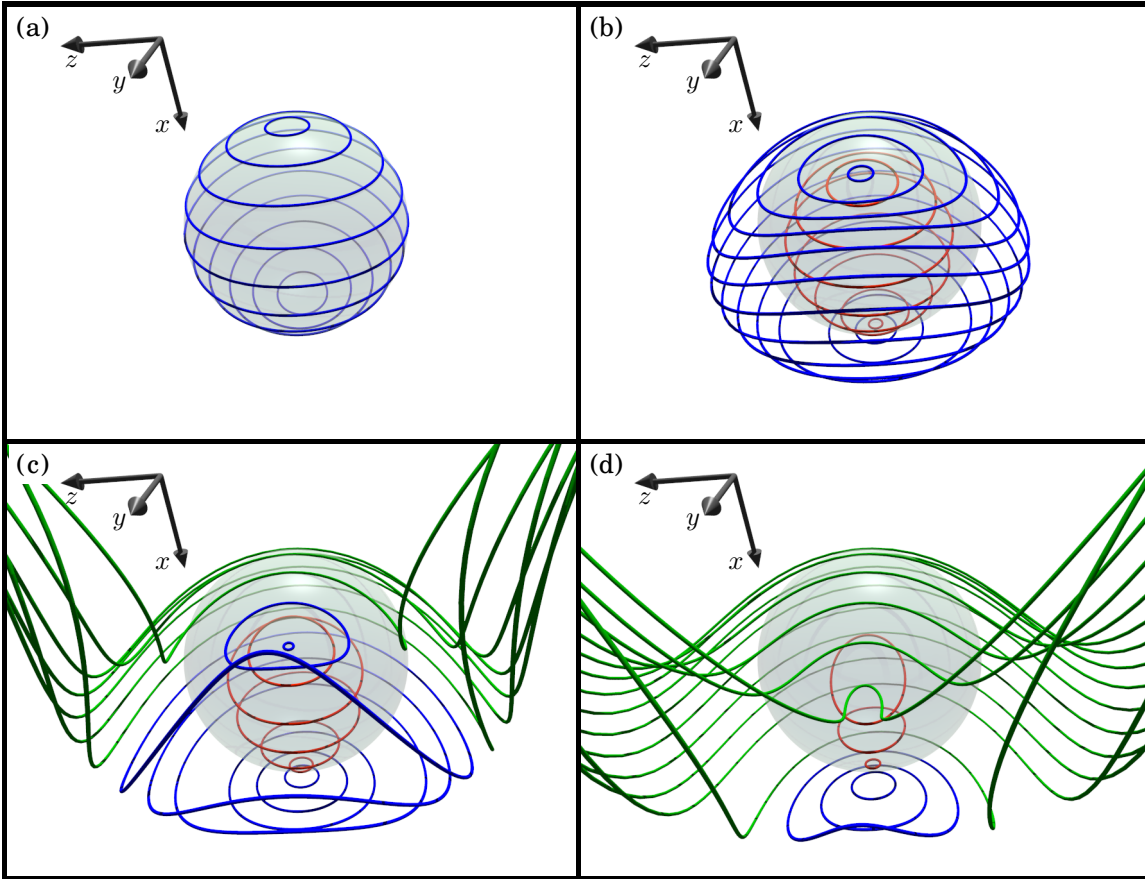


Figure 4.2.: The Bloch sphere (transparent sphere) represents all states of unity norm. Shown in blue, red and green are trajectories starting at  $\theta = \pi/2$ , i.e., on a central meridian. The orientation is chosen in such a way, that points on the left side represent states where the left well is strongly occupied, while points on the right side represent the case of strongly inhabited right wells. The nonlinearity is set identically to  $U = 0.5$  in all figures, while the in- and out-coupling strength is varied. The Hermitian case  $\gamma = 0$  (a) conserves the norm, with all states oscillating from the left to the right well. For  $\gamma = 0.5$  (b) the norm is no longer conserved. The red lines depict states with a norm lower than unity and start on the front side of the sphere, while blue lines depict states with higher norm, all of which originate at the back side. Thus, the highest possible norm of each trajectory is reached when it is nearest to the observer. Even though, the spectrum for  $\gamma = 0.7$  (c) is still entirely real, some trajectories from the backside of the sphere shown in green are diverging. For  $\gamma = 0.9$  (d), the excited state is clearly unstable.

stable, i.e., both fixed points are surrounded by elliptic closed curves. Every non-stationary state oscillates between the right and the left well. However, even before any one of these points become unstable on the Bloch sphere, i.e., the  $\mathcal{PT}$ -broken states have not yet emerged, trajectories start to diverge. This case is shown by Fig. 4.2(c), where this new type of trajectories (green lines) start from the backside of the sphere. A detailed analysis of the trajectories shows that the diverging behavior starts at high norm values. Thus, the strong norm oscillations are responsible for the unstable behavior. In the last region, between this bifurcation point, at which the  $\mathcal{PT}$ -broken states emerge, and the tangent bifurcation, at which both  $\mathcal{PT}$ -symmetric states vanish, the excited state is unstable. This is visible in Fig. 4.2(d), where the first diverging trajectory indicates a repulsive fixed point. Trajectories starting near this point can either diverge or start to oscillate around the stable ground state.

### 4.4. Spatially extended double well

For the sake of simplicity, all calculations shown so far were done in the two-mode approximation. Indeed, almost all results transfer seamlessly to the case of spatially extended potentials. The spectrum shows nearly no difference and the dynamics are qualitatively the same. However, there are some important differences leading to new effects. To present and understand these effects, consider the three dimensional potential

$$V(\mathbf{r}) = \frac{1}{4}x^2 + y^2 + z^2 + 5e^{-x^2}e^{-\frac{1}{10}(y^2+z^2)} + i\gamma \left( e^{-(x+\sqrt{\ln(20)})^2} - e^{-(x-\sqrt{\ln(20)})^2} \right), \quad (4.9)$$

which consists of a cigar-shaped harmonic trap and a Gaussian barrier that is small in  $x$ - but quite elongated in  $y$ - and  $z$ -direction. Two one-dimensional imaginary Gaussian functions, which are positioned in the wells' minima and scaled with the parameter  $\gamma$ , describe the particle in- and out-coupling in the two wells. Note that all other numbers in the potential were fixed such that the results are comparable with those of double-well potentials in previous studies [20, 22].

This potential supports an infinite number of stationary states, of which only the energetically lowest two, i.e., the ground and first excited state in  $x$ -direction, are studied using the finite-element method from Sec. 3.2. The corresponding real part of the eigenvalue spectrum is shown for different nonlinearities  $Na$  in Fig. 4.3(a). In contrast to the two-mode calculations, the position of the tangent bifurcation, at which the two  $\mathcal{PT}$ -symmetric states vanish, does not match the position of the exceptional point at  $Na = 0$ . Instead, it is shifted to higher values of  $\gamma$ . This is due to the fact that the repulsive interaction is changing the shape of the wave function, i.e., the effective in- and out-coupling at a given parameter  $\gamma$  changes.

Further, by including Fig. 4.3(b) into this discussion, a second difference can be observed. The stability of the excited state does not change at the same point at

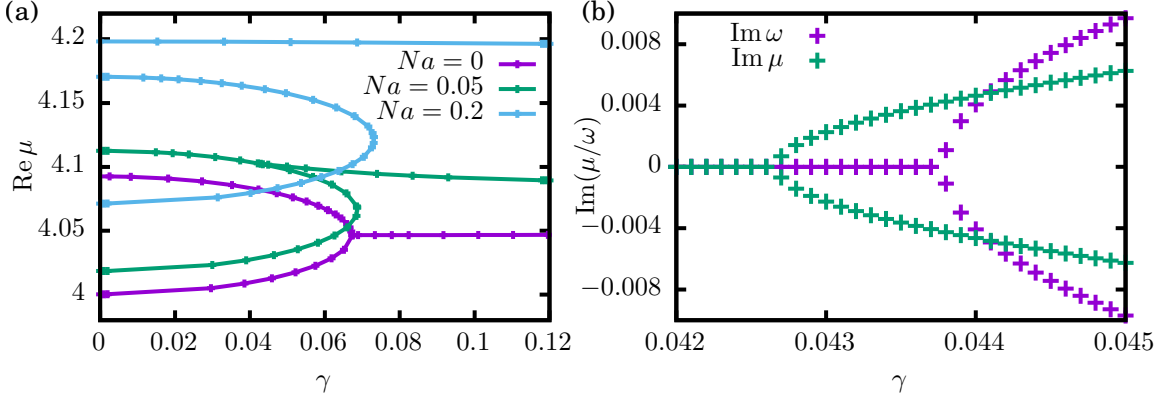


Figure 4.3.: The left panel (a) shows the real part of the eigenvalues of the spatially extended  $\mathcal{PT}$ -symmetric double well over the strength of particle in- and out-coupling  $\gamma$ . The qualitative behavior matches the two-mode calculations in Fig. 4.1. They differ only in the absolute values, a shifted bifurcation point between the  $\mathcal{PT}$ -symmetric states and a small shift in the eigenvalues of the  $\mathcal{PT}$ -broken states. The right panel (b) shows the last non-vanishing imaginary part of the Bogoliubov-de Gennes eigenvalues of the excited state and the imaginary part of the chemical potential of the  $\mathcal{PT}$ -broken states for the case  $Na = 0.05$ . In contrast to the two-mode calculations, the point where the stationary state becomes unstable and the point where the  $\mathcal{PT}$ -broken states emerge do not match.

which the  $\mathcal{PT}$ -broken states emerge. Instead, the stationary state stays dynamically stable for higher values of the in- and out-coupling parameter  $\gamma$ , although  $\mathcal{PT}$ -broken states exist in its vicinity. It has to be emphasized that this effect is not only present in three-dimensional calculations, which omit an unlimited number of stationary states, but also in the one-dimensional double-delta potential, which only supports two stationary states [22, 74]. Even the three-mode system presented in Sec. 6.1 shows a significant stability gap. All these systems have in common that the eigenstates depend on the strength of the nonlinearity. Due to the non-Hermitian Hamiltonian the norm of a wave function is not conserved and, in general, changes over time. The changed norm subsequently changes the effective strength of the nonlinearity since more or fewer particles are involved, i.e., the dynamics unfold to different interaction strengths. Therefore, one cannot determine the system's properties by investigating the fixed points at a specific interaction strength but must take the whole spectrum into account.

The nonlinearities used,  $Na \approx 0.2$ , are still small compared to the realistic values presented in Sec. 2.1. Two examples of effects at high interaction strengths have

#### *4. The $\mathcal{PT}$ -symmetric double well*

---

already been studied. Firstly, Dizdarevic et al. [75] studied the case of a strong attractive interaction that leads to a collapse of the condensate. Secondly, rotating condensates at high repulsive interaction strengths nucleated vortices and are discussed in Chap. 7.

## 5. Existence of real spectra

In Sec. 2.3 a solid interpretation of imaginary potentials in the mean-field description of many-particle systems has been found and it has been made clear that a microscopic description of the in- and out-coupling process is indeed possible. However no mandatory criterion was given under which the resulting system with  $\mathcal{PT}$ -symmetric imaginary potentials leads to a configuration with balanced gain and loss where real stationary states can be found.

Consider a system, in which the  $m$  lowest eigenstates of the Hamiltonian are  $\mathcal{PT}$  symmetric and have real eigenvalues, and one is interested in the stability of these eigenstates. If even one higher excited state were  $\mathcal{PT}$  broken, the corresponding perturbation to the originally stationary state would grow exponentially. But how can it be ensured that a spectrum with an infinite number of eigenvalues is entirely real, i.e., the system has unbroken  $\mathcal{PT}$  symmetry? This chapter deals with this problem examining small perturbations to the Hermitian case without imaginary potentials.

### 5.1. Perturbation theory

A linear system shall be described by the Hamiltonian  $\hat{H} = \hat{H}_0 + \gamma\hat{H}_P$ , where the unperturbed Hamiltonian  $\hat{H}_0$  is Hermitian and the perturbation  $\hat{H}_P$  is anti-Hermitian. If they fulfill the relations

$$\mathcal{P}\hat{H}_0 = \hat{H}_0^\dagger\mathcal{P} = \hat{H}_0\mathcal{P}, \quad (5.1a)$$

$$\mathcal{P}\hat{H}_P = \hat{H}_P^\dagger\mathcal{P} = -\hat{H}_P\mathcal{P}, \quad (5.1b)$$

the Hamiltonian is pseudo-Hermitian with respect to the parity operator,  $\mathcal{P}\hat{H} = \hat{H}^\dagger\mathcal{P}$ . It is obvious that in case of a diagonal matrix representation, the system is  $\mathcal{PT}$  symmetric, where  $\mathcal{T}$  acts as the complex conjugation. This is in particular true in position space where the perturbation is given by an antisymmetric imaginary potential  $i\hat{V}(\hat{x})$ .

Assume that all eigenvalues of  $\hat{H}_0$  are non-degenerate and discrete and behave as continuous functions of the perturbation strength  $\gamma$ . Then a perturbation can always be chosen small enough such that the eigenvalues are not able to coalesce and form exceptional points. Since complex eigenvalues of pseudo-Hermitian and  $\mathcal{PT}$ -symmetric Hamiltonians always appear in complex conjugate pairs [56–58]

## 5. Existence of real spectra

---

the formation of complex eigenvalues can only occur at such exceptional points. In particular, for perturbations small enough all eigenvalues must remain real.

As a first step, the former argument will be presented in a more formal way applying the perturbation theory [76, 77]. This technique has already been used with great success [78, 79] to decide whether a specific linear system stays  $\mathcal{PT}$  symmetric under a non-Hermitian perturbation. Another important power of this approach is that it can be extended to discuss degenerate states.

Since the unperturbed Hamiltonian commutes with the parity operator  $\mathcal{P}$ , all its eigenvectors,  $\{|\psi_m\rangle\}$ , can be chosen either symmetric or antisymmetric, hence  $\mathcal{P}|\psi_m\rangle = \lambda_m|\psi_m\rangle$ ,  $\lambda_m = \pm 1$  holds. The power series for the perturbed energy eigenvalue  $\mu_n$  of the corresponding eigenstate  $|\psi_n\rangle$  reads

$$\mu_n = \mu_{n,0} + \gamma\mu_{n,1} + \gamma^2\mu_{n,2} + \dots \quad (5.2)$$

A useful explicit form of the energy corrections was given by Kato in 1949 [80],

$$\mu_{n,s} = (-1)^{s-1} \text{tr} \sum_{\mathbf{k}_s} S^{k_1} \hat{H}_P S^{k_2} \dots \hat{H}_P S^{k_{s+1}}, \quad (5.3)$$

where the sum is chosen to iterate over all  $\mathbf{k}_s \in \mathbb{N}^{s+1}$  with  $k_1 + \dots + k_{s+1} = s - 1$ . The *reduced resolvent* is defined as

$$S = \sum_{m \neq n} \frac{|m\rangle\langle m|}{\mu_m - \mu_n}, \quad (5.4a)$$

while the zeroth power is treated differently as

$$S^0 = |n\rangle\langle n|. \quad (5.4b)$$

Obviously,  $[S, \mathcal{P}] = 0$  holds, since

$$\mathcal{P}|m\rangle\langle m| = \lambda_m|m\rangle\langle m| = |m\rangle\langle m|\lambda_m = |m\rangle\langle m|\mathcal{P}. \quad (5.5)$$

Pseudo-Hermiticity of  $\hat{H}_P$  ensures that all corrections  $\mu_{n,s}$  are real. This can be seen by using  $\text{tr}(\mathcal{P}\hat{O}\mathcal{P}) = \text{tr}(\hat{O})$  and  $S^\dagger = S$  and calculating the complex conjugate of the energy correction

$$\begin{aligned} \mu_{n,s}^* &= (-1)^{s-1} \text{tr} \sum_{\mathbf{k}_s} \mathcal{P} S^{k_{s+1}} \hat{H}_P^\dagger \dots \hat{H}_P^\dagger S^{k_1} \mathcal{P} \\ &= (-1)^{s-1} \text{tr} \sum_{\mathbf{k}_s} S^{k_{s+1}} \hat{H}_P \mathcal{P} \dots \mathcal{P} \hat{H}_P S^{k_1} \\ &= (-1)^{s-1} \text{tr} \sum_{\mathbf{k}_s} S^{k_1} \hat{H}_P \dots \hat{H}_P S^{k_{s+1}} \\ &= \mu_{n,s}. \end{aligned} \quad (5.6)$$

However, since the anti-Hermiticity of  $\hat{H}_P$  renders every odd energy correction purely imaginary,

$$\begin{aligned}
 \mu_{n,s}^* &= (-1)^{s-1} \text{tr} \sum_{\mathbf{k}_s} S^{k_{s+1}} \hat{H}_P^\dagger \cdots \hat{H}_P^\dagger S^{k_1} \\
 &= (-1)^{s-1} \text{tr} \sum_{\mathbf{k}_s} (-1)^s S^{k_1} \hat{H}_P \cdots \hat{H}_P S^{k_{s+1}} \\
 &= (-1)^s \mu_{n,s},
 \end{aligned} \tag{5.7}$$

i.e., together with Eq. (5.6) they vanish, it can be concluded that the lowest order energy shift is at least quadratic.

The situation changes drastically if one stops assuming non-degenerate eigenvalues. Now consider  $M$  degenerate eigenvectors  $\{\phi_i\}$  with the common eigenvalue  $\mu$ . The first order energy shift is given by the eigenvalues of the matrix

$$S_{ij} = \langle \phi_i | \hat{H}_P | \phi_j \rangle. \tag{5.8}$$

The matrix  $S$  inherits the anti-Hermiticity from the perturbation  $\hat{H}_P$ . Its eigenvalues are therefore either purely imaginary or zero. This means that any perturbation that does not imply  $S = 0$  immediately produces imaginary eigenvalues. For  $\mathcal{PT}$ -symmetric Hamiltonians describing in- and out-coupling of particles, this means that no stable stationary current from particle source to particle sink can exist.

For  $S = 0$ , i.e., all matrix elements between degenerate eigenstates are zero, higher-order perturbations must be taken into account. In this case the considerations for simple eigenvalues from Eq. (5.6) hold, thus all eigenvalues remain real.

Two important problems remain to be addressed: Firstly, the discussion in this section assumed eigenvalues that change only slightly due to a weak perturbation. Discussing the results of Adduci, Mityagin and Siegl [81, 82] in Sec. 5.2 it can be seen that this assumption cannot only be checked in the mathematical framework of *frames* and the *Riesz basis* but the absolute strength of this change can indeed be estimated. Secondly, in Sec. 5.3, the rigorous estimates of these works are tested against the question whether or not they hold even in a nonlinear system.

## 5.2. Riesz basis and general estimates

The study how a non-Hermitian perturbation changes the eigenvalue spectrum of a system leads to the question, whether the perturbed eigensystem builds a Riesz basis [81]. A detailed study of frames and the Riesz basis is out of the scope of this thesis. However, the importance of these concepts can be made clear.

## 5. Existence of real spectra

---

Perturbation theory determines corrected eigenvalues and eigenstates of the perturbed system from the unperturbed case. However, to ensure that this approach is successful, the eigenvalues have to be continuous with respect to the perturbation strength. Within the radius of convergence of the perturbation theory the eigenvalues must behave like a power series around every  $\gamma$ . Any additional deflection  $\delta$  of this parameter then leads to states and eigenvalues again predicted by perturbation theory. Let  $|\psi\rangle$  be an eigenvector to such a further perturbed operator  $\hat{H}(\gamma + \delta)$  and  $|\phi_i\rangle$  the eigenvectors of the case  $\hat{H}(\gamma)$ . Perturbation theory can only work, if the new eigenvector can be written as a linear combination of the unperturbed eigenvectors, i.e., the coefficients  $\langle\psi|\phi_i\rangle$  must be bound. This can be only ensured if the sequence  $\{\phi_i\}$  forms a *frame* [83],

$$A\|\chi\|^2 < \sum_i |\langle\chi|\phi_i\rangle|^2 < B\|\chi\|^2 \quad \forall\chi \in \mathcal{H}, \quad (5.9)$$

with the in general real constants  $A$  and  $B$ . If such a bound cannot be given, eigenvalues and eigenstates can differ very strongly even for a weak perturbation. A frame that is exact, i.e., it is no longer a frame if one state is removed, is called a *Riesz basis*.

This shows the strong connection between the search for the existence of a Riesz basis and the possibility to provide estimates for the change of eigenvalues under a small perturbation. Obviously, considering Eq. (5.9), every basis of a finite-dimensional Hilbert space is a Riesz basis and for finite systems, perturbation theory works whenever the system is analyzed sufficiently away from an exceptional point [71]. Thus, when checking the condition for the whole sequence, a finite number of states can be left out as long as the remaining infinite members of the sequence are considered.

To ensure that weak perturbations of Hermitian systems conserve the real spectrum of the unperturbed Hamiltonian, all eigenvalues must either be finitely spaced and therefore be simple, or must correspond to states on which the perturbation does not act according to Eq. (5.8). An even stronger assumption allows for the phrasing of rigorous estimates: The system is supposed to behave like a harmonic oscillator for high excitations. This means that between two adjacent eigenvalues a constant gap, w.l.o.g. of size one, can be found. Adduci and Mityagin [82] and Siegl and Mityagin [81] have recently analyzed how  $\mathcal{PT}$ -symmetric perturbations behave in such an oscillator.

Siegl and Mityagin presented a condition,

$$\exists\alpha > 0, \quad \exists M > 0, \quad \forall m, n \in \mathbb{N}, \quad \left| \langle\psi_m|\hat{B}|\psi_n\rangle \right| \leq \frac{M}{m^\alpha n^\alpha}, \quad (5.10)$$

where  $\hat{B} = \gamma\hat{H}_P$  is the perturbation operator and  $|\psi_m\rangle$  are the eigenfunctions of the harmonic oscillator. The constant  $M$  depends on the specific form of  $\hat{B}$  and

therefore on the perturbation strength  $\gamma$ . Under this criterion they proved that there exists a positive integer  $k$  such that the eigenvalues become simple for high quantum numbers  $n > k$  and the root system forms a Riesz basis. Not only does this condition ensure well behaved eigenvalues, but it also allows the authors to give an estimate about how far eigenvalues of different excitations can vary due to the perturbation:

For a given perturbation strength  $\gamma$ , each eigenvalue in the simple region  $\mu_i, i > k$ , is altered by the value  $\Delta\mu_i$ . Then the authors [81] show that

$$|\Delta\mu_i| < D_k = \frac{\tilde{M}}{k^{2\alpha}}, \quad (5.11)$$

where  $D_k$  is a disc around each eigenvalue that serves as an upper bound for the differences  $\Delta\mu_i$ . The parameter  $\alpha$  is the same as in Eq. (5.10), and  $\tilde{M}$  is a new but universal constant for a given parameter  $\gamma$  and all possible excitation numbers  $k$ .

In the next section the case of singular perturbations is used to answer two questions: Firstly, is the upper bound given in Eq. (5.11) optimal? And secondly, does it even hold for nonlinear systems?

## 5.3. Numerical test of estimates for singular perturbations

### 5.3.1. Properties of the $\mathcal{PT}$ -symmetric harmonic trap

The estimates of the previous section were derived for the case of equally spaced eigenvalues. Therefore this section considers a one-dimensional harmonic oscillator as a trapping potential. The perturbing operator is given by imaginary delta functions to model balanced gain and loss of particles. The nonlinear Gross-Pitaevskii equation with the appropriate potentials reads

$$\mu\psi(x) = \left( -\frac{d^2}{dx^2} + x^2 + i\gamma(\delta(x-b) - \delta(x+b)) + g|\psi(x)|^2 \right) \psi(x). \quad (5.12)$$

Here  $2b$  gives the distance between the two delta functions and  $\gamma$  denotes the strength of the non-Hermiticity, i.e., the strength of the particle in- and out-coupling. The parameter  $g$  stands for the effective nonlinearity of the one-dimensional system and is considered to vanish for the linear systems, which are considered first. Please note that since the system is one-dimensional, the nonlinearity is not scaled with the factor  $8\pi Na$  given in Eq. (2.14). Instead, the concrete strength of the interaction depends on the specific form of the trapping potential in the neglected dimensions.

The unperturbed spectrum shows the known solutions of the one-dimensional harmonic oscillator. The eigenvalues are given by  $\mu_n = 2n + 1$ , where the quantum

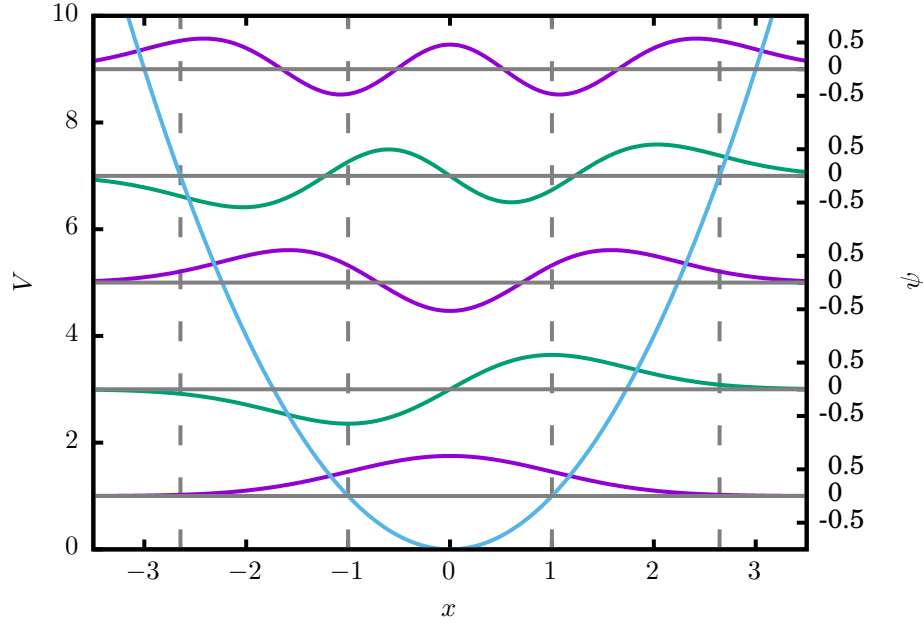


Figure 5.1.: Unperturbed spectrum and the five lowest lying wave functions of the harmonic oscillator. At  $x = \pm 1$  and  $x = \pm\sqrt{7}$  vertical lines designate two important possible positions of the delta functions at classical turning points of the states  $n = 0$  and  $n = 3$  respectively.

number  $n$  is a natural number including zero. The trapping potential, and the five lowest lying states' wave functions are shown in Fig. 5.1. The vertical lines depict the turning points of the classical harmonic oscillator for the quantum numbers  $n = 0$  and  $n = 3$ . In the discussion of the eigenvalue spectrum in Sec. 5.3.2 these turning points ( $b = 1$  and  $b = \sqrt{7}$ ) are used as positions for the delta functions. Outside the turning points, in the classically forbidden regime, the wave functions drop exponentially. It is obvious that only such states will be significantly affected by the perturbations for which the delta functions lie within the classically allowed region.

The system studied fulfills the condition for the existence of a Riesz basis (5.10). Calculating the left side of the inequality gives

$$\left| \langle \psi_m | \hat{B} | \psi_n \rangle \right| = 2|\gamma| |\psi_m(b)\psi_n(b) - \psi_m(-b)\psi_n(-b)|. \quad (5.13)$$

The eigenfunctions of the harmonic oscillator obey the parity  $(-1)^n$ . Since the perturbation is antisymmetric,  $|\langle \psi_m | \hat{B} | \psi_n \rangle| = 0$  holds for all pairs of wave functions with the same parity. For odd  $n$  and even  $m$  or vice versa an estimation of the eigenstates is required. Using an inequality from [81], Example 6, for the Hermite

polynomials  $h_n(x)$ ,

$$|h_n(b)| \leq \tilde{C}n^{-1/4}, \quad b^2 \leq 2(2n+1), \quad (5.14)$$

where  $\tilde{C}$  is a constant that can be chosen uniform for all  $n$ , the eigenstates at the positions  $\pm b$  can be estimated. For high quantum numbers  $n$ , inequality (5.10) yields

$$\left| \langle \psi_m | \hat{B} | \psi_n \rangle \right| \leq 2|\gamma| \tilde{C}m^{-1/4}n^{-1/4}. \quad (5.15)$$

The eigenvalue boundary disc  $D_k$  from Eq. (5.11) then shrinks with the rate

$$k^{-1/2}. \quad (5.16)$$

However, for this special case of singular perturbations it can be shown that this estimate is not ideal. Instead, Mityagin [36] proposed stronger estimates, where the disks shrink with the rate

$$k^{-3/2} \log k. \quad (5.17)$$

In the next sections, numerical results are presented to which both boundaries are compared.

### 5.3.2. Eigenvalue spectra

Since the system (5.12) is one-dimensional, the eigenvalues  $\mu$  can be obtained using the integration method presented in Sec. 3.1. Especially the singular perturbations can be modeled easily by introducing a jump of the first derivative in the integration of the differential equation. Figure 5.2 shows the lower section of the harmonic oscillator spectrum. The eigenvalues are shown for the linear system,  $g = 0$ , and increasing perturbation strengths  $\gamma$ . The perturbations are used at three different positions, close to the center of the harmonic oscillator,  $b = 0.2$  (a),(b), at the turning point of the ground state,  $b = 1$  (c), and at that of the third excited state,  $b = \sqrt{7}$  (d).

Observing the real (a) and imaginary (b) parts of the eigenvalues in Fig. 5.2, one recognizes that successive pairs of eigenvalues coalesce in exceptional points, from where onwards they turn into complex conjugate pairs. This is the expected behavior for a  $\mathcal{PT}$ -symmetric system as the double well presented in Chap. 4. Going up in the spectrum, the branch points are shifted to larger values of  $\gamma$ . For the most part, the real parts of the eigenvalues of the  $\mathcal{PT}$ -broken states remain approximately constant beyond the branch points. The imaginary parts quickly tend to zero after their initial growth. What is surprising is that the eighth and ninth excited state experience huge shifts in both their real and imaginary parts of the eigenvalue shortly after the bifurcation. Eventually they saturate at a value above the 30th excited state.

For perturbations further away from the center, shown in Figs. 5.2 (c),(d), only the real part of the eigenvalues is shown. The delta functions reside outside the

## 5. Existence of real spectra

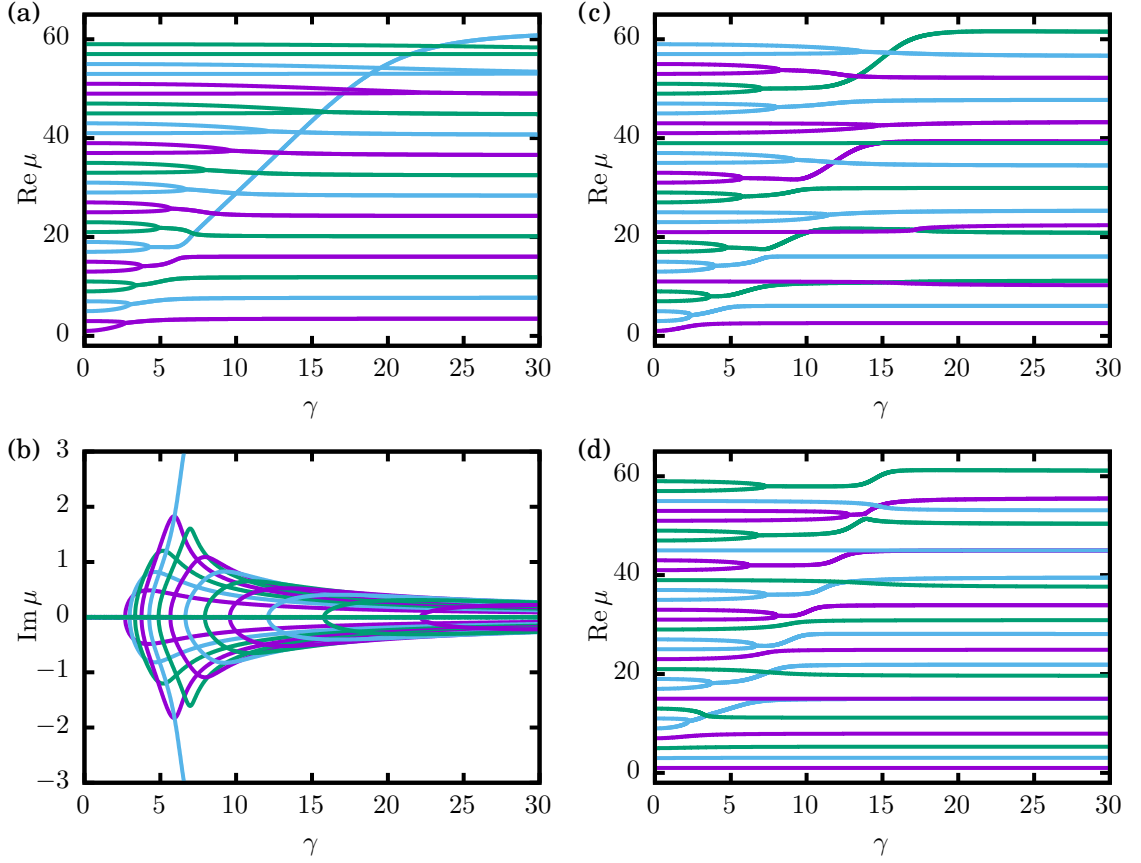


Figure 5.2.: Eigenvalues  $\mu$  evolving from the unperturbed levels of the harmonic oscillator with  $n = 0, \dots, 29$  in dependence of the coupling strength  $\gamma$  of the non-Hermiticity for the linear ( $g = 0$ ) Gross-Pitaevskii equation (5.12). For singular perturbations near the origin  $b = 0.2$ , the real (a) and imaginary (b) parts are shown. Every two adjacent eigenvalues bifurcate and two  $\mathcal{PT}$ -broken states with  $\text{Im } \mu \neq 0$  emerge. For higher distances between the center and the perturbations,  $b = 1$  (c), the perturbation lies at the classical turning point of the ground state. Accordingly, the ground state is not involved in any bifurcation scenario. At  $b = \sqrt{7}$  (d), i.e., the turning point of the state with  $n = 3$ , all states up to the third excited state remain  $\mathcal{PT}$  symmetric.

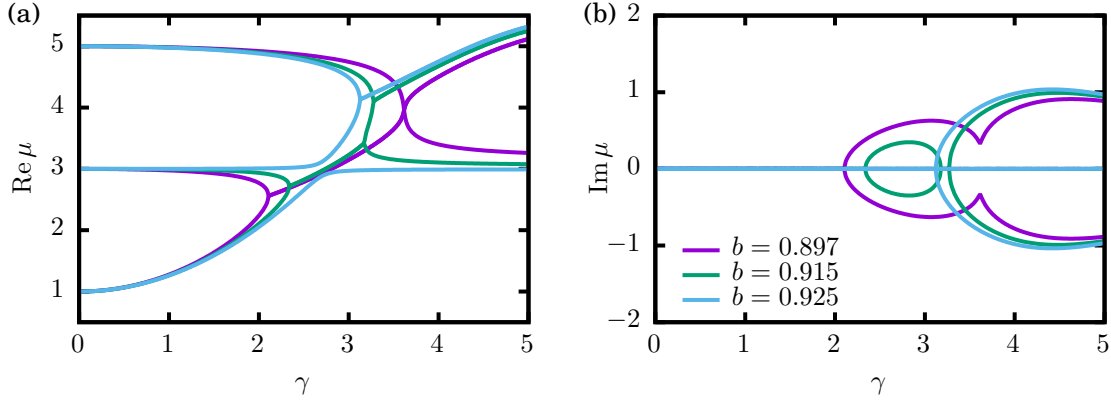


Figure 5.3.: Transition of the bifurcation partner of the unperturbed energy level  $n = 1$ , i.e., the first excited state, from the ground ( $n = 0$ ) to the second excited state ( $n = 2$ ) by varying the position of the delta functions in the vicinity of  $b = 0.9$ . The real (a) and imaginary (b) parts of the eigenvalues are shown.

classically allowed region of the unperturbed ground state  $n = 0$  (c) or all states up to  $n = 3$  (d) respectively. Thus, it is no surprise that for  $b = 1$  the ground state no longer “feels” the delta functions, and therefore no longer unites with the first excited state at a branch point. Rather its eigenvalue remains real for any perturbation strength  $\gamma$ . The same can be observed for the states with  $n = 0, 1, 2, 3$  in Fig. 5.2(d). However, these states are not the only *robust* [84] states of this system. If the delta functions reside near a node of the wave function, their effect is also too weak for the state to form a branch point. For the case  $b = \sqrt{7}$  this behavior is found for many states, namely  $n = 6, 7, 10, 11, 14, 19, 22$ , and 27.

Comparison of Figs. 5.2(a) and (c) shows, that for  $b = 0.2$  the first excited state forms a branch point with the ground state, while for  $b = 1$  it branches with the second excited state. The transition from one coalescence behavior to the other is illustrated in Fig. 5.3. The real and imaginary parts of the eigenvalues emerging from the lowest lying three eigenstates are shown as functions of  $\gamma$  and the three positions of the delta functions  $b = 0.897$ ,  $b = 0.915$ , and  $b = 0.925$  are compared. It is evident that at  $b = 0.897$  the ground and first excited state still coalesce, giving rise to a pair of complex conjugate eigenvalues. Following the real part of these eigenvalues reveals a crossing with the second excited state. It has to be emphasized that the states are not degenerate due to the finite imaginary part of the broken states, i.e., only the real parts cross. After the crossing the state remains  $\mathcal{PT}$  broken.

The behavior for  $b = 0.915$  is similar at first, since the first branch point still exists. However the eigenvalues resulting from this coalescence of the ground and

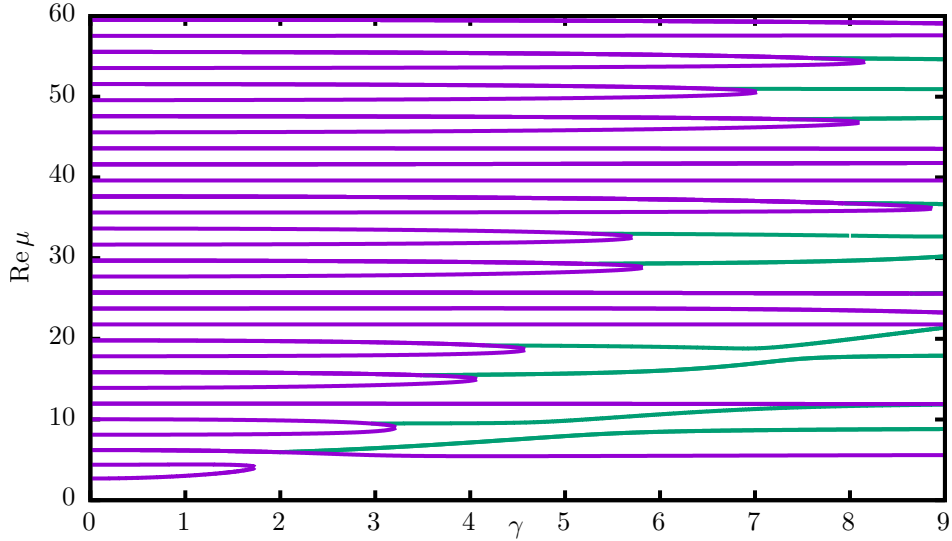


Figure 5.4.: Real parts of the eigenvalues of (5.12) with a nonvanishing nonlinearity  $g = 5$  perturbed by the two delta functions with distance  $b = 1$  from the trap center. Eigenvalues evolving from the unperturbed levels up to  $n = 29$  are shown. Magenta lines depict purely real, i.e.,  $\mathcal{PT}$ -symmetric states, whereas the real parts of every two complex conjugate eigenvalues are shown by single green lines. These complex eigenvalues no longer start at the branch points of the real eigenvalues but bifurcate at previously unspecific perturbation strengths  $\gamma$  from any  $\mathcal{PT}$ -symmetric state's eigenvalue.

first excited state does not stay  $\mathcal{PT}$  symmetric. Instead they again split into two real eigenvalues, the lower of which remains real for any  $\gamma$ . The upper eigenvalue again collides with the second excited state, this time forming a branch point and giving birth to a new pair of complex eigenvalues. In a last step for  $b = 0.925$ , the transition is completed. The two branch points have merged and the intermediate real eigenvalue has vanished. The ground state is represented by a single real energy level while the first two excited states coalesce. A similar behavior, the emergence as well as the transition between *robust* and *fragile* states, has already been discussed for singular perturbations in a square well [84, 85].

The present work, however, deals with Bose-Einstein condensates whose interaction renders the characterizing differential equation nonlinear. Eq. (5.12) already implements the appropriate term for contact interactions, the strength of which is controlled by the parameter  $g$ . Figure 5.4 shows the real part of the eigenvalue spectrum for a nonlinearity  $g = 5$  with the delta functions placed at  $b = 1$ . A direct comparison with the linear case in Fig. 5.2(c) shows major differences. Even though the perturbation lies at its classical turning point of the linear system, the

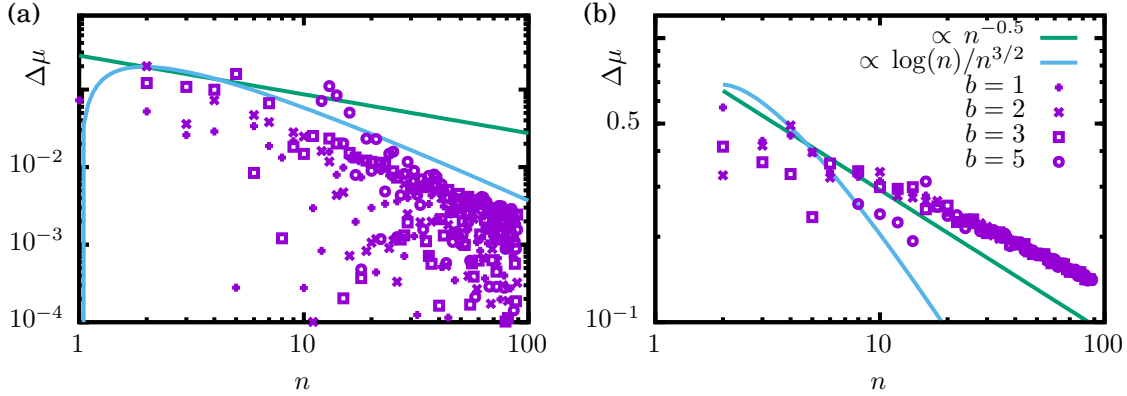


Figure 5.5.: Comparison between rigorous estimates (fully drawn curves) and numerical data. The shift of the eigenvalues for a perturbation with strength  $\gamma = 1$  at different positions  $b$  from the unperturbed levels as a function of the quantum number  $n$  is shown. The linear case (a) shows a perfect agreement between data and estimate while the nonlinear case (b) shows a slower decay behavior of approximately  $n^{-0.37}$ .

ground state still coalesces with the first excited state revealing an increase in the wave function's extension due to the repulsive interaction. However, at the branch point both states vanish with no  $\mathcal{PT}$ -broken state emerging. One should emphasize that an analytic continuation could once more reveal new states, which would still arise from the tangent bifurcation [21, 68].

Like in the double-well system presented in Chap. 4, the broken states are shifted away due to the nonlinear contribution and emerge at new previously unspecific points in the spectrum. As a matter of fact, the lowest lying broken state arises from the robust third excited state that does not break symmetry for any parameter  $\gamma$ . In general, thus, it is not sufficient to account for  $\gamma$  to pinpoint where complex eigenvalues emerge. However, the calculations in the nonlinear double well indicate that such an emergence of symmetry-broken states does not necessarily lead to a stability transition in states not involved in the bifurcation.

### 5.3.3. Eigenvalue shifts

For a given perturbation strength  $\gamma$ , Eqs. (5.16) and (5.17) predict how strongly the eigenstates change in dependence of the excitation quantum number  $n$ . Since the prediction is meant to hold for high quantum numbers  $n \rightarrow \infty$  the exact position of the delta function should not matter for the overall shrinking rate. Figure 5.5 shows the deviations of the eigenvalues  $\Delta\mu$  from their unperturbed energy levels  $\mu_n$  as a function of the quantum number  $n$ . The perturbation strength  $\gamma = 1$  and

## 5. Existence of real spectra

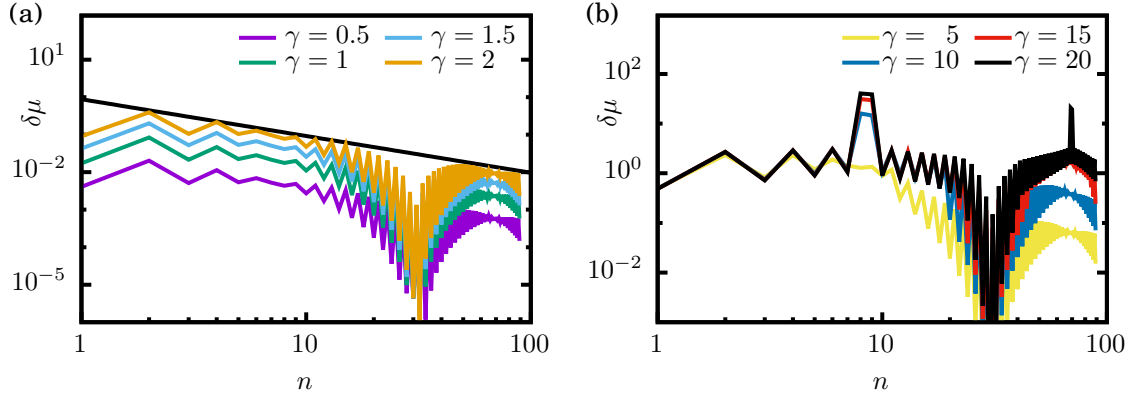


Figure 5.6.: Absolute eigenvalue shift  $\delta\mu = |\Delta\mu|$  for a linear system  $g = 0$  and delta perturbations at the position  $b = 0.2$ . The shifts are shown as a function of the quantum number  $n$  and compared for different perturbation strengths  $\gamma$ . For weak perturbations (a), the ideal perturbation  $\log(n)/n^{3/2}$  (black line) holds even for very low quantum numbers. For higher perturbation (b) outliers at  $n = 8, 9$  and  $n \approx 75$  breach the estimations.

multiple different positions of the delta function are chosen to draw a comparison with the shift rate  $n^{-1/2}$  (green line) and the improved estimate of  $\log(n)/n^{3/2}$  (blue line). For the linear case (a) not only is the  $n^{-1/2}$  dependence an upper bound on the shrink rate, but the improved estimate is in excellent agreement with the numerical data, irrespective of the position of the delta functions.

When a non-vanishing nonlinearity  $g = 2$  is considered, as done in Fig. 5.5(b), again a decay of the eigenvalue shifts in dependence of the quantum number can be seen. However, already by a comparison with the scales of the vertical axis in Fig. 5.5(a) the much slower shrinking behavior becomes obvious. While the linear case shows shifts below  $10^{-2}$  for high quantum numbers  $n \approx 100$ , the nonlinear energy levels are still above  $10^{-1}$ . Furthermore, both rigorous mathematical estimates for the linear case undercut the numerical values. Instead, the decay behavior is found to be approximately proportional to  $n^{-0.37}$ .

Two open questions remain to be answered in this section: Does the strength of the perturbation influence the applicability of the estimates, in particular if for high strengths, complex eigenvalues exist? And how does the decay of eigenvalue shifts respond to a change of the nonlinearity?

To address the first question, Fig. 5.6 shows the eigenvalue shifts for  $g = 0$  and different perturbation strengths  $\gamma = 0.5 \dots 20$ . Since for the position chosen,  $b = 0.2$ , the first complex eigenvalues exist already for  $\gamma \gtrsim 3$  the absolute eigenvalue shift  $\delta\mu = |\Delta\mu|$  must be used. For  $\gamma \leq 2$  Fig. 5.6(a) shows that the ideal estimate (5.17)

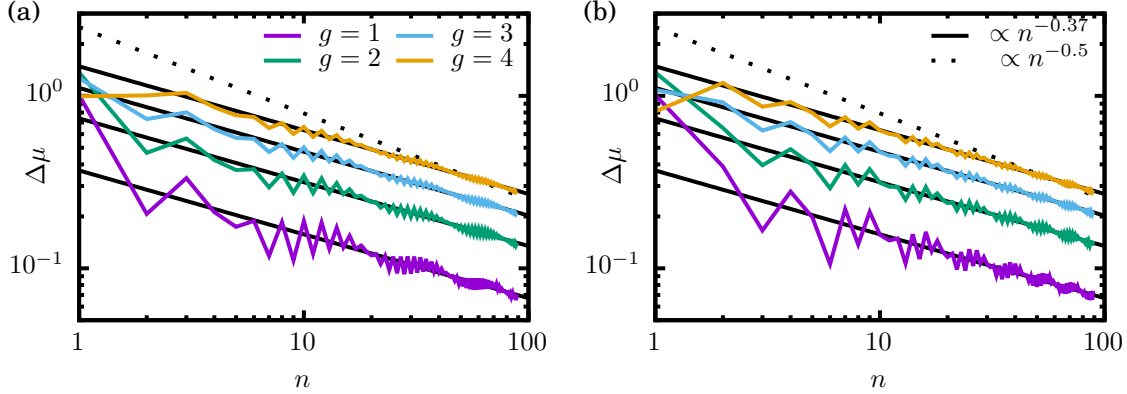


Figure 5.7.: Real eigenvalue shifts for  $\gamma = 1.5$  at  $b = 0.5$  (a) and  $b = 1$  (b) for different values of the nonlinearity  $g$ . All calculations show the same overall decay, while the oscillation amplitude and number of oscillations vary for different positions  $b$ . The upper limit  $n^{-0.5}$  known from the linear case is depicted as a black dotted line, while the solid black lines that fit the data points decay slower with a rate  $n^{-0.37}$ .

can be used independently of  $\gamma$ . However, for higher perturbation strengths  $\gamma \geq 10$ , as visible in Fig. 5.6(b), extreme deviations can be found. These outliers are caused by the giant changes of the real and imaginary parts of the eigenvalues beyond some branch points. This was observed already in Fig. 5.2 for the states  $n = 8$  and  $n = 9$ . For such strong perturbations the estimates are only applicable for quantum numbers of  $n \gtrsim 10$ . For  $\gamma = 20$  new outliers around  $n = 75$  enter the picture, rendering the estimations valid only for  $n \gtrsim 80$ . Please note that even for such parameters only the complex eigenvalues can grow beyond their bond, real eigenvalues still show the expected behavior.

Finally, Fig. 5.7 investigates the effect the nonlinearity has on the eigenvalue shifts for the two perturbations at positions  $b = 0.5$  and  $b = 1$  and strength  $\gamma = 1.5$ . Since even a weak nonlinearity  $g = 2$  shows an immense impact on the eigenvalue shifts, one would assume that by varying the nonlinearity further changes can be observed. However, the eigenvalue shifts oscillate around straight lines with the slopes  $-0.37$ , irrespective of the strength of the nonlinearity. The amplitude of the oscillations, however, and their number depend on the position of the delta functions. Together with the now found slope  $n^{-0.37}$ , Fig. 5.7 depicts the steeper original upper bound  $n^{-1/2}$ .

This closes the analysis of the properties of the perturbed harmonic oscillator. The extraordinary good natured behavior of the harmonic trap makes it a reasonable choice for the extended trapping potentials considered in the next chapters: In the linear case, the existence of a Riesz basis ensures that the perturbation

## 5. *Existence of real spectra*

---

theory is applicable, i.e., weak perturbations ensure real stationary solutions. For nonlinear systems, even though these simple considerations fail, the numerical study suggests that the non-Hermitian influence weakens considerably for higher excitations.

At last, one has to emphasize that real atomic traps have a finite height and therefore include the case of free particles in a quasi-continuous spectrum. It could therefore be worthwhile to analyze, how this atom cloud responds to the particle exchange.

## 6. $\mathcal{PT}$ -symmetric currents in modified double wells

The double-well potential is the simplest and most accessible trapping potential for a  $\mathcal{PT}$ -symmetric condensate. However, reality offers a rich zoo of possible perturbations and asymmetries, especially in a three-dimensional realization. These modifications of the classical double-well potential can both provide deeper insight, and have to be accounted for to avoid experimental difficulties. The focus of this chapter lies on the question, how a selection of characteristic modifications affect the results given in Chap. 4.

As a first step, this question is tackled in Sec. 6.1 where a three-mode approximation of a system of three wells is discussed. The coupling of the double well to an additional well provides a new particle channel from the gain to the loss well. Section 6.2 expands this discussion to a spatially extended double-well potential, where the channel is implemented by opening the double-well trap around the central barrier. Asymmetric in- and out-couplings, as they are inevitable in experimental realizations, will finally be discussed in Sec. 6.3.

### 6.1. Three-mode approximation

The simplest model of the double well is the two-mode system presented in Chap. 4. To facilitate an additional channel, this model must be augmented by an additional mode, modeling a third well leading to a three-mode Gross-Pitaevskii equation with on-site interactions,

$$\sum_{j=1}^3 H_{ij} \psi_j + U |\psi_i|^2 \psi_i = \mu \psi_i, \quad (6.1)$$

described by the Hamiltonian

$$H = \underbrace{\begin{pmatrix} 0 & -J & -1 \\ -J & 0 & -J \\ -1 & -J & 0 \end{pmatrix}}_{\hat{H}_0} + \gamma \underbrace{\begin{pmatrix} i & 0 & 0 \\ 0 & 0 & 0 \\ 0 & 0 & -i \end{pmatrix}}_{\hat{H}_P}. \quad (6.2)$$

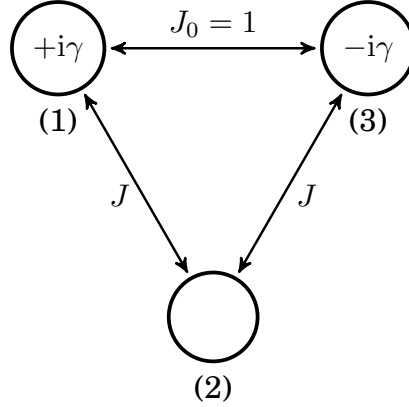


Figure 6.1.: Scheme of the three-mode model. The imaginary on-site energies provide a particle influx to well 1 and an outflux from well 3. These two wells are coupled by a constant strength, set to unity, while the coupling  $J$  to well 2 is varied.

The parameter  $U$  specifies the strength of the nonlinear on-site interaction. The chemical potential  $\mu$  takes the role of the energy and, for the linear case,  $U = 0$ , is given by the eigenvalues of the Hamiltonian. Therefore the three terms are used as synonyms.

The Hamiltonian describes a system of three coupled wells, in the first of which particles are injected into the system while particles are removed from the third well at the same rate  $\gamma$ . The tunneling rate between the gain and loss well is fixed to unity while the second, additional, well is coupled to both of them by the same variable coupling strength  $J$ . A scheme of the setup is shown in Fig. 6.1.

It is obvious that this Hamiltonian is  $\mathcal{PT}$ -symmetric and pseudo-Hermitian with respect to

$$\mathcal{P} = \begin{pmatrix} 0 & 0 & 1 \\ 0 & 1 & 0 \\ 1 & 0 & 0 \end{pmatrix}.$$

The results of Sec. 5.1 are therefore applicable. In the case  $J = 1$  all three wells are coupled with equal strengths. This will cause degeneracies in the eigenvalues of the unperturbed system, i.e., the system without gain and loss of particles. Therefore, the  $\mathcal{PT}$  symmetry will be broken even for very weak particle in- and out-coupling, thus prohibiting any stable stationary currents through the system. Additionally, since this thesis deals with Bose-Einstein condensates, the impact of the nonlinear contact interaction from the Gross-Pitaevskii equation will be taken into account. In this case the stability has to be investigated separately using the Bogoliubov-de Gennes equations.

### 6.1.1. Linear matrix model

The effects leading to the symmetry breaking mentioned in the beginning of the section are discussed in the linear system,  $U = 0$ . Without the perturbation, i.e.  $\gamma = 0$ , the eigenvalues are given by the simple expressions

$$\mu_1 = -\sqrt{2J^2 + 1/4} - 1/2, \quad (6.3)$$

$$\mu_2 = +\sqrt{2J^2 + 1/4} - 1/2, \quad (6.4)$$

$$\mu_3 = 1. \quad (6.5)$$

There are two cases that deserve special attention. For  $J = 0$  the second well is not coupled to the remaining double-well system. This case has already been discussed in detail in Chap. 4. In this case, the  $\mathcal{PT}$  symmetry breaks at  $\gamma = 1$ . The second notable case is  $J = 1$ , in which the system becomes totally symmetric. In this situation the two eigenvalues  $\mu_2 = \mu_3 = 1$  become degenerate. Applying perturbation theory to this case and evaluating Eq. (5.8) leads to the matrix

$$S = \begin{pmatrix} 0 & 2i \\ 2i & 0 \end{pmatrix} \neq 0, \quad (6.6)$$

immediately breaking the  $\mathcal{PT}$  symmetry.

The transition from the double well to the symmetric triangular case is now studied in more detail. The complete analytic expressions for  $\gamma \neq 0$  do not provide further insight, therefore the discussion can be restricted to numerical results starting with the linear spectrum in Fig. 6.2. For  $J = 0$ , where the system corresponds to a double-well potential and one independent well, the ground and excited state of the double well coalesce in a branch point where they vanish and two  $\mathcal{PT}$ -broken states emerge. From Chap. 4 it is known that this branch point is an exceptional point of second order (EP2). The states have complex conjugate eigenvalues with a finite imaginary part. The remaining  $\mathcal{PT}$ -symmetric state exists for all  $\gamma$  and is completely localized in the decoupled well 2, while the double well is empty. However, after the emergence of the  $\mathcal{PT}$ -broken states at  $\gamma = 1$ , this state is unstable since even a single particle in the remaining two wells leads to an exponential growth of the particle number.

For  $J > 0$  the structure changes and the ground state stays  $\mathcal{PT}$ -symmetric for all values of  $\gamma$ . The EP2, however, is still present, now occurring between the two excited states of the three-well system. For increasing coupling strengths  $J$  the difference of the excited states' eigenvalues shrinks. Thus, the EP2 is shifted to lower parameters  $\gamma$  breaking the  $\mathcal{PT}$  symmetry of these states and rendering the system unstable at smaller values of  $\gamma$ .

For  $J = 1$  the EP2 reaches  $\gamma = 0$  where it vanishes due to the Hermiticity of the system and is replaced by a degeneracy of two eigenvalues. For this case,

## 6. $\mathcal{PT}$ -symmetric currents in modified double wells

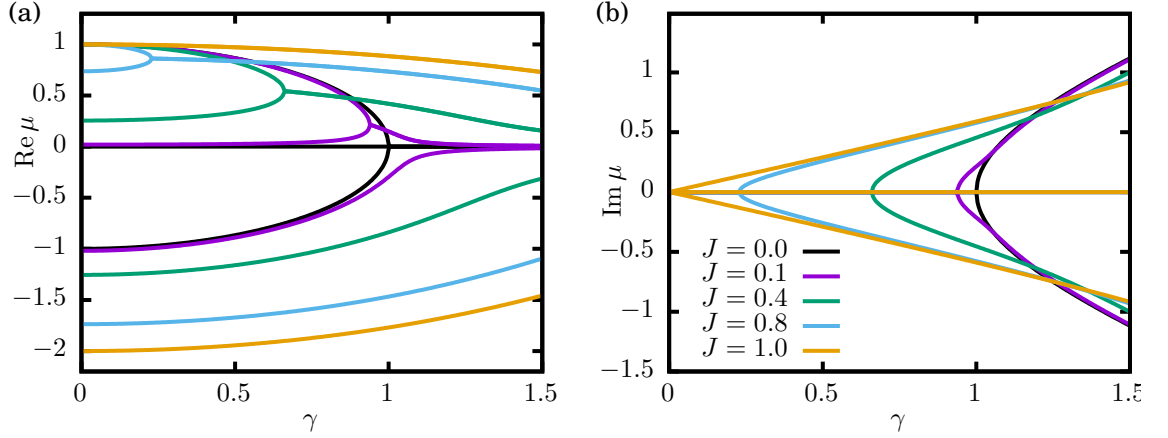


Figure 6.2.: Real (a) and imaginary (b) parts of the eigenvalue  $\mu$  for different values of the coupling strength  $J$  as a function of the in- and out-coupling parameter  $\gamma$ . For  $J = 0$  the ground and second excited state form a branch point at  $\gamma = 1$ , at which  $\mathcal{PT}$ -symmetric states vanish and two  $\mathcal{PT}$ -broken states emerge. The first excited state, located only in well 2, is completely independent of the other eigenstates. For  $J > 0$  the first excited state coalesces with the second excited state, while the ground state is shifted to smaller energies and retains its  $\mathcal{PT}$  symmetry for all values of  $\gamma$ . For increasing values of  $J$ , the energy difference between the two excited states decreases, and the branch point is shifted to smaller values of  $\gamma$ . At  $J = 1$ , two  $\mathcal{PT}$ -broken states emerge directly at  $\gamma = 0$  with degenerate eigenvalues  $\mu = 1$ .

as predicted from perturbation theory, the  $\mathcal{PT}$  symmetry is broken for even the smallest values of  $\gamma$ .

The coupling to an additional well, and thus the availability of an additional channel, seems to diminish the capability of the system to support a stable current. The net current through the system is given by the particle current from the external source to the gain well 1. The continuity equation for this well reads

$$\frac{\partial}{\partial t} |\psi_1|^2 = \underbrace{2\gamma |\psi_1|^2}_{j_{\text{ext}}} - \underbrace{\frac{J}{i} (\psi_1^* \psi_2 - \psi_1 \psi_2^*)}_{j_{12}} - \underbrace{\frac{1}{i} (\psi_1^* \psi_3 - \psi_1 \psi_3^*)}_{j_{13}}, \quad (6.7)$$

where  $\psi_i$  are the components of the eigenvector, the particle currents  $j_{ij}$  run from well  $i$  to  $j$  and  $j_{\text{ext}}$  denominates the external current of particles entering the gain well. For stationary states  $j_{\text{ext}} = j_{12} + j_{13}$  holds. At the same time the in-coupling in well 1 and the out-coupling in well 3 are balanced, thus  $j_{\text{ext}}$  specifies the net current.

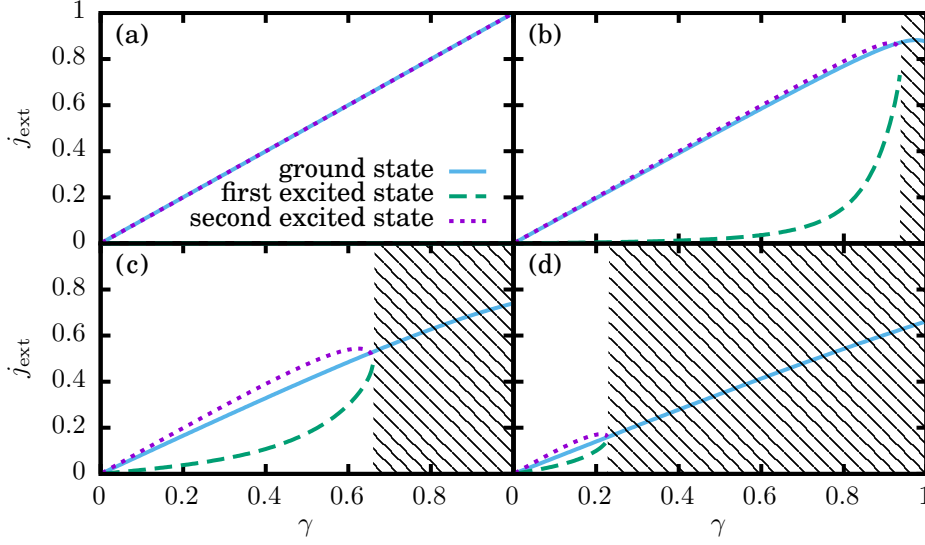


Figure 6.3.: Net current through the system  $j_{\text{ext}}$  as function of  $\gamma$  for  $J = 0$  (a),  $J = 0.1$  (b),  $J = 0.4$  (c),  $J = 0.8$  (d). The hatched areas show regions, in which  $\mathcal{PT}$ -broken eigenstates with complex eigenvalues exist, thus rendering all stationary states unstable. The maximum current,  $j_{\text{ext}} = 1$ , is obtainable only for  $J = 0$ . For  $0 < J < 1$  the second excited state supports the highest net current slightly before the EP.

Figure 6.3 shows the net flow  $j_{\text{ext}}$  for all three states and different coupling strengths  $J$ . For  $J = 0$  the ground state and the second excited state, which are the solutions to an equivalent two-mode problem, support equally strong currents. The maximum current  $j_{\text{ext}} = 1$  is reached at the exceptional point at  $\gamma = 1$ . If the additional well 2 is coupled with  $0 < J < 1$ , the ground state is no longer involved in the EP2 and provides a stationary current even after the two excited states have vanished. However, in this region the state is no longer stable with respect to any small perturbation. The strongest current is achieved by the second excited state for a value of  $\gamma$  slightly smaller than that of the EP2. The  $\mathcal{PT}$  symmetry breaking at the EP2 is therefore the main reason for the decrease of the maximal currents as the coupling  $J$  is increased.

Up till now only the net current was discussed. As a next step the partial particle flows from the gain well 1 to the loss well 3,  $j_{13}$ , i.e., the direct channel, and to the neutral well 2,  $j_{12}$ , i.e., the additional channel, are analyzed. These currents are compared in Fig. 6.4 for different coupling strengths  $J$ . The ground state is the only stationary state supporting a positive current through the additional channel. For growing coupling parameters  $J$  an increasing part of the particles is transported through well 2. At  $J = 0.8$  (Fig. 6.4(d)) this applies to approximately a

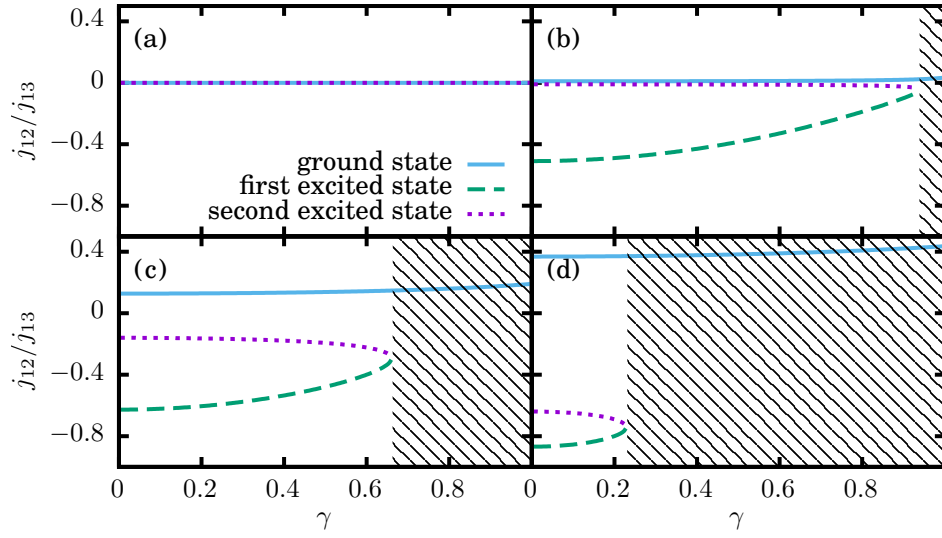


Figure 6.4.: Ratio of the current  $j_{12}$  through the additional well and  $j_{13}$  directly to the loss well as a function of  $\gamma$  for  $J = 0$  (a),  $J = 0.1$  (b),  $J = 0.4$  (c),  $J = 0.8$  (d). Since the current  $j_{13}$  is always positive, negative ratios represent negative currents  $j_{12}$ . Again the hatched areas show regions, in which  $\mathcal{PT}$ -broken eigenstates exist. For  $J = 0$  no particles can be transferred through well 2. After coupling the additional well to the system, the ground state supports a positive current through the well, while the excited states possess negative currents. For  $J \rightarrow 1$  their ratio approaches  $-1$ .

third of the whole net current.

In contrast to this behavior the excited states do not at all support a positive current through well 2. Since the current  $j_{12}$  is negative, the additional channel transports particles from the loss to the gain well. The relative strength of this reverse current increases with higher parameters  $J$ , and becomes comparable to the current from the gain to the loss well  $j_{13}$  for  $J \rightarrow 1$  (Figs. 6.4(c),(d)). For  $J \approx 1$  a small parameter  $\gamma$  is sufficient to induce a strong circular current, breaking the  $\mathcal{PT}$  symmetry even though only very few particles enter the system.

### 6.1.2. Nonlinear three-mode approximation

Up to now only linear systems, i.e., systems without inter-particle interaction were considered. However, in most Bose-Einstein condensates at least a contact interaction, described by the on-site interaction in Eq. (6.1), is present. In the nonlinear case, the stability of a stationary state  $\psi$  is no longer determined by the

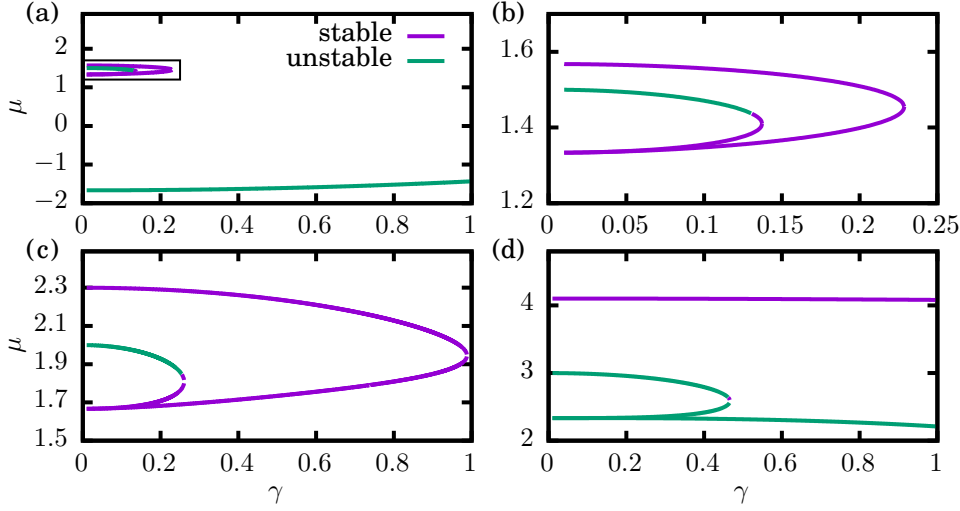


Figure 6.5.: Chemical potential  $\mu$  of  $\mathcal{PT}$ -symmetric states against the strength of the parameter  $\gamma$  for coupling parameter  $J = 1$  and nonlinearity parameter  $U = 1$  (a),(b),  $U = 2$  (c),  $U = 4$  (d). Introducing the nonlinearity (a) gives rise to four new states for  $\gamma \neq 0$ , which are shown in the enlarged figures (b),(c),(d). For  $U = 1$  and  $U = 2$  three of them are stable (magenta lines) and one is unstable (green line), for  $U = 4$  all states except the highest excited are unstable.

complex eigenspectrum but by the linear Bogoliubov-de Gennes equations (2.15) introduced in Sec. 2.1,

$$\sum_{j=1}^3 H_{ij} u_j + 2U |\psi_i|^2 u_i + U \psi_i^2 v_i - \mu u_i = \omega u_i, \quad (6.8a)$$

$$\sum_{j=1}^3 H_{ij}^* v_j + 2U |\psi_i|^2 v_i + U \psi_i^{*2} u_i - \mu^* v_i = -\omega v_i, \quad (6.8b)$$

which determines the linearized evolution of a perturbation. If all eigenvalues  $\omega$  are real, the state is considered to be stable, while positive imaginary parts render it unstable.

Figure 6.5 shows the chemical potential of stable and unstable states for  $J = 1$  and different strengths of the nonlinearity  $U$ . Since  $\mathcal{PT}$ -broken eigenstates are not stationary, only  $\mathcal{PT}$ -symmetric states are shown. The first point to notice is that every nonlinearity strength gives rise to a set of four new  $\mathcal{PT}$ -symmetric states, best seen in Figs. 6.5(a) and (b) for  $U = 1$ . Since three of these states are stable, the particle interaction supports a stationary transport through the system although the symmetry of the system inhibits all stable currents in the linear case. The four

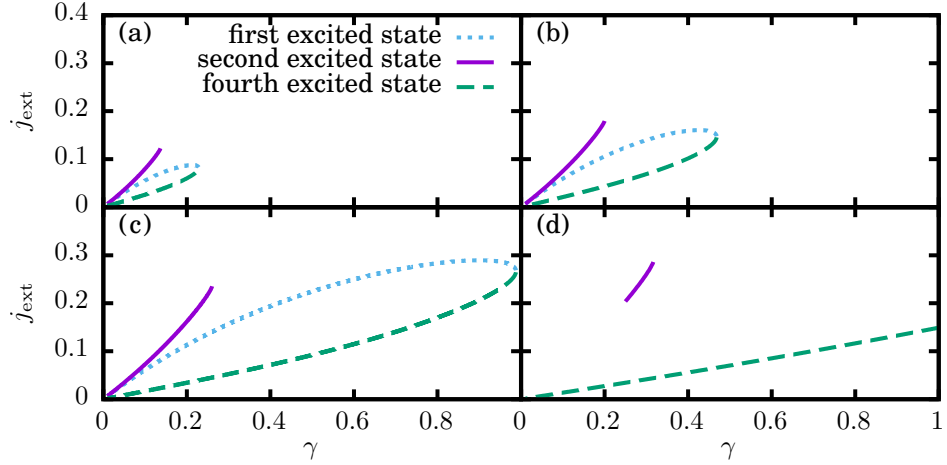


Figure 6.6.: Net current through the system given by the in-coupling external current  $j_{\text{ext}}$  against  $\gamma$  for  $U = 1$  (a),  $U = 1.5$  (b),  $U = 2$  (c),  $U = 2.5$  (d). Only the three stable  $\mathcal{PT}$ -symmetric states introduced in Fig. 6.5 are shown. For nonlinearities of  $U$  up to 2, all three states are able to sustain a similar current, which reaches a maximum of approximately 0.3 at  $U \approx 2$ . For higher nonlinearities stable states become unstable until only the highest excited state remains which occupies mainly the neutral well 2, hence the low net current.

states vanish in two independent tangent bifurcations. For a stronger nonlinearity  $U = 2$  (Fig. 6.5(c)) two stable states are available up to  $\gamma = 1$ . For  $U = 4$  (Fig. 6.5(d)) only the highest excited stationary state is still stable.

At this point one should focus on Fig. 6.5(b) and the first tangent bifurcation between the two middle new states. For the two-mode system described in Chap. 4 the stability of stationary states does only change at bifurcations. However, the upper state of the present branch point becomes stable slightly before the bifurcation is reached. Obviously the three-mode system shows an effect that is not visible in a two-mode approximation of the double well, but is only known from the spatially extended calculations, in which the eigenstates explicitly depend on the strength of the nonlinearity. However, since this gap is usually small and its size changes strongly with varying nonlinearities, this subtlety is neglected in the following discussion, and the states are categorized as completely stable or unstable.

The three states supporting stationary currents are now discussed in more detail. For that purpose, Fig. 6.6 shows the particular net current for different strengths of the nonlinearity. For lower nonlinearities the three stable states support a similar maximum net current that is reached at different values of  $\gamma$  respectively (Fig. 6.6(a)). This is due to different values of the modulus square of the different wave functions at wells 1 and 3. The second excited state resides nearly completely

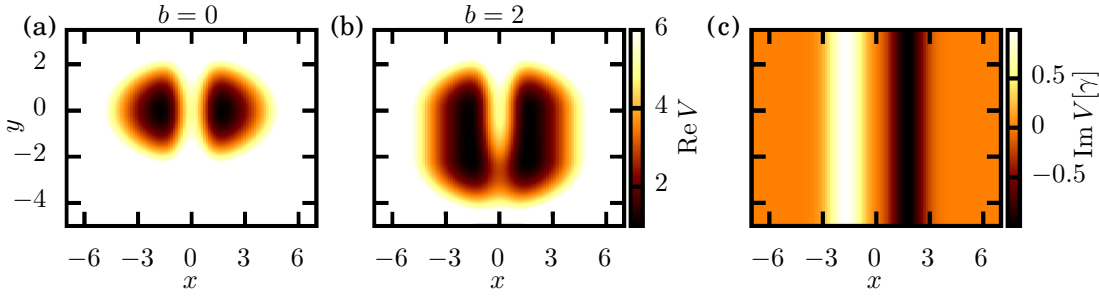


Figure 6.7.: Real part of the symmetric double well potential with  $b = 0$  (a) and the deformed double well potential with  $b = 2$  (b). Their common imaginary part is shown in (c). For  $b = 2$  an additional passage around the central barrier is created.

inside these wells. Thus, this state is already supporting a strong current at lower values of  $\gamma$  and consequently vanishing much earlier. As already seen in Fig. 6.5, the new stable states exist for higher parameters  $\gamma$ , and therefore support higher net currents. For  $U \approx 2$  the in- and out-coupling reaches its maximum of about 0.3, i.e., a third of the maximum current found in the double well with  $J = 0$ . For higher values of  $U$  the first and second excited state become unstable. The fourth excited state, although remaining stable, supports only a weak particle exchange due to the low population in the gain and loss well.

## 6.2. Extended double well with side channel

Modifications to the double well cannot only be discussed in a multi-mode approximation. Using the same potential and method as in Sec. 4.4, a more realistic example of an additional channel can be studied. To this end, the potential (4.9) is modified,

$$\begin{aligned}
 V(\mathbf{r}) = 5e^{-x^2} e^{-\frac{1}{10}(y^2+z^2)} + \frac{1}{4}x^2 + z^2 + \begin{cases} y^2 & \text{if } y > 0 \\ (y+b)^2 & \text{if } y < -b \\ 0 & \text{else} \end{cases} \\
 + i\gamma \left( e^{-(x+\sqrt{\ln(20)})^2} - e^{-(x-\sqrt{\ln(20)})^2} \right), \quad (6.9)
 \end{aligned}$$

where the new deformation is controlled by the parameter  $b$ . Figure 6.7(a) shows the undeformed case,  $b = 0$ , where the potential is symmetric with respect to a rotation inside the  $y$ - $z$ -plane. As already seen in Sec. 4.4, the double well is created by elongating the trap in  $x$ -direction and separating it into two wells by a Gaussian barrier. The imaginary part of the potential shown in Fig. 6.7(c) consists of two

one-dimensional Gaussian functions positioned exactly over the minima of the double well in  $x$ -direction. For a nonvanishing deformation  $b > 0$  the harmonic trap in  $y$ -direction is cut in two parts and the lower part is shifted down from zero to  $-b$ . It opens an additional passage for the particle transport between the two wells. This is shown in Fig. 6.7(b) for the special case  $b = 2$ . The passage should weaken the barrier and therefore strongly increase the amount of particle in- and out-coupling, for which  $\mathcal{PT}$  symmetry can be observed. Since the imaginary part is homogeneous in  $y$ - and  $z$ -direction, the rate of in- and out-coupling does not depend on the position of the condensate, which will shift due to the deformation  $b$ .

Figure 6.8 shows a comparison of the spectra of the original double well (left panel) and the deformed potential (right panel) for the linear system,  $Na = 0$ . Since the given linear problem can be separated into its three dimensions, the excitation numbers in  $x$ -,  $y$ - and  $z$ -direction are used as quantum numbers characterizing the  $\mathcal{PT}$ -symmetric states  $|n_x, n_y, n_z\rangle$ . The blue solid lines including the ground and first excited state show the eigenvalues of the states without excitations in  $y$ - or  $z$ -directions,  $|n_x, 0, 0\rangle$ . The magenta dotted (green dashed) lines depict the eigenvalues of states which are excited in the  $y$ -( $z$ -)direction,  $|n_x, 1, 0\rangle$  ( $|n_x, 0, 1\rangle$ ).

For a Hermitian system with  $\gamma = 0$  all eigenstates are  $\mathcal{PT}$ -symmetric rendering the eigenvalues entirely real. Increasing the parameter  $\gamma$  one finds that the undeformed (Fig. 6.8 left panel) system stays  $\mathcal{PT}$ -symmetric until the ground state and the first excited state coalesce and vanish in an exceptional point at  $\gamma \approx 0.07$ . Two  $\mathcal{PT}$ -broken states emerge at this point. As is always the case for  $\mathcal{PT}$ -symmetric systems their eigenvalues are related by a complex conjugation. This behavior has already been studied extensively and is in complete compliance with the two-mode calculations and spatially extended results presented in Chap. 4. All consecutive pairs of  $x$ -excitations reproduce this scenario within a manifold defined by a fixed  $y$ - and  $z$ -quantum number,  $|i, n_y, n_z\rangle$  and  $|i + 1, n_y, n_z\rangle$ .

For the deformed potential with  $b = 2$  shown in the right panel of Fig. 6.8, the situation changes drastically. Most states confirm the assumption that the system should support much higher currents remaining in the  $\mathcal{PT}$ -symmetric phase. The exceptional points of all states with no excitations in  $y$ -direction,  $n_y = 0$ , are shifted to higher values of  $\gamma$ . By contrast, the remaining two states with  $n_y = 1$ , shown in Fig. 6.8, coalesce at nearly the same value of  $\gamma$ . For the overall system this means that the  $\mathcal{PT}$  symmetry still breaks at only a slightly higher value than before. This time, however, the cause is not the bifurcation of the pair with the lowest energies but instead the  $\mathcal{PT}$  breaking of the states excited in  $y$ -direction.

Please note that even if the ground state still exists and has a purely real energy it is no longer experimentally realizable the moment the  $\mathcal{PT}$  symmetry gets broken. In the linear system, every small deformation will lead to a contribution of the  $\mathcal{PT}$ -broken states, which will result in an infinite growth of the probability amplitude due to the state with  $\text{Im } \mu > 0$ .

Notwithstanding that the new passage connects the two wells and weakens

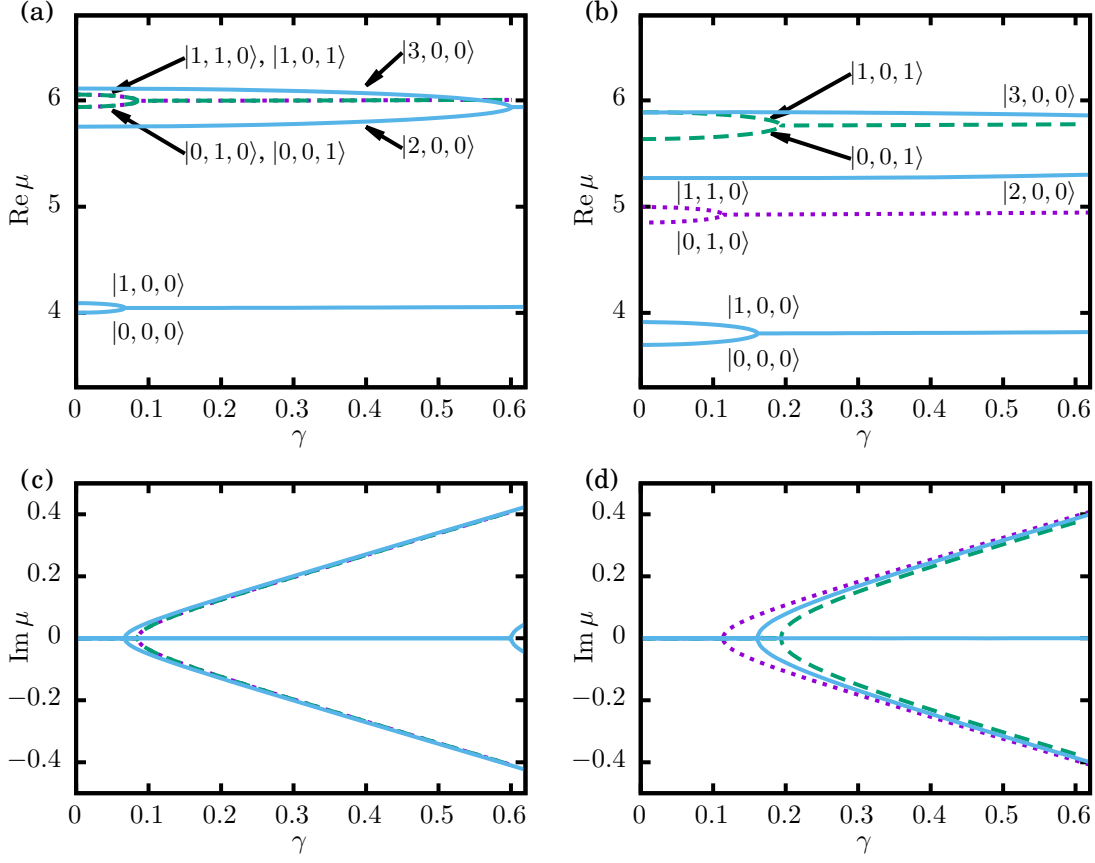


Figure 6.8.: Real (upper panel (a),(b)) and imaginary (lower panel (c),(d)) parts of the eigenvalues of the eight lowest lying states of the double-well potential (left panel (a),(c)) and the deformed potential (right panel (b),(d)) with  $b = 2$  in the linear case as functions of the strength of the in- and out-coupling parameter  $\gamma$ . The branches are denominated using the excitation numbers in  $x$ -,  $y$ - and  $z$ -direction as quantum numbers,  $|n_x, n_y, n_z\rangle$ . The blue solid lines represent states with  $n_y = n_z = 0$  while the magenta dotted (green dashed) lines depict states with  $n_y = 1$  ( $n_z = 1$ ). Every pair of states with consecutive excitations in  $x$ -direction but fixed quantum numbers  $n_y$  and  $n_z$  coalesces in an exceptional point, vanishes, and gives birth to a set of two  $\mathcal{PT}$ -broken states. For the deformed potential all exceptional points with  $n_y = 0$  are shifted to higher values of  $\gamma$ .

## 6. $\mathcal{PT}$ -symmetric currents in modified double wells

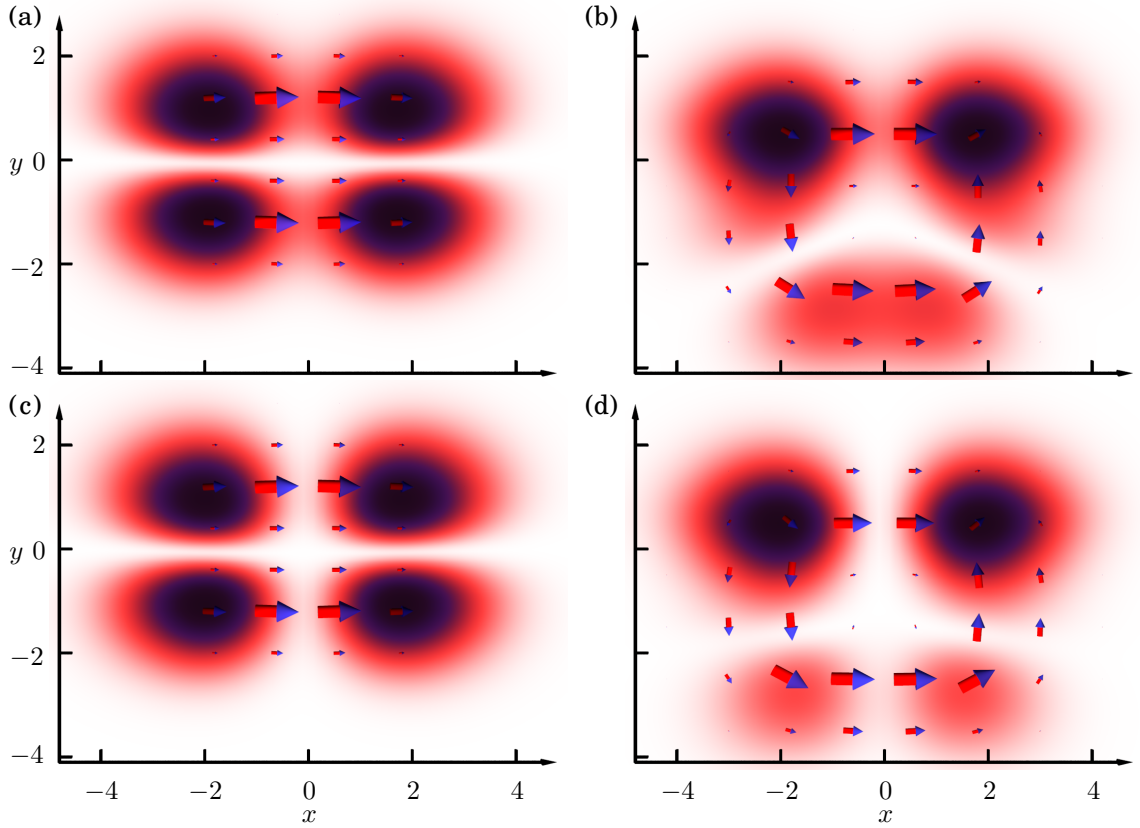


Figure 6.9.: View onto the  $x$ - $y$ -plane of the double-well potential without (a),(c) and with (b),(d) a shift of the barrier. The particle density of two eigenstates is shown as a color map, in which darker regions correspond to higher densities, while the currents are depicted by blue-headed arrows. The state  $|0, 1, 0\rangle$  (a),(b) is symmetric, while the state  $|1, 1, 0\rangle$  is antisymmetric (c),(d) in  $x$ -direction irrespective of the shift  $b$ . In the symmetric double well ( $b = 0$ ) the particles are symmetrically distributed between the two maxima in  $y$ -direction while in the shifted case ( $b = 2$ ) most particles remain near  $y = 0$ .

the barrier, the system still cannot support a much stronger current in the  $\mathcal{PT}$ -symmetric phase. To fully understand this effect, the wave functions of the states excited in  $y$ -direction are studied in detail. Figure 6.9 shows the states  $|0, 1, 0\rangle$  (upper two panels) and  $|1, 1, 0\rangle$  (lower two panels) for the double-well potential (left panel) and the deformed potential (right panel). The probability density is presented as an absorption image while the current density is depicted by arrows. In the double-well case (Fig. 6.9 left panel) both states show a nodal line in  $y$ -direction. Additional views of the wave functions confirm that both wave functions

are symmetric in  $z$ -direction. The energetically lower lying state with  $n_x = 0$  (Fig. 6.9(a)) shows a higher particle density in the  $x = 0$  plane than the second state with  $n_x = 1$  (Fig. 6.9(c)), since that state originated from an antisymmetric state in  $x$ -direction. The current density exhibits a strong flow of particles from the left to the right well. The highest fraction of these currents is present at the maxima of the particle density in  $y$ -direction.

When the barrier in  $y$ -direction is shifted downwards and the potential is no longer symmetric with respect to the  $x$ - $z$ -plane the two states become asymmetric as well. Both the symmetric (Fig. 6.9(b)) and the antisymmetric state in  $x$ -direction (Fig. 6.9(d)) follow the shift of the barrier. This places one of the two maxima in  $y$ -direction nearer to  $y = 0$ , i.e., nearer to the center of the original double well. This maximum becomes much stronger while the other one is damped indicating that the particles are accumulating at  $y = 0$ . Due to the node in  $y$ -direction the current from the upper to the lower maxima is significantly reduced. Therefore approximately half of the net current from the left to the right well still leads over the top of the potential barrier in  $x$ -direction, as is known from the double well's ground state, in which only one maximum resides in each of the wells.

Since the excited states in  $y$ -direction become similar to the ground and first excited state of the symmetric double well  $b = 0$ , it is reasonable to compare these two sets of states also in the case of a nonvanishing particle-particle interaction. This comparison is done in Fig. 6.10, where the left panels show the ground and first excited state of the original potential ( $n_z = n_y = 0$ ) and the right panels show the  $y$ -excited states ( $n_y = 1$ ) for the shifted potential  $b = 2$ . One sees immediately that both states behave similarly when the interaction strength is varied.

The upper two panels in Fig. 6.10 show the case  $\gamma = 0.06$  well before the symmetry breaking. For an decreasing scattering length  $a$  the interaction grows stronger, leading to a separation of the two  $\mathcal{PT}$ -broken states (blue lines) from the energetically lower states even though the gain and loss of particles in the system is still low enough to support  $\mathcal{PT}$ -symmetric states. For parameters  $\gamma$  well beyond the exceptional point shown in Figs. 6.10(c) and (d), only the corresponding  $\mathcal{PT}$ -broken states exist for all scattering lengths shown.

### 6.3. Asymmetries in the particle flux

In the previous two sections asymmetries in the potential perpendicular to the  $\mathcal{PT}$ -symmetric current were shown to leave the real stationary states mostly intact. However, in real systems a perfect control of the in- and out-coupling of particles is not feasible. Therefore also asymmetries in the imaginary potential are to be considered. If the imaginary potentials are not antisymmetric, the system is not  $\mathcal{PT}$  symmetric and no real eigenvalues can be expected for small in- and out-coupling strengths  $\gamma$ . However, increasing this parameter even further to a

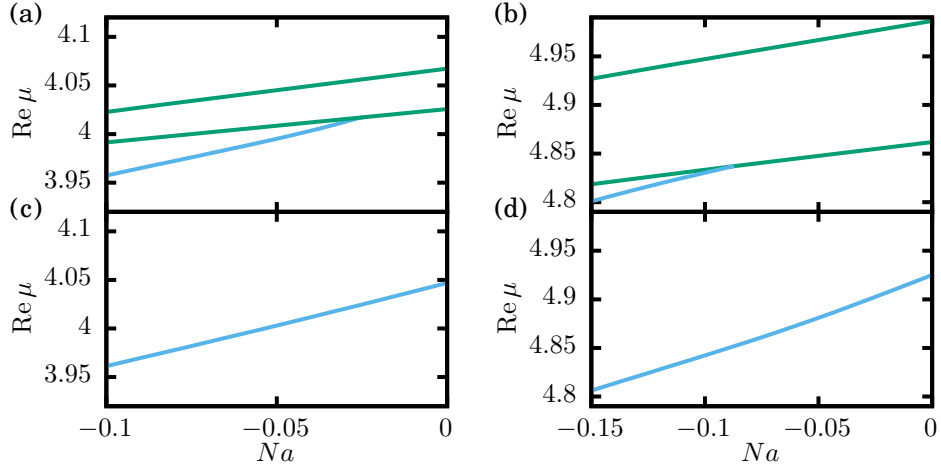


Figure 6.10.: Real part of the chemical potential of stationary states in the symmetric (a),(c) and the perturbed (b),(d) case. For  $\gamma = 0.06$  (a) the ground and first excited states (green lines) exist for all shown nonlinearities. For  $Na \lesssim -0.03$  two  $\mathcal{PT}$ -broken states (blue lines) emerge from the ground state. For  $\gamma = 0.12$  (c) the  $\mathcal{PT}$ -symmetric states vanish and only the broken states remain. On the right panel (b),(d) the deformed potential with  $b = 2$  is used and instead of the ground and first excited state, the  $y$ -excited states with  $n_y = 1$ ,  $|0, 1, 0\rangle$  and  $|1, 1, 0\rangle$ , are shown. They show a similar behavior as the ground and first excited state in (a) and (c).

specific strength can restore a single real eigenvalue.

This section recapitulates some results obtained together with Philipp Lunt during his Bachelor's thesis [86]. The work made use of the finite-element method from Sec. 3.2 for an extended one-dimensional system. The general idea that provides the basis of this extensive work can be illustrated in the two-mode approximation introduced in Sec. 3.5. The asymmetric system described by the Hamiltonian

$$H = \begin{pmatrix} i\gamma(1 + a_I) & -1 \\ -1 & -i\gamma(1 - a_I) \end{pmatrix}, \quad (6.10)$$

with the real asymmetry parameter  $a_I$ , has the eigenvalues

$$\mu = i\gamma a_I \pm \sqrt{1 - \gamma^2}. \quad (6.11)$$

These are the common double-well eigenvalues with a linear purely imaginary shift proportional to the unbalance in the in- and out-coupling. At the exceptional point, the two corresponding eigenvectors coalesce and form a  $\mathcal{PT}$ -symmetric state. It is trivial to see that one of the states emerging from the exceptional point will eventually cut the axis  $\text{Im } \mu = 0$  rendering itself stationary.

One fact should be emphasized. At the point  $\gamma = \sqrt{1/(1 - a_I^2)}$  where one state becomes stationary, the other state of the two-mode system has the eigenvalue  $\mu = 2i\gamma a_i$  which means that it grows exponentially for asymmetries favoring the gain part and decays for stronger particle loss. The same holds true for higher excited states of a spatially extended double well system. The real eigenstate is therefore stable if and only if the loss contribution is favored against the gain of particles.

In this configuration one major problem remains. The real stationary state exists only for one specific parameter  $\gamma$  for a given asymmetry. This leaves the experimental realization with the same problem as before since a fluctuating gain or loss of particles can cause the state to grow exponentially. However, the problem can be overcome by introducing a nonlinear contact interaction term.

Such a contribution renders the spectrum norm dependent since the wave function's modulus square adds to the on-site energies in both wells. Thus, the parameter  $\gamma$ , for which the stationary state is found, changes with a growth or decay of the wave function. As seen in Chap. 4 in case of the double well, a positive nonlinearity shifts the bifurcation of  $\mathcal{PT}$ -broken states to lower values of  $\gamma$ . Therefore it is a solid hypothesis that an increase of the nonlinear contribution in the same parameter range also shifts the position of the stationary states to lower in- out-coupling parameters. This can either happen by strengthening the interaction parameter  $U$  or, intrinsically, by the growth of the wave function due to a positive imaginary chemical potential.

Solving the Gross-Pitaevskii equation,

$$\sum_{j=1}^2 H_{ij}\psi_j + U |\psi_i|^2 \psi_i = \mu\psi_i, \quad (6.12)$$

and the corresponding Bogoliubov-de Gennes equations numerically as described in Sec. 3.5 for the nonlinearity parameters  $U = 0, 0.5, 1$  and  $1.5$  leads to the spectrum and stability analysis presented in Fig. 6.11. There the asymmetry  $a_I = -0.2$  is used. The numerical results show that the general shape of the spectra are still those of a double well superimposed by an overall decrease of  $\text{Im } \mu$  for increased parameter  $\gamma$ . Not only is the aforesaid hypothesis confirmed, but it can be used to understand the stability properties of the system.

Consider an experimental system in which the non-Hermiticity or gain-loss parameter  $\gamma$  is chosen too large. The ground state, instead of staying stationary, is then growing ( $\text{Im } \mu > 0$ ). This effectively increases the nonlinearity and shifts the crossing point of  $\gamma$ , at which the true stationary state with  $\text{Im } \mu = 0$  can be found, to even lower values. The distance between the chosen and the correct value of  $\gamma$  increases and, thus, the error is amplifying itself due to the nonlinearity. This results in the unstable (positive) Bogoliubov-de Gennes eigenvalues shown in Fig. 6.11(b).

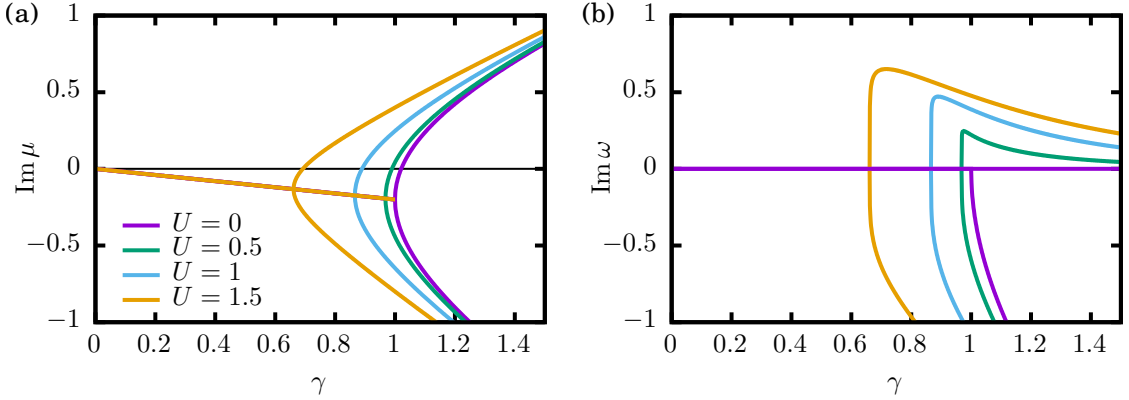


Figure 6.11.: Imaginary part of the nonlinear spectrum (a) of the asymmetric double well (6.10) with  $a_I = -0.2$  representing itself as a simple double-well spectrum superimposed by a linear slope. For *stronger* nonlinearity parameters  $U$  the upper branches intersect the axis  $\text{Im } \mu = 0$  (black line) for *lower* parameters  $\gamma$ . The imaginary part of the Bogoliubov-de Gennes eigenvalues  $\omega$  (b) are given for the upper branch that contains the stationary state. In the nonlinear case this state is unstable.

The influence of the nonlinearity in this simple model not only fails to stabilize the stationary states against small deviations of  $\gamma$  but adds a worse instability even for well chosen parameters. To get rid of this new instability the exact converse behavior is necessary: One possibility would be to invert the imaginary part of the chemical potential so that too large values of the parameters  $\gamma$  lead to a decay of the wave function instead of a growth. However, to inhibit unstable perturbations at high excitation energies, the loss contribution must always be stronger than the particle gain. The alternative is to invert the movement of the crossing point in the spectrum, such that it is shifted to higher parameters  $\gamma$  if the interaction is amplified and vice versa.

To influence the overall form of the spectrum a new parameter has to be introduced. The inversion of the crossing point movement can be achieved by introducing an asymmetry in the real part of the potential. Once again, the necessary calculations are very simple if done in a two-mode approximation. Figure 6.12 shows the same values as Fig. 6.11 but for the asymmetric Hamiltonian

$$H = \begin{pmatrix} i\gamma(1 + a_I) + a_R & -1 \\ -1 & -i\gamma(1 - a_I) - a_R \end{pmatrix}, \quad (6.13)$$

with  $a_R = -0.15$  and  $a_I = -0.2$ .

Introducing an increased on-site energy on the loss and a decreased energy on

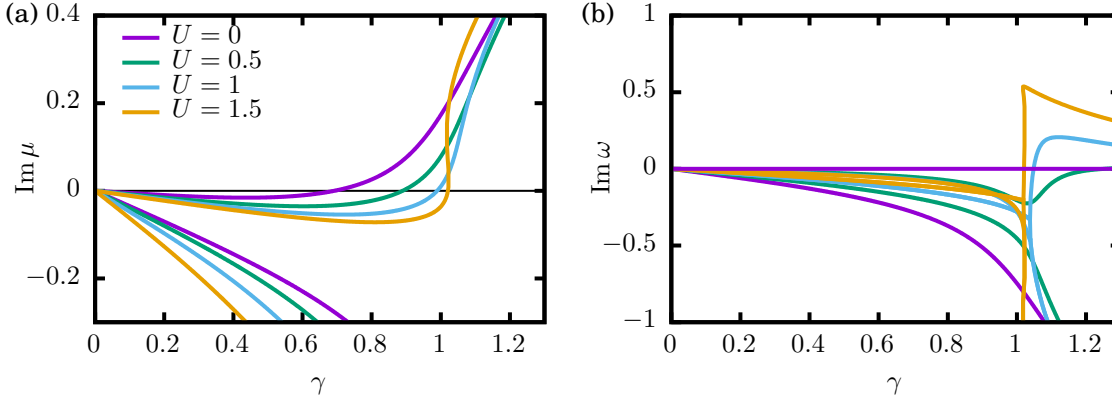


Figure 6.12.: Imaginary part of the nonlinear spectrum (a) of the asymmetric double well (6.13) with  $a_I = -0.2$  and a real on-site asymmetry  $a_R = -0.15$ . The bifurcation vanishes in favor of two independent states. For *stronger* nonlinearity parameters  $U$  the upper branches cut the axis  $\text{Im } \mu = 0$  (black line) for *higher* parameters  $\gamma$ . The imaginary part of the Bogoliubov-de Gennes eigenvalues  $\omega$  (b) are given for the upper branch that contains the stationary state. For all shown values of  $U$  the stationary case is now stable.

the gain well gets rid of the exceptional point. This is obvious since the probability densities in the two wells now differ for the ground and excited state, i.e., either the gain or the loss well is favored. The ground state resides in the energetically lower gain well, therefore its out-coupling of particles is weakened significantly and the imaginary part of the chemical potential is shifted upwards. As a result, the crossing point for  $U = 0$  is shifted to a lower parameter  $\gamma$ .

However, in this new situation, a repulsive interaction equalizes both densities. This counters the effect of the real asymmetry and shifts the imaginary part of the chemical potential down to lower values, thus, the crossing point migrates to higher values of  $\gamma$ . Now, as predicted, all Bogoliubov-de Gennes eigenvalues apart from the trivial solution  $\omega = 0$  of an ineffective phase shift have negative imaginary parts at the crossing point, at which the stationary state with  $\text{Im } \mu = 0$  resides. The stationary state is therefore not only stable, but acts as an attractor. If the parameters of the system are not perfectly set, the wave function grows or decays exactly to match the appropriate interaction strength to stay stationary.

The results of this two-mode model hold true also for extended potentials, where it was shown that almost all parameter ranges of  $\gamma$  that are accessible in the  $\mathcal{PT}$ -symmetric double well can also be reached in an asymmetric model by varying the interaction strength  $U$  [86].



# 7. Rotating condensates in $\mathcal{PT}$ -symmetric potentials

Up to this chapter systems with steady laminar currents were discussed. The imaginary potentials described a separate in- and out-coupling of particles and the condensate provided a steady current between the respective positions. This is justified since the ground state, which is the easiest achievable state of a Bose-Einstein condensate, is typically smooth and does not show any turbulences. However, by rotating the system very fast the condensate is forced to nucleate vortices.

Section 7.1 will shortly revisit the behavior of vortices as well as the basic properties of rotating condensates. The numerical calculations are divided into two sections. In Sec. 7.2 two-dimensional calculations are used to discuss a  $\mathcal{PT}$ -symmetric particle gain and loss that is rotating along with the condensate. Three-dimensional calculations are finally used to discuss particle currents parallel to the vortices (Sec. 7.3).

## 7.1. Introduction to rotating systems

### 7.1.1. Vortices in coherent wave functions

As shown in the more elaborate discussion of Bose-Einstein condensates in general in Chap. 2, condensates in mean-field theory are described by a coherent wave function. In polar representation, this wave function reads

$$\psi(\mathbf{r}) = \sqrt{\rho(\mathbf{r})} e^{i\phi(\mathbf{r})}, \quad (7.1)$$

with its modulus square  $\rho$  representing the particle density and the real function  $\phi$  representing a spatial-dependent phase. The particle current itself is defined by the quantum mechanical probability current density

$$\mathbf{j}(\mathbf{r}) = \frac{1}{2i} (\psi^*(\mathbf{r}) \nabla \psi(\mathbf{r}) - \psi(\mathbf{r}) \nabla \psi^*(\mathbf{r})) = \rho \nabla \phi(\mathbf{r}). \quad (7.2)$$

A vortex is defined by a circular current. Thus, the current and therefore the gradient of the phase are always positive when encircling the center of an vortex.

## 7. Rotating condensates in $\mathcal{PT}$ -symmetric potentials

---

To be continuous the wave function must show a change of  $2n\pi$ ,  $n \geq 1$  around the vortex. An imminent consequence of this fact is that the center of the vortex of a Bose-Einstein condensate is always a node.

The simplest example, a single vortex in an otherwise uniform Bose-Einstein condensate, was studied by Pitaevskii and Gross in 1961 using their Gross-Pitaevskii equation [45, 46]. The most important results are now summarized in dimensionless units. For exact results in physical units please refer to the aforementioned references.

The homogeneity of the gas ensures that the modulus square of the wave function depends solely on the distance from the vortex. The same argument forces the phase to increase with a constant slope when encircling the node. Assuming the vortex possesses the weakest possible angular momentum, i.e., the phase increases by  $2\pi$ , the wave function around the singular vortex is given by the term

$$\psi(\mathbf{r}) = f(r) e^{i\phi}. \quad (7.3)$$

The radial function was calculated numerically by Ginzburg, but can be approximated reasonably well by the function  $f_{\text{var}}(r) = r/\sqrt{r^2 + 2}$  [87, 88]. Compared with the uniform case without vortex the energy inside a given radius  $R$  is increased by  $E_v \propto \sqrt{\rho} \ln 1.46R$  [46].

### 7.1.2. Rotating coordinate frame

Due to the additional energy provided by each vortex, a ground state commonly does not contain any vortices. However, this changes drastically if one forces the condensate to rotate with a defined frequency  $\Omega$ . In this example this is done by a rotating trapping potential. To achieve this, the Gross-Pitaevskii equation is transformed into a counterclockwise rotating frame,

$$\mathbf{r}'(t) = -D_z(\Omega t)\mathbf{r}, \quad (7.4)$$

where the  $z$ -axis is used as a rotation axis. The transformed wave function reads

$$\psi'(\mathbf{r}', t) = e^{-i\hat{L}_z\Omega t}\psi(\mathbf{r}, t), \quad (7.5)$$

with the angular momentum operator  $\hat{L}_z = -i(\mathbf{r} \times \nabla)_z$ .

The potential rotates with the same frequency  $\Omega$ . However, beyond this rotation it is not time-dependent. Therefore, inside the rotating frame the potential  $V'(\mathbf{r}', t) = V_{\text{rot}}$  only depends on the rotating spatial coordinates. The transformed wave function yields some simple relations,

$$|\psi'(\mathbf{r}', t)|^2 = |\psi(\mathbf{r}, t)|^2, \quad (7.6a)$$

$$i\frac{\partial}{\partial t}\psi'(\mathbf{r}', t) = i\frac{\partial}{\partial t}\psi(\mathbf{r}, t) + \hat{L}_z\Omega t, \quad (7.6b)$$

$$\Delta'\psi'(\mathbf{r}', t) = \Delta\psi(\mathbf{r}, t), \quad (7.6c)$$

and allows for the formulation of the Gross-Pitaevskii equation in rotating coordinates. To improve the legibility of the formulae, the transformed functions and parameters are no longer marked by primes,

$$i\frac{\partial}{\partial t}\psi(\mathbf{r}, t) = \left(-\Delta + V_{\text{rot}}(\mathbf{r}) + 8\pi Na|\psi(\mathbf{r}, t)|^2 - \Omega\hat{L}_z\right)\psi(\mathbf{r}, t). \quad (7.7)$$

The solutions  $\psi(\mathbf{r}, t) = \psi(\mathbf{r})e^{i\mu t}$  are stationary with respect to the rotating frame. They fulfill the stationary rotating Gross-Pitaevskii equation,

$$\mu\psi(\mathbf{r}) = \left(-\Delta + V_{\text{rot}}(\mathbf{r}) + 8\pi Na|\psi(\mathbf{r})|^2 - \Omega\hat{L}_z\right)\psi(\mathbf{r}). \quad (7.8)$$

Please note from Eq. (7.5) that for  $t = 0$  the wave functions are the same in both coordinate frames.

Evidently the mean-field energy now reads

$$E_{\text{MF,rot}} = E_{\text{MF}} - \Omega\langle\hat{L}_z\rangle. \quad (7.9)$$

If the potential lacks complete rotational symmetry, the systems cannot relax to the non-rotating state. In this case, this modified mean-field energy  $E_{\text{MF,rot}}$  determines the ground state of the system.

As a first linear example, consider a harmonic trap  $V(r) = \omega^2 r^2/4$  in radial direction, providing a cylindrical symmetry around the rotating axis for particles without interaction,  $Na = 0$ . The stationary states of the non-rotating frame can then be chosen to be eigenfunctions of the  $\hat{L}_z$  operator with the eigenvalue  $l_z$ , corresponding to states with no ( $l_z = 0$ ) or one vortex with quantized angular momentum,  $l_z = 1, 2, \dots$ , at their center. The same set of eigenfunctions can therefore be used in both frames, however, the energy is modified by the summand

$$E_v = -l_z\Omega. \quad (7.10)$$

In the harmonic oscillator the angular momentum is bounded by the kinetic excitation number  $|l_z| \leq n$ . The minimal mean-field energy for a fixed quantum number  $n$  is reached for  $n = l_z$ ,

$$E(n) = n(\omega - \Omega) + \omega/2. \quad (7.11)$$

This leads to the formulation of the simple condition  $\Omega \leq \omega$ . For higher rotation frequencies the harmonic trap cannot exert the necessary centripetal force and the gas flies apart [31]. The energy has no lower bound and diverges to negative infinity for large quantum numbers  $n$ .

Introducing an interaction changes the observed behavior drastically. Butts and Rokhsar [31] used a variational approach with a linear combination of the low-energy angular-momentum eigenstates of the harmonic oscillator. They showed

that when raising the rotating frequency, the number of vortices in the ground state increases. Only months later, these calculations were experimentally verified by Madison et al. [32]. By now, numerical methods such as the finite-element method presented in Sec. 3.2 make the exact numerical study of these systems possible providing a much higher precision [89]. For all further information on the properties of rotating trapped Bose-Einstein condensates please refer to the very extensive review by Fetter [88].

## 7.2. Two-dimensional calculations

Due to the enormous numerical advantage, it is quite reasonable to start with two-dimensional calculations, i.e., the lowest dimensional system that is able to rotate at all. To illustrate the reduction from three to two dimensions consider a harmonic oscillator with the radial trapping frequency  $\omega_r = 1$  and the axial trapping frequency  $\omega_z$ ,

$$V(r, z) = \frac{1}{4}r^2 + \frac{1}{4}\omega_z^2 z^2. \quad (7.12)$$

For a linear system, a separation into the radial and the axial system is possible. Due to strong axial trapping frequencies  $\omega_z \gg 1$  excitations in this direction become improbable and the wave function assumes the shape of the ground state.

The interaction energy in the two-dimensional remainder,  $\int 8\pi Na|\psi(x, y)|^4$ , equals the interaction energy in the original three-dimensional system if one assumes  $\omega_z \approx 4\pi$  for the trapping  $z$ -direction. In this case, the rotating Gross-Pitaevskii equation in two dimensions assumes the form

$$\mu\psi(x, y) = \left( -\Delta + \frac{1}{4}(x^2 + y^2) + 8\pi Na|\psi(x, y)|^2 - \Omega\hat{L}_z \right) \psi(x, y), \quad (7.13)$$

where the interaction strength  $8\pi Na$  appears unmodified. For stronger repulsive contact interactions, this approximation is not exact and an even tighter trapping in  $z$ -direction must be employed. However, for the whole course of this section, an adequately strong trapping frequency is assumed and fixed interaction strengths are considered.

The  $\mathcal{PT}$ -symmetric imaginary potential

$$V_I(y) = -i\gamma \text{sign}(y) \quad (7.14)$$

is used. For positive values of  $\gamma$  the potential describes a gain of particles in the lower half of the  $x$ - $y$ -plane and a loss of particles in the upper half. The potential is constant in both regions. This ensures that the same amount of particles is coupled in and out of the system for every possible  $\mathcal{PT}$ -symmetric wave function. Thus, a comparisons between different parameter sets and different numbers of

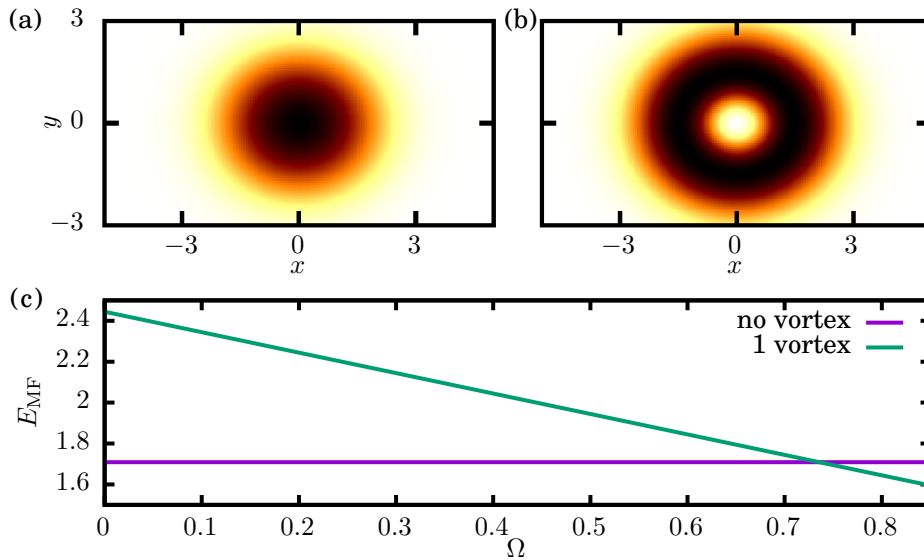


Figure 7.1.: Wave functions (a),(b) and mean-field energies (c) of two stationary states of the rotating harmonic oscillator in two dimensions. The wave function's particle density is shown as a color map, in which darker regions correspond to higher densities. The state with no vortices (a) does not change due to the rotation. The state with one vortex in the center (b) depends on the exact rotation frequency and is shown for  $\Omega = 0.85$ . Its mean-field energy decreases for higher rotation frequencies, crosses the energy value of the original ground state and becomes the new ground state of the system for  $\Omega \approx 0.7356 < 1$ .

vortices is much easier. It must be emphasized that the potential is used inside the rotating frame and therefore is itself rotating around the point  $x = y = 0$ , i.e., the gain and loss contributions are rotating alongside the wave function.

Please note that the ground state does not need to be the state with the lowest chemical potential but instead minimizes the energy of the many-particle system. Therefore, to simplify the identification of the ground state, the mean-field energy of all states is discussed in the following sections.

### 7.2.1. Numerical solutions without gain and loss

The starting point for this discussion is the case  $\gamma = 0$  of an isolated system. For the first part of this analysis, the strength of the nonlinearity is fixed to  $Na = 1$ . The formation of the first vortex in a ground state of this system can be demonstrated using the finite-element method from Sec. 3.2. Figure 7.1 shows the wave function of the original ground state of the harmonic oscillator and the first excited state

## 7. Rotating condensates in $\mathcal{PT}$ -symmetric potentials

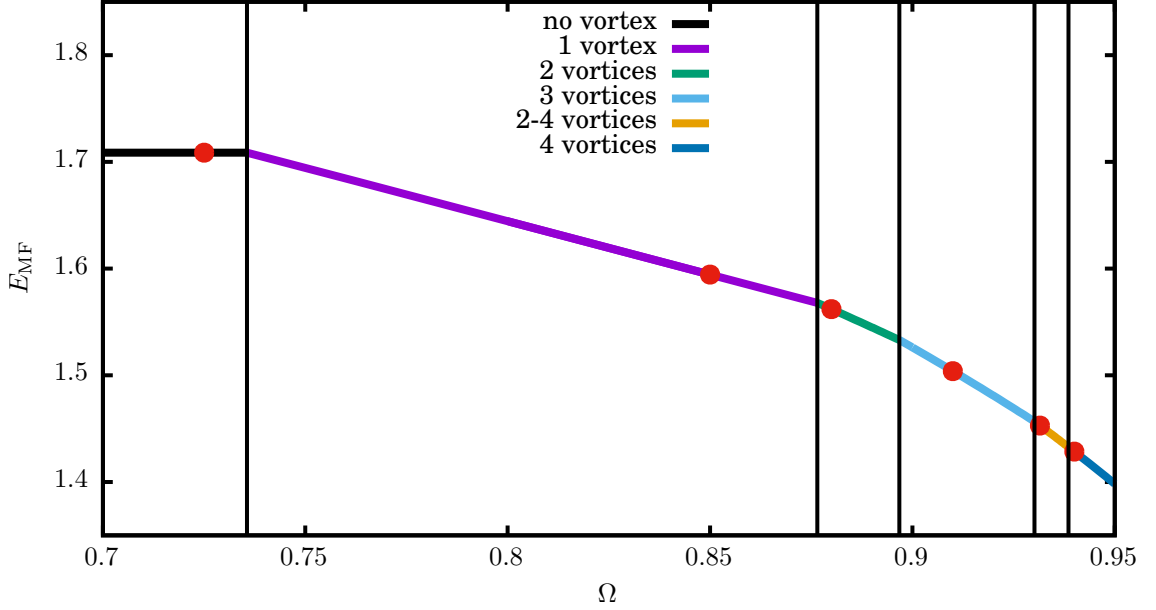


Figure 7.2.: Mean-field energy of the ground states of the rotating harmonic oscillator in two dimensions. The borders of each region, at which the ground state changes, are shown by black bars. Figure 7.3 shows the corresponding wave functions for each red dot.

with  $l_z = 1$ . The state without vortices ( $v_0$ , Fig. 7.1(a)) is not affected by the rotation. Since it has no angular momentum, the mean-field energy stays constant for all values of  $\Omega$ . The first excited state ( $v_1$ , Fig. 7.1(b)) with one vortex and  $\hat{L}_z|v_1\rangle = |v_1\rangle$  also stays nearly constant in its shape. However, due to the angular momentum, this results in a linear decay of the mean-field energy. Already for  $\Omega \approx 0.7356$  the state  $v_1$  becomes the new ground state of the system.

Increasing the rotation frequency further gives rise to additional vortices, as the mean-field energies of even higher excited states cross the current ground state. To reveal these states, various vortex configurations were created to act as initial values for the nonlinear root search used in the finite-element method. Figure 7.2 shows the mean-field energy of all states that act as ground state anywhere in the parameter regime discussed of  $\Omega < 0.95$ . The number of vortices increases from zero to four vortices in five distinguishable areas. While the areas in which no or one vortex exists are relatively large, from  $\Omega \approx 0.88$  on the number of vortices increases very fast.

One additional remark has to be made on the full eigenvalue spectrum: Due to a high number of bifurcations, portraying every stationary state would be incredibly complicated. For a growing rotation frequency  $\Omega$ , the number of vortices in the ground state increases. To this end, new states bifurcate from the existing

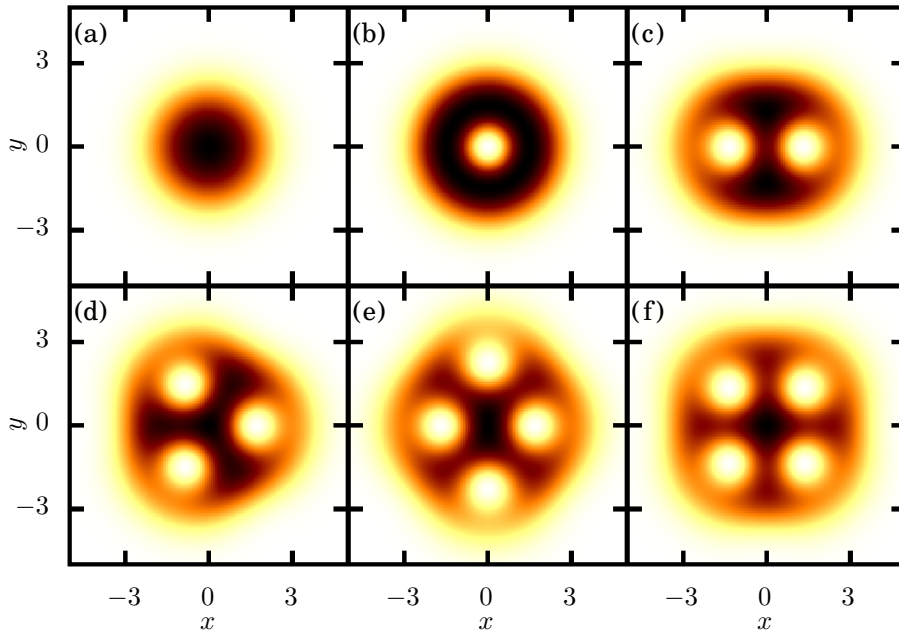


Figure 7.3.: The particle densities of the ground states of the rotating two dimensional harmonic oscillator are shown as color maps, in which darker regions correspond to higher densities. For each region distinguished in Fig. 7.2 one wave function is shown. The original ground state (a) has no vortex ( $v_0$ ) and does not change for any value of  $\Omega$ . For  $\Omega = 0.85$  (b) the ground state has one central vortex ( $v_1$ ). The states with two vortices ( $v_2$ , (c),  $\Omega = 0.88$ ), three vortices ( $v_3$ , (d),  $\Omega = 0.91$ ) and four vortices ( $v_4$ , (f),  $\Omega = 0.94$ ) have their vortices equally spaced around the center of coordinates. At  $\Omega = 0.9315$  the four vortices already exist ( $v_{2-4}$ , (e)) but only a 2-fold rotational symmetry is present.

branches featuring higher number of vortices. However, the number of vortices is not even constant for a given branch of solutions. If the rotation frequencies increase, new vortices may appear in the stationary state although no bifurcation occurs. In the region from  $\Omega = 0.7$  to  $\Omega = 0.95$  presented in Fig. 7.2 a total of five different branches of solutions contribute to the six different ground states. Figure 7.3 shows the wave functions corresponding to the different ground states that are labeled by red dots in Fig. 7.2.

Three classes of wave functions can be distinguished. The states  $v_0$  and  $v_1$  have full cylindrical symmetry. One should emphasize that these two states are the only ground states shown in Fig. 7.3 that exist even for  $Na = 0$  and  $\Omega = 0$ . The states  $v_2$ ,  $v_3$ , and  $v_4$  have emerged from the state  $v_0$  at some point featuring off-center vortices that break the rotational symmetry spontaneously. Instead, they exhibit a 2-, 3- and 4-fold rotational symmetry according to their number of vortices. The last class

## 7. Rotating condensates in $\mathcal{PT}$ -symmetric potentials

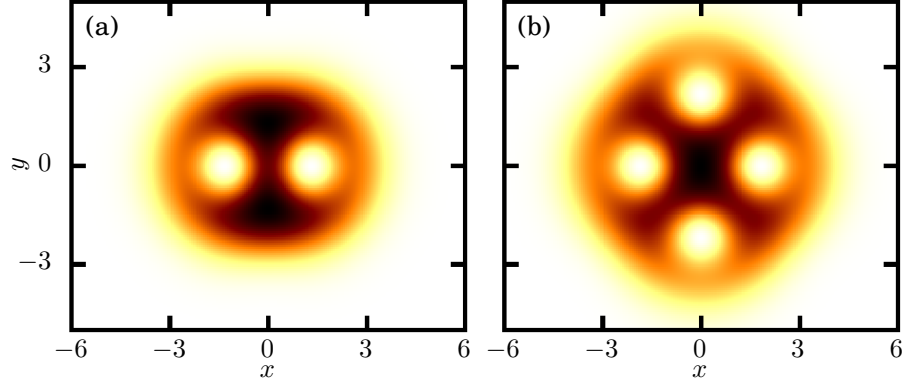


Figure 7.4.: The particle densities of the state  $v_2$  for the rotation frequency  $\Omega = 0.88$  and  $Na = 1$  (a) and  $Na = 2$  (b) of the rotating two dimensional harmonic oscillator are shown as color maps, in which darker regions correspond to higher densities. Due to the higher interaction strength, two new vortices appear.

is represented by the state  $v_{2-4}$  which has only a 2-fold symmetry although four vortices are present. Indeed, this configuration of vortices has not been created in an bifurcation from the state  $v_0$  but developed continuously from the state  $v_2$ , i.e., the ground state at  $\Omega = 0.88$ . While ramping up the rotation frequency to  $\Omega = 0.9315$ , two additional vortices drift into the wave function. However, since these vortices are farther away from the rotation center, only the 2-fold symmetry remains. This behavior is a typical example for a branch of solutions with a varying number of vortices.

Up to now, the interaction strength was locked to  $Na = 1$ . However, since the occurrence of non-central vortices is only possible in nonlinear systems, the precise strength of the interaction should strongly influence the stationary states. Figure 7.4 compares the wave functions of the state  $v_2$  at  $\Omega = 0.88$  and  $Na = 1$  (a) and after increasing the nonlinearity to  $Na = 2$  (b). Two additional vortices appear and the original vortices are shifted slightly outwards as if the vortices reject each other. Moreover, a comparison with Fig. 7.3(c) reveals that the ground state for  $\Omega = 0.9315$  and  $Na = 1$ , i.e.  $v_{2-4}$ , and the vortex state discovered at  $\Omega = 0.88$  and  $Na = 2$  are nearly the same. This conclusion is again in agreement with the results from Butts and Rokhsar [31]. In case of weak interaction strengths, they found that the transition from a non-rotating ground state to the first vortex state happens at  $\Omega = 1 - ca$  where  $c$  is some potential-dependent constant and  $a$  is the scattering length. A stronger nonlinearity has the same effect on the choice of the ground state as if the rotation frequency is increased.

Since the states with two and more vortices break the cylindrical symmetry of the potential, the system exhibits an intrinsic infinite degeneracy. Each wave

function can be rotated by an arbitrary angle and still presents itself as a solution of the Gross-Pitaevskii equation. To select only  $\mathcal{PT}$ -symmetric solutions one must require the modulus square of the wave functions to be symmetric with respect to the space reflection  $y \rightarrow -y$ . This extracts a finite number of wave functions from the infinitely degenerate ground states.

### 7.2.2. Numerical solutions including gain and loss

Introducing the  $\mathcal{PT}$ -symmetric potential (7.14), the stationary states  $v_1, v_2, v_3$  and  $v_4$  will now undergo a gain and loss of particles. The imaginary part of the potential and therefore the particle exchange rotates concurrently with the wave function. For each state not only the square modulus of the wave function is analyzed but the particle current density (7.2) is studied in detail to understand how the currents around the vortices contribute to the net current enforced by the particle gain and loss. Please note that Eq. (7.2) defines the current in the non-rotating frame, and thus, all figures in this section show the wave function in the laboratory non-rotating frame at  $t = 0$ .

Since this study is explicitly interested in setups that are experimentally accessible, the stability of all states is analyzed along with their general shape, current density and mean-field energy. The stability properties are explored via the Bogoliubov-de Gennes equations (2.15) in the rotating frame,

$$\Delta u(\mathbf{r}) = \left( V(\mathbf{r}) - \mu - \omega + 2g|\psi_0(\mathbf{r})|^2 - \Omega \hat{L}_z \right) u(\mathbf{r}) + g\psi_0^2(\mathbf{r})v(\mathbf{r}), \quad (7.15a)$$

$$\Delta v(\mathbf{r}) = \left( V^*(\mathbf{r}) - \mu^* + \omega + 2g|\psi_0(\mathbf{r})|^2 + \Omega \hat{L}_z \right) v(\mathbf{r}) + g\psi_0^{*2}(\mathbf{r})u(\mathbf{r}). \quad (7.15b)$$

The central vortex state  $v_1$  has full cylindrical symmetry; hence, there is only one possible discriminable configuration that is  $\mathcal{PT}$  symmetric. Figure 7.5 presents a detailed analysis of this simplest vortex state in the presence of particle gain and loss. The figure is composed of a spectrum (b), in which the mean-field energies of the stationary state  $v_1$  and its bifurcation partner are plotted, and illustrations of the wave functions for any extraordinary points of the spectrum (a),(b-f).

The discussion follows the spectrum in Fig. 7.5(b) that is plotted in dependency of the parameter  $\gamma$ . Next to the mean-field energy it also illustrates the stability of the respective stationary states. Since the graph is clearly symmetric with respect to  $\gamma$ , it is sufficient to limit the discussion to positive parameters  $\gamma$ . Negative parameters invert the net current. Referring to the Gross-Pitaevskii equation (7.13) this inversion is equivalent to a reflection of both coordinates  $x$  and  $y$ . This relates both cases, and maps the wave functions (a) and (d) onto the cases (c) and (f).

The ground state, which is stationary for  $\gamma = 0$  is shown in Fig. 7.5(e). In addition to the density profile already presented in Fig. 7.3, the current density is depicted using blue arrows. Increasing the in- and out-coupling of particles, i.e., increasing  $\gamma$ , enforces a current from the lower to the upper half of the  $x$ - $y$ -surface.

## 7. Rotating condensates in $\mathcal{PT}$ -symmetric potentials

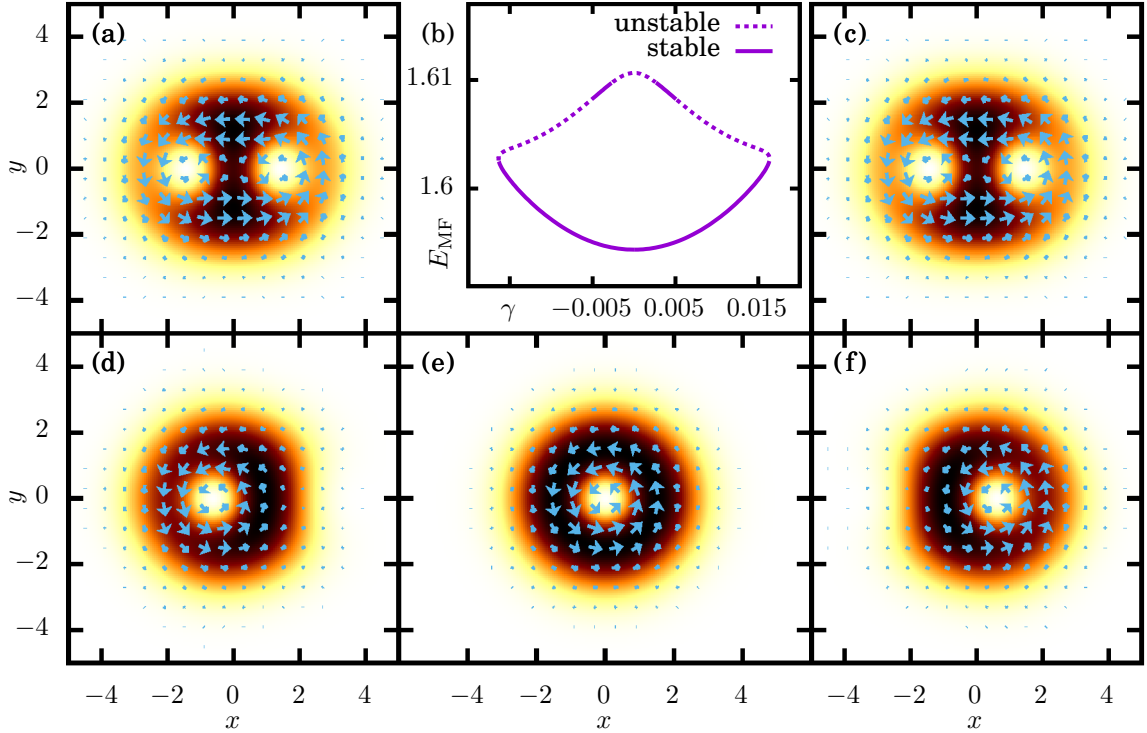


Figure 7.5.: Wave functions (a),(c-f) from the bifurcation scenario (b) of the stationary state  $v_1$  for  $\Omega = 0.85$  under variation of the in- and out-coupling strength  $\gamma$ . The ground state  $v_1$  at  $\gamma = 0$  (e) forms the lower branch which coalesces at  $\gamma \approx -0.0164$  (d) and  $\gamma \approx 0.0164$  (f) with the same upper branch, i.e., with the same bifurcation partner  $v_2$  (a),(c). The particle density is shown as a color map, in which darker regions correspond to higher densities, while the currents are depicted by blue arrows. Their lengths are proportional to the current strength.

For the parameter  $\gamma \approx 0.0164$  the current reaches its maximum. Figure 7.5(f) depicts the wave function at this point where the central vortex is shifted slightly to the right. From  $\gamma = 0$  up to this point the state remains completely stable. Directly at this point, the state vanishes in a bifurcation. The bifurcation partner is shown in Fig. 7.5(c) for  $\gamma = 0$ , and is found to be the state  $v_2$ . However, an analysis of the Bogoliubov-de Gennes eigenvalues shows that this state is unstable for most parameters  $\gamma$ .

To understand how the configuration of vortices contributes to the net current in positive  $y$  direction, it is instructive to follow the excited bifurcation partner  $v_2$  on the transition from  $\gamma = 0$  to the bifurcation and back to the ground state. At  $\gamma = 0$ , the state has two vortices aligned at the axis  $y = 0$  (Fig. 7.5(c)). Three regions

can be distinguished. Left of the vortices, the particle current points in negative  $y$ -direction while the region right of the vortices provides a compensating current in positive  $y$ -direction. Between both vortices the circular currents around the vortices cancel each other. By increasing  $\gamma$ , both vortices are shifted to the left, such that the left vortex almost leaves the wave function and the right vortex is placed near the center of the harmonic trap. As shown in Fig. 7.5(f), the higher particle density strengthens the current on the right side of the vortex and increases the particle transport in positive  $y$ -direction.

Up until now, the different regions identified in the state  $v_2$  remained nearly intact. Even though the left vortex is shifted slightly stronger than the right one, the currents in the region between them still cancel each other. This changes drastically when the parameter  $\gamma$  is decreased, following the lower branch of the bifurcation. While the right vortex stays in the center of the trap, the left vortex vanishes, its effect on the current wears off, and the downwards current on the left side of the remaining current increases. At  $\gamma = 0$  the ground state  $v_1$  is recovered and the corresponding Fig. 7.5(e) reveals only one vortex with no net current up- or downwards.

Since the bifurcation partner of the state  $v_1$  at  $\Omega = 0.85$  happened to be  $v_2$ , the logical step is to investigate, whether the same combination can be found for the two-vortex ground state at  $\Omega = 0.88$ . This is analyzed in Fig. 7.6. At the first glance, the two bifurcation partners from Fig. 7.5 and the same intermediate states are found in this calculation, while the original ground and first excited states have exchanged their roles. This is due to the fact, that the same effects are responsible for the creation of the net current:

- Both vortices move alongside each other to reduce or strengthen some segments of their circular currents by shifting them out of or into areas of high particle densities.
- Vortices are added from or released to the outside of the particle cloud to allow for different combinations of vortex currents.

However, a detailed analysis reveals crucial differences. Contrary to expectation, the bifurcation partner is not the state  $v_1$ . Indeed the partner (Figs. 7.6(a),(c)) is not a single, but a two-vortex state in an asymmetric configuration. The persistent presence of the left vortex is counteracted by shifting the right vortex slightly to the right. Naturally, in contrast to the  $\Omega = 0.85$ -case, the ground state  $v_2$  is stable. But this time even the asymmetric bifurcation partner is stable for all parameters  $\gamma$  except  $\gamma = 0$  and a small region around it.

Since the state  $v_2$  breaks the cylindrical symmetry of the system, it represents not only one but an infinite set of degenerate eigenstates. In addition to the configuration discussed in Fig. 7.6, rotating the state by an angle of  $\pi/2$  leads to a second  $\mathcal{PT}$ -symmetric configuration. Both vortices are then aligned along the

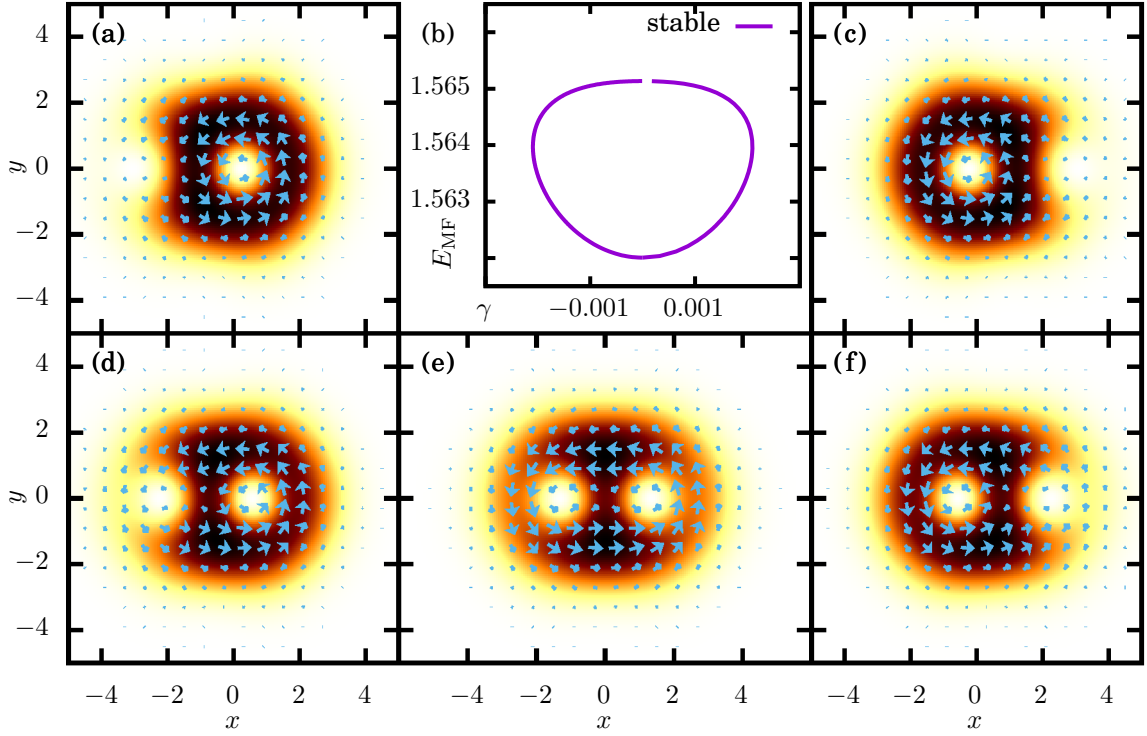


Figure 7.6.: Wave functions (a),(c-f) from the bifurcation scenario (b) of the stationary state  $v_2$  for  $\Omega = 0.88$  under variation of the in- and out-coupling strength  $\gamma$ . The ground state  $v_2$  at  $\gamma = 0$  (e) forms the lower branch. Its bifurcation partners are two degenerate asymmetric two-vortex states (a),(c), which differ by a  $\pi$ -rotation. At  $\gamma \approx -0.0021$  (d) the ground state coalesces with the state (a), while at  $\gamma \approx 0.0021$  (f) the second bifurcation partner is reached. In both cases, the coalescing branches vanish. The particle density is shown as a color map, in which darker regions correspond to higher densities, while the currents are depicted by blue arrows. Their lengths are proportional to the current strength.

$y$ -axis at  $x = 0$ , i.e., in direction of the current. This wave function along with the analysis of all possible configurations of the state  $v_4$  are shown in Appendix A for the interested reader. They show the same effects already known from the last two discussions, although, due to the higher number of vortices, the wave functions are more complicated.

The one remaining state that is then left to discuss is  $v_3$  at  $\Omega = 0.91$ . This is done in Fig. 7.7. The reason why this state is worth of being discussed separately is its anomalous lack of symmetry against a reflection in  $x$ -direction. This leads to an asymmetric behavior with respect to a commutation of the particle gain and

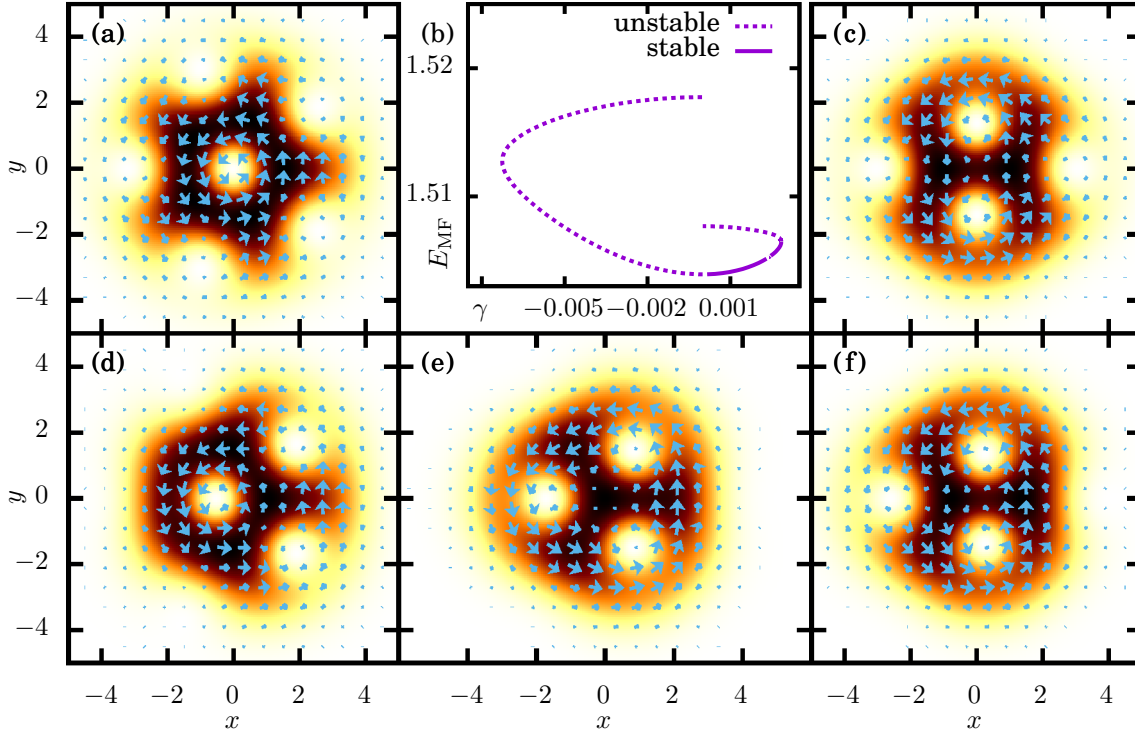


Figure 7.7.: Wave functions (a),(c-f) from the bifurcation scenario (b) of the stationary state  $v_3$  for  $\Omega = 0.88$  under variation of the in- and out-coupling strength  $\gamma$ . The ground state  $v_3$  at  $\gamma = 0$  (e) forms the lower branch. Due to the asymmetric shape in  $x$ -direction, two distinguished bifurcation partners exist. A central-vortex state with six vortices (a) coalesces with the ground state in a tangent bifurcation for the negative in- and out-coupling strength  $\gamma \approx -0.0073$  (d). The other bifurcation partner, the state  $v_{2-4}$  (c) coalesces with the ground state at a positive value  $\gamma \approx 0.0028$  (f). The particle density is shown as a color map, in which darker regions correspond to higher densities, while the currents are depicted by blue arrows. Their lengths are proportional to the current strength.

loss. As already discussed in the symmetric cases before, the stationary states after such a commutation cannot be constructed by a reflection of the  $y$ -axis, since this would reverse the rotation of the condensate particles. To restore the rotation, a combined transformation  $x \rightarrow -x, y \rightarrow -y$  is required. Such a transformation maps two degenerate  $\mathcal{PT}$ -symmetric configurations onto each other, i.e., the single vortex can either reside on the left or the right side.

Positive and negative values of  $\gamma$  must therefore be discussed separately. In both

cases all three vortices are shifted alongside each other to either the left or right to increase the right or left current, respectively. For positive values of  $\gamma$  the current in positive  $y$ -direction on the right side of the state must be enhanced; the state is shifted to the left. Figure 7.7(f) shows the state at the tangent bifurcation with its first bifurcation partner, the state  $v_{2-4}$ . As it is visible in Fig. 7.7(c), the upward current in this configuration is again countered by the newly formed vortex on the right side. Negative values of  $\gamma$  accordingly lead to a shift to the right and a net current in negative  $y$ -direction. In contrast to the positive case, this downward current is not stopped by the appearance of a single new vortex. Instead, while tuning the parameter  $\gamma$  back to zero, new vortices are added symmetrically to build a central-vortex state with a total of six vortices (Fig. 7.7(a)). Of all these branches, only the lower branch for positive  $\gamma$  stays stable. All other parts of the scenario are unstable.

This concludes the  $\mathcal{PT}$ -symmetric rotating configurations that are studied in two dimensions. To realize a gain and loss of particles that does not rotate alongside the wave function, the two-dimensionality must be waived.

### 7.3. Three-dimensional calculations

While many configurations of imaginary potentials in rotating systems could be discussed in two dimensions, there is one trivial configuration that is three-dimensional per se. In this section, instead of looking into rotating gain and loss contributions, a net current in direction of the vortices is considered. To this end, the gain and loss of particles must be homogeneous in the  $x$ - $y$ -plane and vary only in  $z$ -direction. In contrast to the two-dimensional case, the trapping in  $z$ -direction is not tight but equal to the radial trapping. With this condition,  $\omega_r = \omega_z$ , an isotropic trapping potential is constructed,

$$V(r) = \frac{1}{4}r^2. \quad (7.16)$$

The imaginary potential

$$V_I(z) = -i\gamma \text{sign}(z) \quad (7.17)$$

with positive values of  $\gamma$  implements a gain of particles below the  $x$ - $y$ -plane and a loss of particles above. The imaginary part of the potential is again constant in each of these regions to ensure that an equal amount of particles is coupled in and out of the system for any shape of the wave function.

To gain access to numerical results, the finite-element method must be provided with initial values for its root search. As long as one is interested in the ground state of the system, excitations in the  $z$ -direction can be excluded from this search. A good approximation to the three-dimensional wave function can therefore be

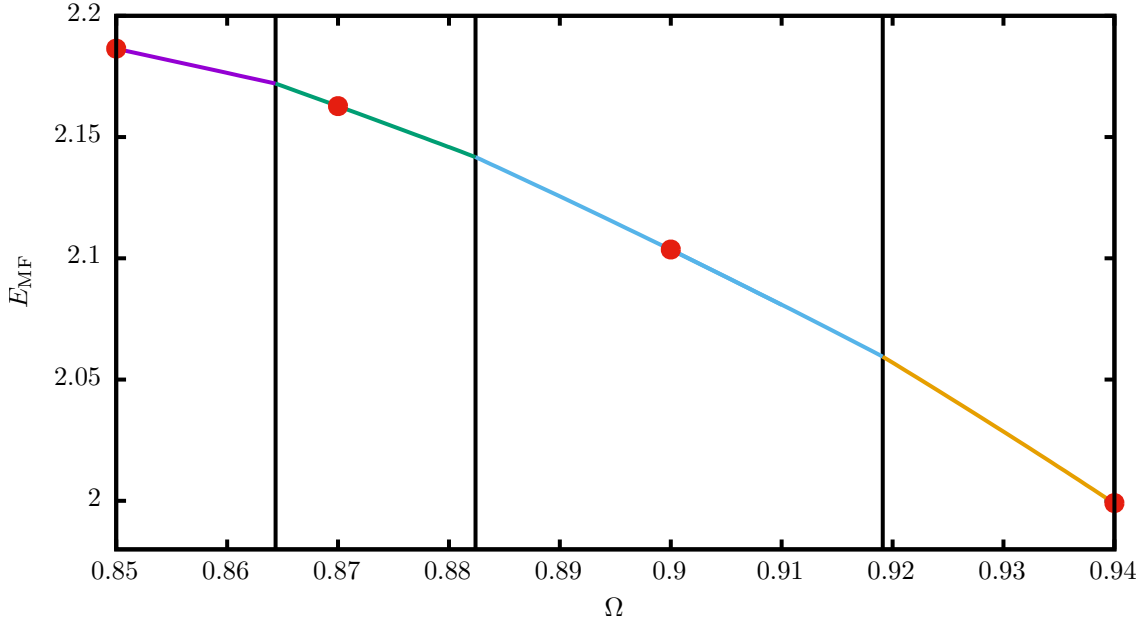


Figure 7.8.: Mean-field energy of the ground states of the rotating isotropic harmonic oscillator in three dimensions. The borders of each region, at which the ground state changes, are shown by black bars. Figure 7.9 shows the corresponding wave functions for each red dot.

found using a product state of the two-dimensional solution in  $x$ - and  $y$ -directions and a Gaussian ground state in  $z$ -direction.

However, to confidently postulate initial values for the ground state the two- and three-dimensional systems must be comparable to start with. Since the trapping potential in  $z$ -direction is much weaker than in the two-dimensional case, the modulus square of the mean-field wave function is smaller. To counterbalance this effect the particle number is increased to provide  $Na = 5$ . The Gross-Pitaevskii equation then reads

$$\mu\psi(\mathbf{r}) = \left( -\Delta + \frac{1}{4}r^2 - i\gamma \text{sign}(z) + 40\pi|\psi(\mathbf{r})|^2 - \Omega\hat{L}_z \right) \psi(\mathbf{r}). \quad (7.18)$$

The discussion will firstly cover the case  $\gamma = 0$ , in which no particles are injected or removed from the condensate. The two-dimensional case showed that for increasing rotation frequencies  $\Omega$  the ground state contains more and more vortices.

Figure 7.8 is the three-dimensional counterpart of Fig. 7.2 and shows the mean-field energy of the ground states for changing frequencies  $\Omega$ . As suspected, the number of vortices increases from one to four vortices over a range from  $\Omega = 0.85$  to 0.94. Obviously the transitions from one ground state to the next are not at the exactly same values as in the two-dimensional case. Furthermore, in the

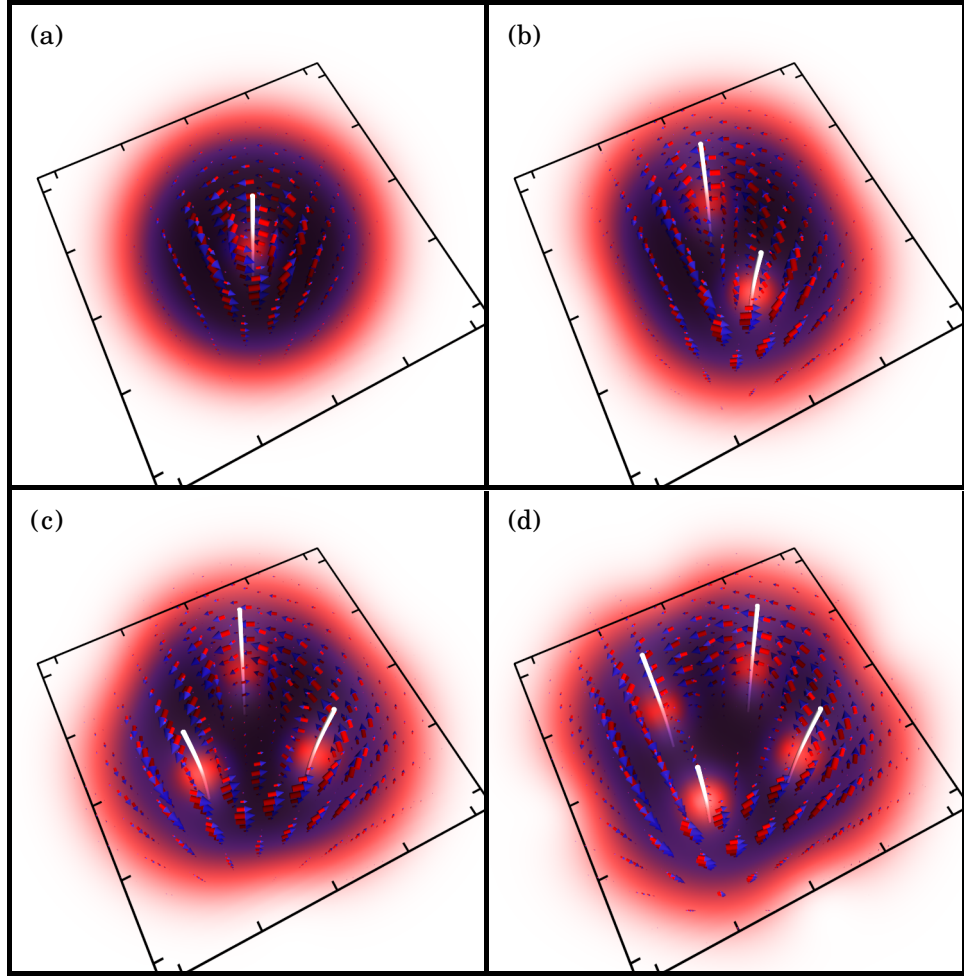


Figure 7.9.: The particle density of the four ground states with one to four vortices is shown as a color map, in which darker regions correspond to higher densities, while the currents are depicted by blue-headed arrows. The vortex centers are highlighted by white lines. For  $\Omega = 0.85$  (a) one central vortex exists, while for  $\Omega = 0.87$  (b),  $\Omega = 0.9$  (c) and  $\Omega = 0.94$  (d) all vortices are located off center.

parameter regime discussed, the three-dimensional case only provides ground states whose  $p$ -fold symmetry corresponds to their number of vortices. The state  $v_{2-4}$  is not found. Figure 7.9 shows the three-dimensional wave functions of the ground states with one to four vortices at the rotation frequencies marked by red dots in Fig. 7.8, i.e., it is the three-dimensional counterpart of Fig. 7.3.

As in Sec. 7.2 all wave functions are shown in the non-rotating laboratory system at time  $t = 0$ . Therefore the figure reveals an overall circular current of particles that is consistent with the rotation of the wave function. The concrete path of a

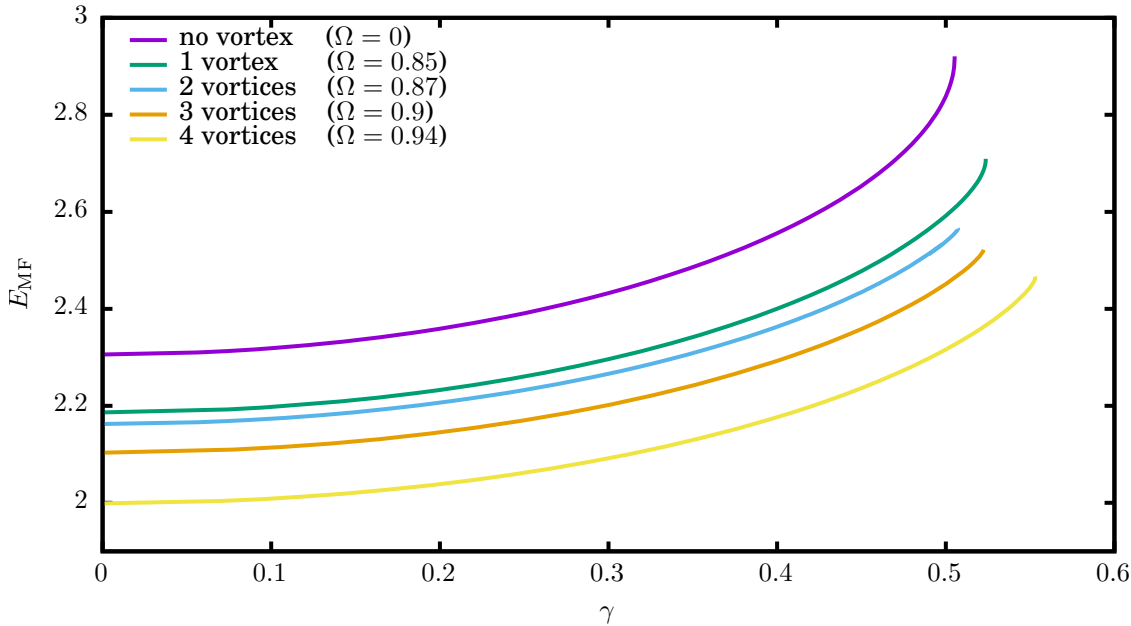


Figure 7.10.: Mean-field energy of the ground states with zero to four vortices. The in- and out-coupling parameter  $\gamma$  is increased until the mean-field energy undergoes a tangent bifurcation where they vanish. The bifurcation partners are not shown and correspond to the same states with an additional excitation in  $z$ -direction.

vortex in  $z$ -direction is defined by its nodal line. To permit an unobstructed view of this path, the nodal line is highlighted by white lines. Special attention should be given to the state with three vortices in Fig. 7.9(c). The vortex lines are bent inwards towards the rotation center.

By increasing the parameter  $\gamma$ , the in- and out-coupling actuates a new current in the system; particles have now to be transported upwards parallel to the vortices. In case of the unrotated ground state and the four states discussed in Fig. 7.9 this leads to an increase of the mean-field energy, as shown in Fig. 7.10. The first eye-catching result of this analysis is certainly that all these ground states behave largely the same. Indeed, the bifurcation scenario resembles the behavior of the double-well system or the harmonic oscillator studied in previous chapters. All states break the  $\mathcal{PT}$  symmetry shortly after  $\gamma = 0.5$  in a typical tangent bifurcation. Since the rotation, controlled by the parameter  $\Omega$ , changes the wave function considerably, not only by increasing or decreasing the number of vortices but also by broadening the wave, this similarity is quite surprising. It indicates that the  $x$ - $y$ -plane and the third dimension are only weakly coupled, even though the nonlinearity already provides a major contribution to the planar solutions.

At the bifurcation point the wave functions support the strongest possible current

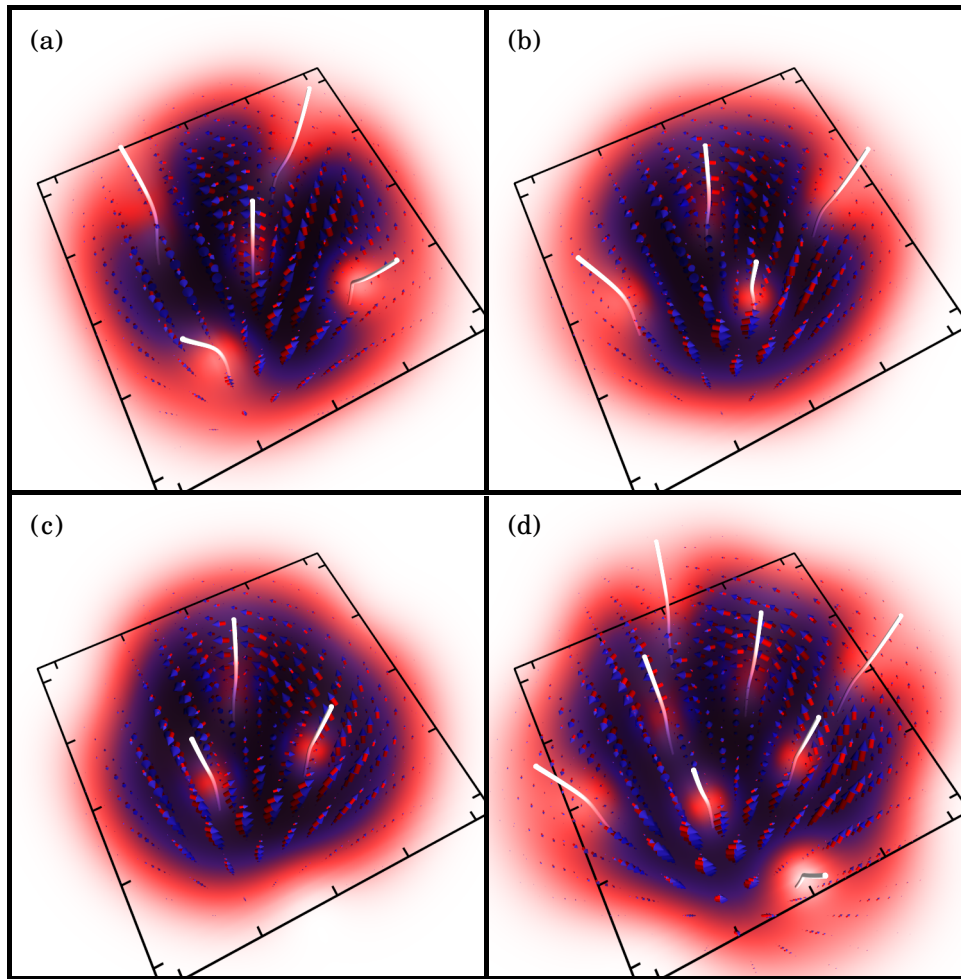


Figure 7.11.: The four ground states with one to four vortices after evolving to their maximum  $\gamma$ . The particle density is shown as a color map, in which darker regions correspond to higher densities, while the currents are depicted by blue-headed arrows. The vortex centers are highlighted by white lines. Additional vortices are added to the ground state at  $\Omega = 0.85$  and  $\gamma = 0.52$  (a),  $\Omega = 0.87$ ,  $\gamma = 0.5$  (b) and  $\Omega = 0.94$ ,  $\gamma = 0.54$  (d). The three vortex state  $\Omega = 0.9$ ,  $\gamma = 0.51$  (c) is mainly unchanged.

upwards. Figure 7.11 shows these exact wave functions for the same states as in Fig. 7.9. Two important effects are visible in these maximum-current wave functions: Firstly, the number and position of the vortices in the  $x$ - $y$ -plane are changing. This is exceptionally easy to see in Fig. 7.11(d). Not only have four new vortices entered the picture, the original vortices are pushed much tighter together. The new vortices have also increased the dilatation of the wave function. This effect

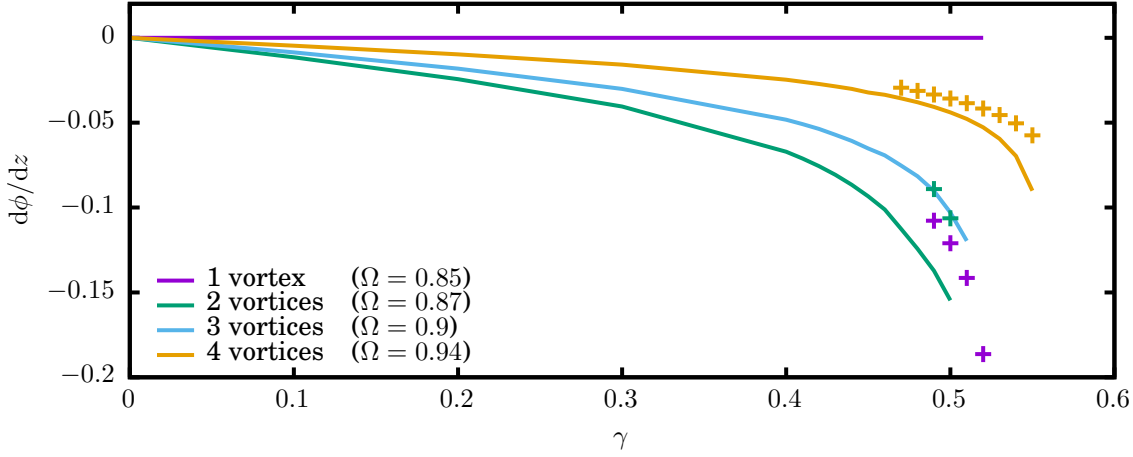


Figure 7.12.: The screwing strength, given as  $d\phi/dz|_{z=0}$  of the parametrized vortex, as a function of  $\gamma$  and for different rotation frequencies  $\Omega$ . The original vortices existing from  $\gamma = 0$  upwards are shown as solid lines while the new vortices arising for higher parameters  $\gamma$  are depicted as crosses.

is expected from an increased rotation frequency or a strengthened interaction. To understand this relation, the findings from Chap. 4 have to be taken into account. Due to the  $\mathcal{PT}$ -symmetric current in  $z$ -direction, this component of the wave function cannot be chosen exactly symmetric, i.e., it does not take the shape of a Gaussian. Instead, an antisymmetric contribution is needed, considerably reducing the modulus square at  $z = 0$ . The particles are then forced to the top and bottom of the trap, increasing the particle density and the impact of the interaction at these points.

Secondly, the previously discussed bend to the center of the trap is not the only deformation the vortex lines undergo. Following the direction of the  $\mathcal{PT}$ -symmetric current upwards, the vortex lines are screwed in clockwise direction, i.e., in the opposite direction of the frame's rotation. To chart this screwing, each vortex must be parametrized by the coordinate  $z$  in cylindrical coordinates  $r(z), \phi(z)$ . The vortex screwing is then purely described by the non-constant function  $\phi(z)$ , which is antisymmetric with respect to the  $x$ - $y$ -plane; the differential  $d\phi/dz$  defines a screwing strength. This value is shown in Fig. 7.12 as a function of  $\gamma$ .

The shape of all these functions are the same. Only the maximum obtainable  $\gamma$  and the overall slope differ. In fact, additional illustrations confirm, that all lines can be made congruent by appropriately rescaling both axes. The different maximum parameters  $\gamma$  are an obvious consequence of the different positions of the tangent bifurcations at which the ground states vanish. The different inclinations are particularly distinct for low parameters  $\gamma$ . In this regime, two

## 7. Rotating condensates in $\mathcal{PT}$ -symmetric potentials

---

rough dependencies are visible: Firstly, the central vortex is not bent at all. Secondly, vortices of a stationary state with  $n$  non-center vortices are screwed  $m/n$  times as strong as in the case of  $m$  vortices. This fact supports the suggestion that the vortex screwing supports the upwards current in the system and each vortex makes an equal contribution. The strongest screwed vortices are therefore found in the two-vortex case. For stronger gain and loss new non-center vortices arise, depicted as points in Fig. 7.12. These are, with the exception of the central vortex state, screwed less than the original vortices

## 8. Summary and Outlook

This thesis presented numerical results to answer the question how Bose-Einstein condensates in realistic trapping potentials behave in the presence of  $\mathcal{PT}$ -symmetric particle in- and out-coupling.  $\mathcal{PT}$ -symmetric systems often have real eigenvalues. This well known statement always has to be supported by a range of examples to particularize the term *often*. One such exemplary system is the  $\mathcal{PT}$ -symmetric double well, for which many hitherto existing results were summarized in Chap. 4.

To derive a mandatory criterion for the existence of  $\mathcal{PT}$ -symmetric stationary states, perturbation theory was used starting from the unperturbed case of a Hermitian closed system in Chap. 5. A weak  $\mathcal{PT}$ -symmetric perturbation  $\hat{H}_P$  keeps the real eigenvalue spectrum intact, provided that all sets of degenerate eigenvectors  $\{\phi_i\}$  satisfy  $\langle \phi_i | \hat{H}_P | \phi_j \rangle = 0$ .

If the effect of the perturbation smears out and, thus, is damped for highly excited states, a harmonic trapping potential ensures that the results of the perturbation theory stay correct even in infinite-dimensional systems. For the example of two point-like perturbations, one of which acts as a particle source and the other as a drain, rigorous analytic estimates were confirmed. Even though the estimates fail for the nonlinear Gross-Pitaevskii equation, i.e., in the interacting case, a sufficient damping of the perturbation's influence was found. Thus, one can assume that in harmonically trapped systems with bounded perturbations modeling balanced gain and loss of particles, the  $\mathcal{PT}$  symmetry remains unbroken.

These results confirm that the spatially extended double-well presented in Chap. 4 is suitable for the realization of  $\mathcal{PT}$ -symmetric systems. However, what if this meticulously set-up double well is perturbed, if additional particle channels are opened, or the in- and out-coupling of particles cannot be balanced completely?

In Chap. 6 three important modifications to the double-well system were examined. The first two sections addressed the question, how an additional channel from the loss to the gain well of the  $\mathcal{PT}$ -symmetric double well facilitates the particle transport. In both systems the particle transport does not profit from this channel. However the fashion of these effects differs notably.

In the first part, the second channel was provided by an additional well. The particle in- and out-coupling effectively induces a ring current through the system. This reduces the net current even though the partial current through the original double well increases. The mathematical reason for this effect can be found in Sec. 5.1. Due to the degeneracy that occurs when all three wells are equally strongly coupled, even a weak in- and out-coupling immediately breaks

## 8. Summary and Outlook

---

the symmetry.

If the new channel is, in contrast to the three well case, realized by a spatially extended trench that opens between the wells, higher excited states with even more modes have to be considered. While it would be possible for the ground state to carry a higher particle current, it will eventually become unstable when perturbations arise which provide a nodal plane within the course of the new particle channel. This was studied in the linear regime, where it was shown that the first excited state that provides such a node behaves very similar to the original double-well ground state.

These two modifications only interfered with the real part of the potential and if, instead, the  $\mathcal{PT}$  symmetry is primarily broken by an asymmetric imaginary potential all hitherto presented results become invalid. However, if the overall loss contributions are stronger than the particle gain, and the trapping potential can be controlled, this issue was shown to be easily overcome. Providing a weak repulsive interaction is present, a dynamical attractor can be found for any fixed in- and out-coupling strength. Particles are then induced or removed from the condensate until the particle number matches this state.

As a last step, the field of stationary traps was left behind when rotating condensates were studied in Chap. 7. Rotating condensates exhibit a new feature that belongs to the most central effects of interacting condensates and superfluids, the nucleation of vortices. Since vortices introduce complex intrinsic currents to the condensate, it is of great interest how these singularities behave in the presence of a  $\mathcal{PT}$ -symmetric current. Ground states up to four vortices were discussed to establish a reliable analysis of such current combinations.

A first, numerically cheaper, approach dealt with two-dimensional condensates. The Gross-Pitaevskii equation in a rotating frame was rendered  $\mathcal{PT}$ -symmetric by introducing an equally rotating imaginary potential. The particles in this sense are injected and removed from the condensate not at a fixed point but at circling positions around the rotation center. Increasing the particle in- and out-coupling actuates a current through the rotating condensate. There are in principle two possible impacts on the wave function. The current could either add to the circular vortex currents leaving the overall particle density intact, or the vortices can reposition themselves to change the current. Indeed, it was worked out over the course of the analysis that the net current from the gain to the loss areas is completely composed of the individual currents around the vortices, whose positions in the wave function are shifted complying to two effects. Either, all vortices are moved alongside each other to weaken the currents that are shifted to lower particle densities and vice versa, or some vortices are added from or released to the outside of the particle cloud to permit new combinations of vortex currents. Stability of the stationary states, however, varied greatly. While some configurations of vortices were found to not even support the weakest net currents, others are found to be stable for wide ranges of the parameters.

---

While the two-dimensional calculations scoped with a highly complex case of time-dependent in- and out-coupling, a much more apparent configuration was tackled in three dimensions. Instead of running the net current through vortices, it can be aligned along the vortices nodal line. Since vortices are nucleated in a plane perpendicular to the rotation axis, the  $\mathcal{PT}$ -symmetric current is then parallel to this axis. While increasing the particle in- and out-coupling, all vortices short of those residing on the rotation axis were found to bend and screw themselves around it. Following the course of the particles, the direction of this screwing was identified to be opposite to the rotation direction. Since higher numbers of vortices are screwed more weakly than small numbers, it is conjecturable that this effect contributes to the particle transport which itself is then distributed between the vortices.

## Outlook

This thesis showed extensively that the double-well system is a versatile basis for any future work. The emphasis lies on two distinct effects. Firstly, the  $\mathcal{PT}$  symmetry breaking due to the degeneracy of three circularly-arranged wells. A dynamical, i.e., time-dependent, analysis of this effect leading to a suppression of the double-well current, can prove worthwhile. Possible scenarios include a purely geometric transistor for Bose-condensed particles. Secondly, the appearance of a dynamical attractor in a system with unbalanced gain and loss of particles allows for a more stable experimental realization. It would be worthwhile to investigate, how such an unbalancing would influence many-particle calculations including the predicted purity oscillations by Dast et al. [28].

However, the thesis also discussed rotating condensates. Especially the case of a net current in direction of the rotation axis should be analyzed in more detail, to expose the relationship between the net current and the vortex screwing. Two different approaches come to mind: One could analyze the behavior of an ideal superfluid analytically using the Euler equations. This would clarify if the screwing is a characteristic of any flow parallel to vortices in a coherent atomic gas. On the other hand, the influence of the rotation can be made clearer by introducing a system with a vortex bound to a non-central well in a non-rotating system.



## A. Additional analysis of the two-dimensional rotating system

In Fig. A.1 the state  $v_2$  from the nomenclature introduced in Sec. 7.2 is shown for increasing values of the in- and out-coupling parameter  $\gamma$ . The state is aligned in such a way that both vortices lie on the  $y$ -axis with  $x = 0$ . The current enforced by the particle exchange with the surroundings is generated by weakening the opposing current with the introduction of a new vortex. The bifurcation partner is the three-vortex state  $v_3$ . Apart from three small regions, almost all possible configurations are unstable.

While the other possible two-vortex configuration was already discussed in Sec. 7.2, both possible configurations for the state  $v_4$  are left to discuss. It is obvious, that this state can either be used with one vortex residing in each quadrant of the  $x$ - $y$ -plane (Fig. A.2) or rotated about  $\pi/4$ , such that the vortices reside on the axis at  $x = 0$  and  $y = 0$  (Fig. A.3). These bifurcation scenarios do not reveal entirely new effects. However, the stability properties must be analyzed. In the first configuration, the lower branch is stable for a notable region. In the second configuration even a small particle exchange breaks the stability on the spot.

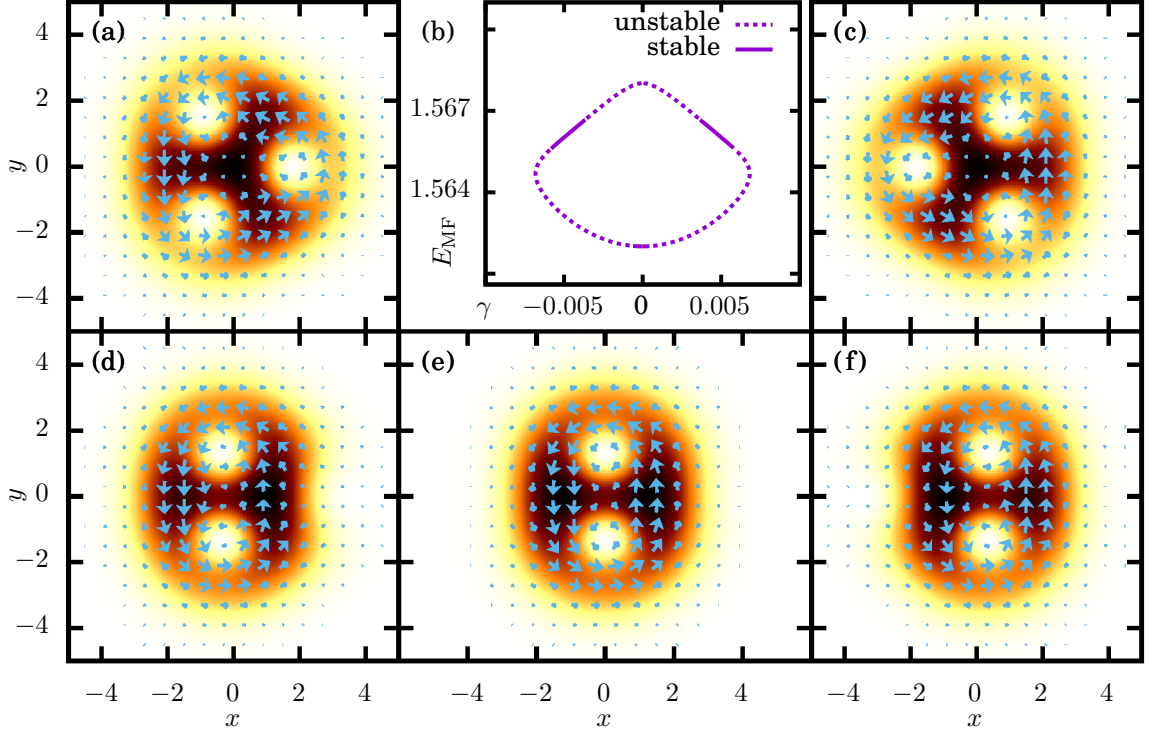


Figure A.1.: Wave functions (a),(c-f) from the bifurcation scenario (b) of the stationary state  $v_2$  for  $\Omega = 0.88$  under variation of the in- and out-coupling strength  $\gamma$ . This state, shown in (e) for  $\gamma = 0$ , forms the lower branch and coalesces at  $\gamma \approx -0.0068$  (d) and  $\gamma \approx 0.0068$  (f) with two different branches. For  $\gamma \rightarrow 0^-$  (a) and  $\gamma \rightarrow 0^+$  (c) the two solutions degenerate and form the state  $v_3$ . The particle density is shown as a color map, in which darker regions correspond to higher densities while the currents are depicted by blue arrows. Their lengths are proportional to the current strength.

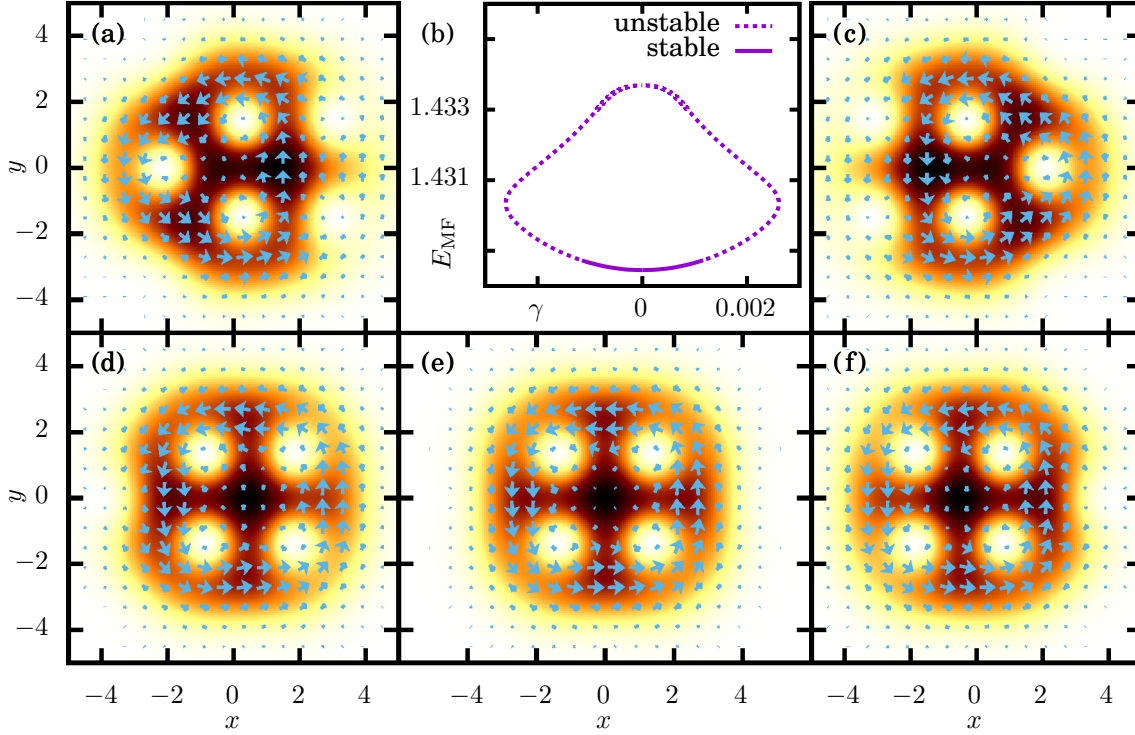


Figure A.2.: Wave functions (a),(c-f) from the bifurcation scenario (b) of the stationary state  $v_4$  for  $\Omega = 0.94$  under variation of the in- and out-coupling strength  $\gamma$ . The state is oriented in such a way that one vortex resides in each quadrant of the  $x$ - $y$ -plane. This state, shown in (e) for  $\gamma = 0$ , forms the lower branch while the two bifurcation partners for  $\gamma \approx -0.0026$  (d) and  $\gamma \approx 0.0026$  (f) form the upper branch. For  $\gamma \rightarrow 0^-$  (a) and  $\gamma \rightarrow 0^+$  (c) the two bifurcation partners degenerate and form an asymmetric five vortex state. The particle density is shown as a color map, in which darker regions correspond to higher densities while the currents are depicted by blue arrows. Their lengths are proportional to the current strength.

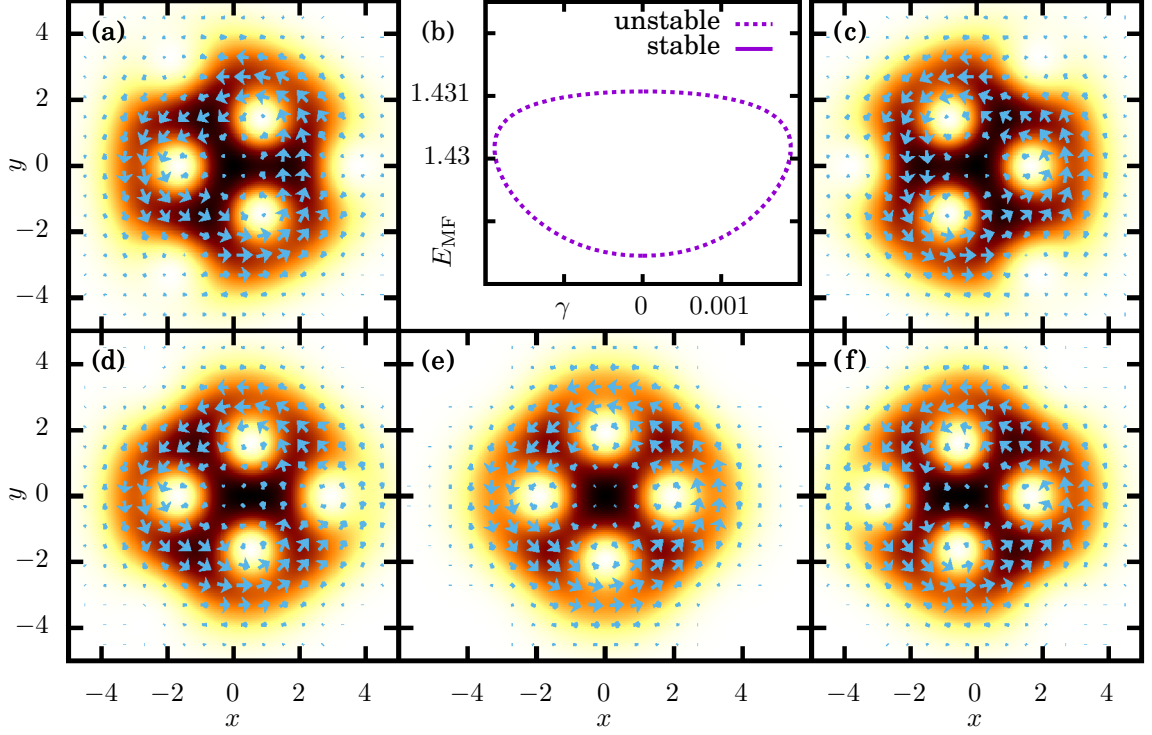


Figure A.3.: Wave functions (a),(c-f) from the bifurcation scenario (b) of the stationary state  $v_4$  for  $\Omega = 0.94$  under variation of the in- and out-coupling strength  $\gamma$ . The state is oriented in such a way that the vortices lay on the  $x$  and  $y$  axis. This state, shown in (e) for  $\gamma = 0$ , forms the lower branch while the bifurcation partners for  $\gamma \approx -0.0019$  (d) and  $\gamma \approx 0.0019$  (f) form the upper branch. For  $\gamma \rightarrow 0^-$  (a) and  $\gamma \rightarrow 0^+$  (c) the two bifurcation partners degenerate and form the state  $v_3$ , which at this point supports three additional vortices. The particle density is shown as a color map, in which darker regions correspond to higher densities while the currents are depicted by blue arrows. Their lengths are proportional to the current strength.

# Bibliography

- [1] C. M. Bender and S. Boettcher, “Real spectra in non-Hermitian Hamiltonians having  $\mathcal{PT}$  symmetry”, Phys. Rev. Lett. **80**, 5243 (1998).
- [2] C. M. Bender, D. C. Brody, and H. F. Jones, “Complex Extension of Quantum Mechanics”, Phys. Rev. Lett. **89**, 270401 (2002).
- [3] A. Mostafazadeh, “ $\mathcal{QT}$ -symmetry and weak pseudo-hermiticity”, J. Phys. A **41**, 055304 (2008).
- [4] A. Mostafazadeh, “Pseudo-Hermitian representation of quantum mechanics”, Int. J. Geom. Methods Mod. Phys. **07**, 1191 (2010).
- [5] R. El-Ganainy, K. G. Makris, D. N. Christodoulides, and Z. H. Musslimani, “Theory of coupled optical  $\mathcal{PT}$ -symmetric structures”, Opt. Lett. **32**, 2632 (2007).
- [6] S. Klaiman, U. Günther, and N. Moiseyev, “Visualization of Branch Points in  $\mathcal{PT}$ -Symmetric Waveguides”, Phys. Rev. Lett. **101**, 080402 (2008).
- [7] Z. Musslimani, K. G. Makris, R. El-Ganainy, and D. N. Christodoulides, “Optical solitons in  $\mathcal{PT}$  periodic potentials”, Phys. Rev. Lett. **100**, 30402 (2008).
- [8] K. G. Makris, R. El-Ganainy, D. N. Christodoulides, and Z. H. Musslimani, “Beam Dynamics in  $\mathcal{PT}$  Symmetric Optical Lattices”, Phys. Rev. Lett. **100**, 103904 (2008).
- [9] K. G. Makris, R. El-Ganainy, D. N. Christodoulides, and Z. H. Musslimani, “ $\mathcal{PT}$ -symmetric optical lattices”, Phys. Rev. A **81**, 063807 (2010).
- [10] A. Guo, G. J. Salamo, D. Duchesne, R. Morandotti, M. Volatier-Ravat, V. Aimez, G. A. Siviloglou, and D. N. Christodoulides, “Observation of  $\mathcal{PT}$ -Symmetry Breaking in Complex Optical Potentials”, Phys. Rev. Lett. **103**, 093902 (2009).
- [11] C. E. Rüter, K. G. Makris, R. El-Ganainy, D. N. Christodoulides, M. Segev, and D. Kip, “Observation of parity-time symmetry in optics”, Nat. Phys. **6**, 192 (2010).
- [12] Y. D. Chong, L. Ge, and A. D. Stone, “ $\mathcal{PT}$ -Symmetry Breaking and Laser-Absorber Modes in Optical Scattering Systems”, Phys. Rev. Lett. **106**, 093902 (2011).

- [13] Z. Lin, H. Ramezani, T. Eichelkraut, T. Kottos, H. Cao, and D. N. Christodoulides, “Unidirectional Invisibility Induced by  $\mathcal{PT}$ -Symmetric Periodic Structures”, *Phys. Rev. Lett.* **106**, 213901 (2011).
- [14] A. Regensburger, C. Bersch, M.-A. Miri, G. Onishchukov, D. N. Christodoulides, and U. Peschel, “Parity-time synthetic photonic lattices”, *Nature* **488**, 167 (2012).
- [15] B. Peng, Ş. K. Özdemir, F. Lei, F. Monifi, M. Gianfreda, G. L. Long, S. Fan, F. Nori, C. M. Bender, and L. Yang, “Parity–time-symmetric whispering-gallery microcavities”, *Nat. Phys.* **10**, 394 (2014).
- [16] J. Schindler, A. Li, M. C. Zheng, F. M. Ellis, and T. Kottos, “Experimental study of active *LRC* circuits with  $\mathcal{PT}$  symmetries”, *Phys. Rev. A* **84**, 040101 (2011).
- [17] N. Bender, S. Factor, J. D. Bodyfelt, H. Ramezani, D. N. Christodoulides, F. M. Ellis, and T. Kottos, “Observation of Asymmetric Transport in Structures with Active Nonlinearities”, *Phys. Rev. Lett.* **110**, 234101 (2013).
- [18] H. Cartarius, D. Haag, D. Dast, and G. Wunner, “Nonlinear Schrödinger equation for a  $\mathcal{PT}$ -symmetric delta-function double well”, *J. Phys. A* **45**, 444008 (2012).
- [19] H. Cartarius and G. Wunner, “Model of a  $\mathcal{PT}$ -symmetric Bose-Einstein condensate in a  $\delta$ -function double-well potential”, *Phys. Rev. A* **86**, 013612 (2012).
- [20] D. Dast, D. Haag, H. Cartarius, G. Wunner, R. Eichler, and J. Main, “A Bose-Einstein condensate in a  $\mathcal{PT}$  symmetric double well”, *Fortschr. Physik* **61**, 124 (2013).
- [21] D. Dast, D. Haag, H. Cartarius, J. Main, and G. Wunner, “Eigenvalue structure of a Bose-Einstein condensate in a  $\mathcal{PT}$ -symmetric double well”, *J. Phys. A* **46**, 375301 (2013).
- [22] D. Haag, D. Dast, A. Löhle, H. Cartarius, J. Main, and G. Wunner, “Nonlinear quantum dynamics in a  $\mathcal{PT}$ -symmetric double well”, *Phys. Rev. A* **89**, 023601 (2014).
- [23] M. Kreibich, J. Main, H. Cartarius, and G. Wunner, “Hermitian four-well potential as a realization of a  $\mathcal{PT}$ -symmetric system”, *Phys. Rev. A* **87**, 051601(R) (2013).
- [24] F. Single, H. Cartarius, G. Wunner, and J. Main, “Coupling approach for the realization of a  $\mathcal{PT}$ -symmetric potential for a Bose-Einstein condensate in a double well”, *Phys. Rev. A* **90**, 042123 (2014).
- [25] M. Holland, K. Burnett, C. Gardiner, J. I. Cirac, and P. Zoller, “Theory of an atom laser”, *Phys. Rev. A* **54**, R1757 (1996).

- 
- [26] T. Gericke, P. Wurtz, D. Reitz, T. Langen, and H. Ott, “High-resolution scanning electron microscopy of an ultracold quantum gas”, *Nat. Phys.* **4**, 949 (2008).
- [27] N. P. Robins, C. Figl, M. Jeppesen, G. R. Dennis, and J. D. Close, “A pumped atom laser”, *Nat. Phys.* **4**, 731 (2008).
- [28] D. Dast, D. Haag, H. Cartarius, and G. Wunner, “Quantum master equation with balanced gain and loss”, *Phys. Rev. A* **90**, 052120 (2014).
- [29] D. Dast, D. Haag, H. Cartarius, and G. Wunner, “Purity oscillations in Bose-Einstein condensates with balanced gain and loss”, *Phys. Rev. A* **93**, 033617 (2016).
- [30] D. Dast, D. Haag, H. Cartarius, J. Main, and G. Wunner, “Bose-Einstein condensates with balanced gain and loss beyond mean-field theory”, *Phys. Rev. A* **94**, 053601 (2016).
- [31] D. A. Butts and D. S. Rokhsar, “Predicted signatures of rotating Bose-Einstein condensates”, *Nature* **397**, 327 (1999).
- [32] K. W. Madison, F. Chevy, W. Wohlleben, and J. Dalibard, “Vortex Formation in a Stirred Bose-Einstein Condensate”, *Phys. Rev. Lett.* **84**, 806 (2000).
- [33] D. Haag, D. Dast, H. Cartarius, and G. Wunner, “Finite element Calculations of  $\mathcal{PT}$ -Symmetric Bose-Einstein Condensates”, *Int. J. Theor. Phys.* **54**, 4100 (2015).
- [34] E.-M. Graefe, “Stationary states of a  $\mathcal{PT}$  symmetric two-mode Bose-Einstein condensate”, *J. Phys. A* **45**, 444015 (2012).
- [35] D. Haag, D. Dast, H. Cartarius, and G. Wunner, “ $\mathcal{PT}$ -symmetric currents of a Bose-Einstein condensate in a triple well”, *Phys. Rev. A* **92**, 053627 (2015).
- [36] B. S. Mityagin, “The Spectrum of a Harmonic Oscillator Operator Perturbed by Point Interactions”, *Int. J. Theor. Phys.* **54**, 4068 (2015).
- [37] D. Haag, H. Cartarius, and G. Wunner, “A Bose-Einstein condensate with  $\mathcal{PT}$ -symmetric double-delta function loss and gain in a harmonic trap: a test of rigorous estimates”, *Acta Polytechnica* **54**, 116 (2014).
- [38] S. Bose, “Plancks Gesetz und Lichtquantenhypothese”, *Zeitschrift für Physik A* **26**, 178 (1924).
- [39] A. Einstein, “Quantentheorie des einatomigen idealen Gases”, *Sitzungsber. Preuss. Akad. Wiss., Phys. Math. Kl.* **22**, 261 (1924).
- [40] A. Einstein, “Quantentheorie des einatomigen idealen Gases II”, *Sitzungsber. Preuss. Akad. Wiss., Phys. Math. Kl.* **1**, 3 (1925).

- [41] M. H. Anderson, J. R. Ensher, M. R. Matthews, C. E. Wieman, and E. A. Cornell, “Observation of Bose-Einstein Condensation in a Dilute Atomic Vapor”, *Science* **269**, 198 (1995).
- [42] K. B. Davis, M.-O. Mewes, M. R. Andrews, N. J. van Druten, D. S. Durfee, D. M. Kurn, and W. Ketterle, “Bose-Einstein Condensation in a Gas of Sodium Atoms”, *Phys. Rev. Lett.* **75**, 3969 (1995).
- [43] I. Bloch, J. Dalibard, and W. Zwerger, “Many-body physics with ultracold gases”, *Rev. Mod. Phys.* **80**, 885 (2008).
- [44] F. Dalfovo, S. Giorgini, L. P. Pitaevskii, and S. Stringari, “Theory of Bose-Einstein condensation in trapped gases”, *Rev. Mod. Phys.* **71**, 463 (1999).
- [45] E. P. Gross, “Structure of a Quantized Vortex in Boson Systems”, *Nuovo Cimento* **20**, 454 (1961).
- [46] L. P. Pitaevskii, “Vortex Lines in an Imperfect Bose Gas”, *Sov. Phys. JETP* **13**, 451 (1961).
- [47] J. R. Anglin and A. Vardi, “Dynamics of a two-mode Bose-Einstein condensate beyond mean-field theory”, *Phys. Rev. A* **64**, 013605 (2001).
- [48] A. Vardi and J. R. Anglin, “Bose-Einstein Condensates beyond Mean Field Theory: Quantum Backreaction as Decoherence”, *Phys. Rev. Lett.* **86**, 568 (2001).
- [49] J. Söding, D. Guéry-Odelin, P. Desbiolles, F. Chevy, H. Inamori, and J. Dalibard, “Three-body decay of a rubidium Bose–Einstein condensate”, *Applied Physics B* **69**, 257 (1999).
- [50] M. Egorov, B. Opanchuk, P. Drummond, B. V. Hall, P. Hannaford, and A. I. Sidorov, “Measurement of  $s$ -wave scattering lengths in a two-component Bose-Einstein condensate”, *Phys. Rev. A* **87**, 053614 (2013).
- [51] S. E. Pollack, D. Dries, M. Junker, Y. P. Chen, T. A. Corcovilos, and R. G. Hulet, “Extreme Tunability of Interactions in a  $^7\text{Li}$  Bose-Einstein Condensate”, *Phys. Rev. Lett.* **102**, 090402 (2009).
- [52] S. Inouye, M. R. Andrews, J. Stenger, H.-J. Miesner, D. M. Stamper-Kurn, and W. Ketterle, “Observation of Feshbach resonances in a Bose-Einstein condensate”, *Nature* **392**, 151 (1998).
- [53] P. A. M. Dirac, *The principles of quantum mechanics*, Fourth (Clarendon Pr., Oxford, 1995).
- [54] C. M. Bender, S. Boettcher, and P. N. Meisinger, “ $\mathcal{PT}$ -symmetric quantum mechanics”, *J. Math. Phys.* **40**, 2201 (1999).
- [55] C. M. Bender, “Making sense of non-Hermitian Hamiltonians”, *Rep. Prog. Phys.* **70**, 947 (2007).

- 
- [56] A. Mostafazadeh, “Pseudo-Hermiticity versus  $\mathcal{PT}$  symmetry: The necessary condition for the reality of the spectrum of a non-Hermitian Hamiltonian”, *J. Math. Phys.* **43**, 205 (2002).
- [57] A. Mostafazadeh, “Pseudo-Hermiticity versus  $\mathcal{PT}$ -symmetry. II. A complete characterization of non-Hermitian Hamiltonians with a real spectrum”, *J. Math. Phys.* **43**, 2814 (2002).
- [58] A. Mostafazadeh, “Pseudo-Hermiticity versus  $\mathcal{PT}$ -symmetry III: Equivalence of pseudo-Hermiticity and the presence of antilinear symmetries”, *J. Math. Phys.* **43**, 3944 (2002).
- [59] Y. Kagan, A. E. Muryshev, and G. V. Shlyapnikov, “Collapse and Bose-Einstein Condensation in a Trapped Bose Gas with Negative Scattering Length”, *Phys. Rev. Lett.* **81**, 933 (1998).
- [60] H.-P. Breuer and F. Petruccione, *The theory of open quantum systems*, 1. publ. (Oxford Univ. Press, Oxford, 2002).
- [61] G. C. Wick, A. S. Wightman, and E. P. Wigner, “The Intrinsic Parity of Elementary Particles”, *Phys. Rev.* **88**, 101 (1952).
- [62] R. Haag, *Local quantum physics: Fields, particles, algebras*, Second Revised and Enlarged Edition (Springer, Berlin, 1996).
- [63] D. Witthaut, F. Trimborn, H. Hennig, G. Kordas, T. Geisel, and S. Wimberger, “Beyond mean-field dynamics in open Bose-Hubbard chains”, *Phys. Rev. A* **83**, 063608 (2011).
- [64] K. Rapedius, “Closed system approach to open systems: tunnelling decay of interacting cold bosons in an optical lattice”, *J. Phys. B* **46**, 125301 (2013).
- [65] M. Powell, “A Hybrid Method for Nonlinear Equations”, in *Numerical Methods for Nonlinear Algebraic Equations*, edited by P. Rabinowitz (Gordon and Breach, 1970) Chap. 6, pp. 87–114.
- [66] J. J. Moré, B. S. Garbow, and K. E. Hillstom, “User Guide for MINPACK-1”, ANL-80-74, Argonne National Laboratory (1980).
- [67] F. Catoni, D. Boccaletti, R. Cannata, V. Catoni, E. Nichelatti, and P. Zampetti, *The Mathematics of Minkowski Space-Time With an Introduction to Commutative Hypercomplex Numbers*, First (Birkhäuser Verlag, Basel, 2008).
- [68] R. Gutöhrlein, J. Main, H. Cartarius, and G. Wunner, “Bifurcations and exceptional points in dipolar Bose-Einstein condensates”, *J. Phys. A* **46**, 305001 (2013).
- [69] C. Schimeczek and G. Wunner, “Accurate 2d finite element calculations for hydrogen in magnetic fields of arbitrary strength”, *Comp. Phys. Comm.* **185**, 614 (2014).

- [70] C. de Boor, “Package for Calculating with B-Splines”, *SIAM J. Numer. Anal.* **14**, 441 (1977).
- [71] T. Kato, *Perturbation theory for linear operators* (Springer, Berlin, 1966).
- [72] G. Demange and E. M. Graefe, “Signatures of three coalescing eigenfunctions”, *J. Phys. A* **45**, 025303 (2012).
- [73] E. M. Graefe, H. J. Korsch, and A. E. Niederle, “Mean-Field Dynamics of a Non-Hermitian Bose-Hubbard Dimer”, *Phys. Rev. Lett.* **101**, 150408 (2008).
- [74] A. Löhle, H. Cartarius, D. Haag, D. Dast, J. Main, and G. Wunner, “Stability of Bose-Einstein condensates in a  $\mathcal{PT}$ -symmetric double- $\delta$  potential close to branch points”, *Acta Polytechnica* **54**, 133 (2014).
- [75] D. Dizdarevic, D. Dast, D. Haag, J. Main, H. Cartarius, and G. Wunner, “Cusp bifurcation in the eigenvalue spectrum of  $\mathcal{PT}$ -symmetric Bose-Einstein condensates”, *Phys. Rev. A* **91**, 033636 (2015).
- [76] F. M. Fernández, *Introduction to perturbation theory in quantum mechanics* (CRC Press, Boca Raton, FL, 2001).
- [77] A. Messiah, *Quantum Mechanics Vol 2* (North-Holland Publishing Company, Amsterdam, 1965).
- [78] F. M. Fernández, R. Guardiola, J. Ros, and M. Znojil, “Strong-coupling expansions for the  $\mathcal{PT}$ -symmetric oscillators  $V(x) = a(ix) + b(ix)^2 + c(ix)^3$ ”, *J. Phys. A* **31**, 10105 (1998).
- [79] F. M. Fernández and J. Garcia, “Parity-time symmetry broken by point-group symmetry”, *J. Math. Phys.* **55**, 042107 (2014).
- [80] T. Kato, “On the Convergence of the Perturbation Method. I”, *Prog. Theor. Phys.* **4**, 514 (1949).
- [81] B. Mityagin and P. Siegl, “Root System of Singular Perturbations of the Harmonic Oscillator Type Operators”, *Lett. Math. Phys.* **106**, 147 (2016).
- [82] J. Adduci and B. Mityagin, “Eigensystem of an L 2-perturbed harmonic oscillator is an unconditional basis”, *Cent. Eur. J. Math.* **10**, 569 (2012).
- [83] O. Christensen, “Frames, Riesz bases, and discrete Gabor/wavelet expansions”, *Bull. Amer. Math. Soc.* **38**, 273 (2001).
- [84] V. Jakubsky and M. Znojil, “An explicitly solvable model of the spontaneous  $\mathcal{PT}$ -symmetry breaking”, *Czech. J. Phys.* **55**, 1113 (2005).
- [85] D. Krejčířík and P. Siegl, “ $\mathcal{PT}$ -symmetric models in curved manifolds”, *J. Phys. A* **43**, 485204 (2010).
- [86] P. Lunt, “Stabilität  $\mathcal{PT}$ -symmetrischer Effekte bei asymmetrischen Potentialanteilen”, Bachelor’s Thesis (Universität Stuttgart, 2016).

- [87] V. L. Ginzburg and L. P. Pitaevskii, “On the theory of superfluidity”, *Sov. Phys. JETP* **7**, 858 (1958).
- [88] A. L. Fetter, “Rotating trapped Bose-Einstein condensates”, *Rev. Mod. Phys.* **81**, 647 (2009).
- [89] W. Bao, “Ground states and dynamics of rotating Bose-Einstein condensates”, in *Transport Phenomena and Kinetic Theory: Applications to Gases, Semiconductors, Photons, and Biological Systems*, edited by C. Cercignani and E. Gabetta (Birkhäuser Boston, Boston, MA, 2007), pp. 215–255.



# Zusammenfassung in deutscher Sprache

## Motivation und Grundlagen

Eines der wichtigen Dirac-von Neumann-Axiome der Quantenmechanik besagt, dass Operatoren, die physikalische Messgrößen repräsentieren, stets Hermitesch sind. Daraus folgt direkt, dass jede Messung reelle, und damit interpretierbare, Ergebnisse liefert [53]. Jedes neue Axiom, welches das Axiom Hermitescher Operatoren ersetzen will, muss diese grundlegendere Eigenschaft erhalten.

Im Jahr 1998 zeigten Bender und Boettcher [1], dass eine ganze Schar nicht-Hermitescher Hamilton-Operatoren reelle Eigenwerte und damit reelle Messwerte hat. Sie begründeten das Verhalten damit, dass die untersuchten Systeme symmetrisch bezüglich einer gleichzeitigen Punktspiegelung des Raums und einer Zeitumkehr sind. Diese Systeme heißen  $\mathcal{PT}$ -symmetrisch. Diesem Fund folgten viele Versuche das Konzept zu verallgemeinern und eine  $\mathcal{PT}$ -symmetrische Quantenmechanik zu formulieren [2–4].

Neben diesen fundamentalen Überlegungen wurden auch bald Konzepte zu einer ersten experimentellen Umsetzung  $\mathcal{PT}$ -symmetrischer Systeme entwickelt. Der bedeutendste Teil dieser Aufgabe besteht in der Interpretation und Realisierung der nicht-Hermiteschen Anteile, die im einfachsten Fall durch imaginäre Potentiale repräsentiert werden. Im Fall optischer Systeme, in denen die ersten erfolgreichen Realisierungen gelungen sind, verursachen diese Potentiale einen Anstieg oder Abfall der elektrischen Feldstärke [5–9]. Umgesetzt wird dies durch zwei gekoppelte Wellenleiter. In einem wird ein absorbierendes Medium eingebracht [10], während im anderen ein aktives Medium eine Verstärkung der Mode verursacht [11]. Inzwischen folgten weitere interessante Anwendungen in anderen Geometrien, die mehrere experimentellen Erfolge zu verzeichnen haben [14, 15].

In dieser Dissertation wird eine weitere Möglichkeit näher untersucht. Für sehr kleine Temperaturen gehen dünne atomare Gase in die Phase der Bose-Einstein-Kondensate über. Dabei nehmen alle Atome denselben Zustand an, sodass das gesamte Gas durch eine einzige Mean-Field-Wellenfunktion beschrieben ist, die jedes einzelne Teilchen einnimmt [39, 40]. Es lässt sich zeigen, dass ein imaginäres Potential auch in diesem Fall zu einem Gewinn oder Verlust, hier jedoch von Teilchen, führt. Der genaue Zusammenhang ist in Kapitel 2 beschrieben. Reelle

Eigenwerte des Hamiltonoperators beschreiben in diesem Fall Zustände, die trotz Teilchenzufluss und -abfluss die Teilchenzahl insgesamt erhalten.

Einem Vorschlag von Klaiman et al. [6] folgend wurde der einfachste Fall einer solchen Falle, das  $\mathcal{PT}$ -symmetrische Doppelmuldenpotential, theoretisch untersucht. Dabei wurden nicht nur bekannte Effekte der Optik wiedergefunden, sondern auch originäre nichtlineare Effekte beschrieben, die eine direkt Folge der Teilchenwechselwirkung darstellen [18–22]. Experimentelle Umsetzungen dieser Arbeiten sind noch nicht gelungen, obwohl Vorschläge existieren:

Die Doppelmulde kann entweder in ein Hermitesches System mit mehr Moden eingebettet [23, 24] oder, durch das Ein- und Auskoppeln von Teilchen von außen, offen sein. Die einzelnen Prozesse des Teilchenaustauschs mit externen Quellen und Senken wurden bereits verwirklicht. Die Streuung eines Elektronenstrahls an der Atomwolke verursacht den erwarteten Teilchenverlust [26] während einzukoppelnde Teilchen von einem darüberliegenden Kondensat einrieseln [27]. Tatsächlich entspräche die Verwirklichung von solchen kohärenten Teilchengewinnen und einer gleich starken Auskopplung einem kontinuierlichen Atom-Lasers [25].

Im Gegensatz zu optischen Experimenten, ist die Verwirklichung von Gewinn und Verlust im Bose-Einstein-Kondensat sehr aufwändig. Neben einer intensiven Untersuchung zu Instabilitäten und experimentellen Störungen der  $\mathcal{PT}$ -Symmetrie ist es daher umso wichtiger, intrinsische Effekte tiefkalter Gase wie die Bildung von Wirbeln zu berücksichtigen. An dieser Stelle setzt die vorliegende Arbeit an. Dazu wird die Gross-Pitaevskii-Gleichung,

$$\mu\psi(\mathbf{r}) = (-\Delta + V(\mathbf{r}) + g|\psi(\mathbf{r})|^2) \psi(\mathbf{r}), \quad (1)$$

verwendet, die von stationären Zuständen so gelöst wird, dass das chemische Potential  $\mu$  reell ist. Dabei gibt  $g$  die Stärke der Nichtlinearität an, die die Wechselwirkung beschreibt, und  $V(\mathbf{r})$  beschreibt das Potential, dessen Realteil die Falle und dessen Imaginärteil den Teilchenaustausch charakterisiert.

Um die Gross-Pitaevskii-Gleichung zu lösen, werden zwei Näherungsmethoden genutzt. Beide basieren auf der selben grundlegenden Eigenschaft. Statt eine beliebige Mean-Field-Wellenfunktion zuzulassen, wird angenommen, dass sie sich durch einen endlichen Satz an Basisfunktionen darstellen lässt. Numerisch exakte Ergebnisse lassen sich erhalten, indem man die Funktion stückweise in sogenannten finiten Elementen durch Polynome beschreibt. Der Vorteil möglichst exakter Näherungslösungen bringt jedoch einen entsprechend hohen numerischen Aufwand mit sich. Oft lassen sich die charakteristischen Effekte einer bestimmten Fallengeometrie auch nachbilden, wenn die Wellenfunktion durch einzelne lokalisierte Basisfunktionen dargestellt wird. Diese sind im vorliegenden Fall beispielsweise nicht angeregte Grundzustände innerhalb einzelner Mulden. Diese Mehrmodennäherung nimmt daher an, dass die zugehörigen Wellenfunktionen

innerhalb der einzelnen Mulden während der Rechnung in ihrer Form unverändert bleibt und keine Anregungen innerhalb der Mulden zu berücksichtigen sind.

## $\mathcal{PT}$ -Symmetrie und stationäre Zustände

Ein lineares System heißt  $\mathcal{PT}$ -symmetrisch, wenn der charakterisierende Hamilton-Operator mit dem  $\mathcal{PT}$ -Operator vertauscht,  $[\hat{H}, \mathcal{PT}] = 0$ . Da der kinetische Teil des Hamiltonoperators,  $\hat{H} = \hat{p}^2/2m + V(\hat{r})$ , bereits einzeln mit der Ortsspiegelung  $\mathcal{P} : \hat{r} \rightarrow -\hat{r}$ ,  $\hat{p} \rightarrow -\hat{p}$  und Zeit- oder Impulskehr  $\mathcal{T} : \hat{p} \rightarrow -\hat{p}$ ,  $i \rightarrow -i$  vertauscht, überträgt sich die Kommutatorrelation direkt auf das Potential,

$$V(\hat{r}) = V^*(-\hat{r}). \quad (2)$$

Es muss sich also um einen symmetrischen Realteil, was einem symmetrischen Fallenpotential entspricht, und einen antisymmetrischen Imaginärteil handeln.

Der Operator ist im Allgemeinen nicht-Hermitesch und die Eigenwerte damit komplex. Man kann jedoch zeigen, siehe dazu Abschnitt 2.2, dass sowohl für ein solches lineares System, als auch für die nichtlineare Gross-Pitaevskii-Gleichung folgende Zusammenhänge gelten: Ist ein Eigenzustand selbst  $\mathcal{PT}$ -symmetrisch, gilt also  $\mathcal{PT}|\psi\rangle = \lambda|\psi\rangle$ , so ist der Energieeigenwert reell. Umgekehrt ist jeder nicht-entartete Zustand mit reellem Eigenwert  $\mathcal{PT}$ -symmetrisch. Sind alle Eigenwerte reell, heißt das System selbst  $\mathcal{PT}$ -symmetrisch. Ist ein Energieeigenzustand  $|\psi\rangle$  nicht  $\mathcal{PT}$ -symmetrisch, so existiert ein zweiter Eigenzustand  $\mathcal{PT}|\psi\rangle$  mit komplex konjugierter Energie.

Diese Eigenschaften erklären zwar den fundamentalen Zusammenhang zwischen  $\mathcal{PT}$ -Symmetrie und reellen Eigenwerten, beantwortet allerdings nicht, für welche Potentiale die Zustände überhaupt  $\mathcal{PT}$ -symmetrisch sind. Mit dieser Frage befasst sich die Arbeit in Kapitel 5. Mithilfe der Störungstheorie [76–79] wurde untersucht, inwieweit für kleine Teilchengewinne und -verluste reelle Eigenwerte und damit echte stationäre Kondensate zu erwarten sind. Dazu wurde ein symmetrisches Fallenpotential betrachtet, das durch einen kleinen Teilchenaustausch  $\gamma\hat{H}_P$  gestört wird.

Es zeigt sich, dass die  $\mathcal{PT}$ -Symmetrie nur dann brechen kann, wenn sich zwei Eigenwerte berühren [56–58]. Solange die Eigenwerte sich also durch die Störung nicht sprunghaft verändern, ist die Symmetrie für einen kleinen Teilchenaustausch gesichert. Im Fall einer Entartung berühren sich zwei oder mehr Eigenwerte bereits ohne jegliche Störung und die Matrixelemente

$$S_{ij} = \langle\phi_i|\hat{H}_P|\phi_j\rangle \quad (3)$$

müssen verschwinden um dennoch  $\mathcal{PT}$ -Symmetrie zu ermöglichen.

In linearen Systemen lässt sich die Wirkung einer Störung auf die stationären Zustände sehr gut abschätzen. Solche Abschätzungen für den Spezialfall einer

harmonischen Falle von Adduci, Mityagin and Siegl [81, 82] zeigen, dass sehr allgemeine Annahmen über die Beschränktheit des Imaginärteils des Potentials ausreichen, um reelle Eigenwerte zu garantieren. Im Abschnitt 5.3 werden sowohl diese, als auch noch spezialisiertere Abschätzungen [36] untersucht.

Es zeigte sich, dass im linearen Fall eine kleinste untere Schranke für die Auswirkungen der Störung auf hochangeregte Zustände gefunden werden konnte. Besonders einfach ist dies in der Abbildung 5.5 auf Seite 47 dargestellt. Bedeutender als die linearen Ergebnisse ist jedoch, dass die numerischen Untersuchungen ermöglichen, auch nichtlineare Systeme zu berücksichtigen. In dem genannten Abschnitt wird daher die Gross-Pitaevskii-Gleichung mit Kontaktwechselwirkung (1) herangezogen. Es zeigt sich, dass das nichtlineare System, vollkommen unabhängig von der genauen Stärke der Nichtlinearität, alle getesteten analytischen Abschätzungen sprengt. Allerdings ergibt sich für alle Stärken eine universelle, numerisch gewonnene obere Schranke für hochangeregte Zustände. Dies legt nahe, dass, auch wenn kein analytischer Nachweis existiert, die  $\mathcal{PT}$ -Symmetrie solcher Systeme für hohe Anregungen erhalten bleibt und es genügen sollte, numerisch eine endliche Anzahl tiefer Anregungen zu betrachten.

## Modifikationen der $\mathcal{PT}$ -symmetrischen Doppelmulde

Als einfachstes Beispiel wird in Kapitel 4 die  $\mathcal{PT}$ -symmetrische Doppelmulde vorgestellt. In einer Mulde werden dabei Teilchen ausgekoppelt während Teilchen in die andere Mulde eingeleitet werden. Abbildung 4.1 auf Seite 31 zeigt das chemische Potential der Lösungen der Gross-Pitaevskii-Gleichung für ein solches System in einer Zwei-Moden-Näherung. Die präsentierten Ergebnisse wurden ursprünglich von Graefe et al. analytisch erlangt und ausgiebig diskutiert [34].

Im linearen Fall,  $g = 0$ , treffen sich die Eigenwerte des Grund- und angeregten Zustands in einer Tangentenbifurkation, an welcher beide Zustände verschwinden und zwei  $\mathcal{PT}$ -gebrochene Zustände mit komplex konjugierten Eigenwerten entstehen. Für steigende Nichtlinearitäten,  $g > 0$ , werden alle Eigenwerte zu höheren Realteilen verschoben. Während beide  $\mathcal{PT}$ -symmetrischen Zustände gleich stark verschoben werden, wachsen die  $\mathcal{PT}$ -gebrochenen Zustände sehr viel stärker und entstehen daher nicht mehr an der Tangenten- sondern an einer neuen Heugabelbifurkation, ausgehend vom angeregten Zustand. Dieser wechselt an dieser neuen Bifurkation außerdem von stabilem zu instabilem Verhalten, während der Grundzustand stabil bleibt. Bei stärkeren Nichtlinearitäten,  $g > 1$ , existieren die gebrochenen Zustände bereits ab  $\gamma = 0$ .

Für repulsive Teilchewechselwirkungen erlaubt der Grundzustand einen stabilen Transport von einer zur anderen Mulde. Die erste Frage, der die vorliegende Dissertation im darauffolgenden Kapitel 6 nachging, ist, wie dieser Teilchentransport durch weitere Kanäle beeinflusst werden kann. Dazu wurde das System um

---

eine weitere Mulde erweitert. Abbildung 6.1 auf Seite 52 zeigt das untersuchte System. Die neue Mulde ist mit einer variablen Kopplungsstärke mit der Quelle und der Senke der Doppelmulde verbunden, sodass Teilchen sowohl über den ursprünglichen Transportweg, als auch über die neue Mulde transportiert werden können. Entgegen der klassischen Annahme eines verstärkten Netto-Teilchenflusses, kommt es zu einer Verringerung desselben durch Ausbildung eines Rückflusses durch den neuen Kanal. Das System bildet einen Kreisstrom und bricht die eigene  $\mathcal{PT}$ -Symmetrie dadurch signifikant früher, wie in Abbildung 6.2 auf Seite 54 deutlich zu sehen ist. Ist die Kopplung an die neue Mulde von gleicher Stärke wie die der Doppelmulde, so ist kein stabiler Strom mehr möglich. Durch Berücksichtigung der Kontaktwechselwirkung der einzelnen Atome, lässt sich die Symmetrie zwischen den ursprünglichen und der neuen Mulde allerdings spontan brechen, sodass wieder Ströme von etwa einem Drittel der Stärke in der ursprünglichen Doppelmulde möglich werden.

Ein solcher Kanal lässt sich natürlich nicht nur über eine weitere Mulde verwirklichen. Im nächsten Schritt wird in Abschnitt 6.2 die Barriere zwischen den zwei Mulden in eine Richtung geöffnet, sodass Teilchen nicht nur im direkten Weg durch die Barriere tunneln, sondern auch um sie herum strömen konnten. Wieder erhöhte selbst diese starke Öffnung den gesamten Teilchenstrom nicht wesentlich. Die Knotenebenen höherer Anregungen verhindern die Nutzung der Öffnung und verursachen damit eine Instabilität, die höhere Ströme direkt stört. Eine Wellenfunktion, deren Knotenebenen für einen entsprechend unterdrückten Teilchenstrom verantwortlich ist, ist in Abbildung 6.9 auf Seite 62 gezeigt.

Die zweite Modifikation der Doppelmulde, die in dieser Arbeit untersucht wurde, bezieht sich nicht auf das Fallenpotential, sondern auf die imaginären Potentialanteile, also auf den Teilchenaustausch. Eine experimentelle Realisierung mit perfekt ausgeglichenen Gewinn- und Verlustanteilen ist unwahrscheinlich, kleinste Störungen würden die Ausbildung eines  $\mathcal{PT}$ -symmetrischen Systems verhindern. Die Frage lautet also, ob und wie stabile stationäre Zustände mit reellen Energien realisiert werden können, wenn ein asymmetrischer imaginärer Potentialanteil vorliegt. Tatsächlich zeigt sich, dass eine entsprechend asymmetrische Falle nicht nur zu reellen Eigenwerten für eine bestimmte Teilchenrate der Ein- und Auskopplung führt. Sofern die Verlustrate die Gewinnrate übersteigt, können diese Zustände sogar dynamische Attraktoren darstellen, d.h. die Teilchenzahl steigt oder fällt gerade so, dass es für die eingestellte Rate zu einem stationären Zustand kommt.

## Rotierende Kondensate in $\mathcal{PT}$ -symmetrischen Potentialen

Die bisherigen Rechnungen haben gemeinsam, dass stets laminare Ströme und Grundzustände ohne höhere Anregungen betrachtet wurden. Zu den wohl bekann-

testen Effekten von Bose-Einstein-Kondensaten gehören jedoch gerade Wirbel, die sich zum Beispiel in Grundzuständen rotierender Kondensate zeigen. Der Kreisstrom um die Wirbel, oder Vortices, wird durch einen Phasengradienten aufrechterhalten. Aus der Stetigkeit der Wellenfunktion ergeben sich zwei Bedingungen: Erstens muss die Phase um den Vortex um ein vielfaches von  $2\pi$  ansteigen, zweitens findet sich im Zentrum des Vortex ein Knoten.

Um das Wechselspiel von  $\mathcal{PT}$ -Symmetrie und solchen Vortices zu untersuchen, wurde die Gross-Pitaevskii-Gleichung in Abschnitt 7.1.2 in ein rotierendes Koordinatensystem transformiert. Nimmt man an, dass das Kondensat in einem asymmetrischen Fallenpotential gefangen ist, das mit derselben Frequenz  $\Omega$  rotiert, ist ein nicht-rotierender stationärer Zustand nicht mehr möglich. Stattdessen finden sich Wellenfunktionen, die in diesen Koordinaten stationär sind. Die Wellenfunktion mit der niedrigsten Mean-Field-Energie im rotierenden System fungiert als Grundzustand.

Als rotierende Falle wurde für diese Arbeit ein harmonischer Oszillator verwendet. Während die Wellenfunktion im ruhenden Fall eine Gauß-Form annimmt, enthält der Grundzustand bei stärker werdenden Rotationsfrequenzen mehr und mehr Vortices, wie in Abbildung 7.3 auf Seite 75 für zwei Dimensionen sichtbar gemacht ist.  $\mathcal{PT}$ -symmetrische Ströme können in diesem System auf zwei Arten eingebracht werden. Im ersten Fall liegen Gewinn, Verlust und Teilchenstrom innerhalb der Rotationsebene. Um stationäre Zustände zu ermöglichen, rotieren all diese Anteile mit dem Koordinatensystem. Diese Konfiguration lässt sich in zwei Dimensionen und damit mit geringem numerischem Aufwand verwirklichen.

Durch den Teilchenaustausch muss die Wellenfunktion einen Strom von der Position des Gewinns zur Position des Verlusts ermöglichen. Es stellt sich damit die Frage, ob die vorhandenen Ströme um Vortices den effektiven Teilchentransport behindern oder verändern. Zwei Möglichkeiten wurden postuliert: Entweder bleiben die Vortices unbeeinflusst und der neue effektive Strom fließt zusätzlich durch das System, oder die Vortices verschieben sich und bedingen damit den Gesamtstrom. In der Arbeit konnte tatsächlich klar gezeigt werden, dass sich der effektive Gesamtstrom von Gewinn- zu Verlustbereich vollständig aus den Strömen um die Vortices zusammensetzt. Dabei lassen sich zwei Methoden unterscheiden:

- Die Gesamtheit der Vortices kann sich verschieben. Dadurch werden bestimmte Randströme zu kleineren Teilchendichten verschoben und damit geschwächt, oder umgekehrt zu größeren Dichten verschoben und gestärkt.
- Neue Vortices können aus dem unendlichen außerhalb der Teilchenwolke ins Kondensat driften, während andere komplett in den Außenbereich dissipieren. Dadurch ergeben sich neue Kombinationen und Gesamtströme.

Während die Prinzipien zum Stromaufbau stets gleich waren, finden sich sehr unterschiedliche dynamischen Stabilitäten der entsprechenden Zustände. In man-

---

chen Fällen sind bereits kleinste Ströme ausreichend um ehemals stabile Grundzustände zu stören. Beide Prinzipien im Fall eines stabilen Zustands sind in Abbildung 7.5 auf Seite 78 gezeigt.

Wie bereits erwähnt ist dies nicht die einzige untersuchte Konfiguration. Anstatt den Teilchengewinn und Verlust innerhalb einer Ebene in zwei Dimensionen einzuführen, kann der Strom auch entlang der  $z$ -Achse und damit parallel zur Rotationsachse und den Vortices realisiert werden. Da der Teilchenaustausch in diesem Fall nicht zeitabhängig ist, liegt diese Verwirklichung sehr viel näher. Das Verhalten bei steigender Rotationsfrequenz entspricht dem des zweidimensionalen Falls. Obwohl der neue Strom senkrecht zu den Vortexströmen und deren Beitrag zum Teilchentransport daher nicht offensichtlich ist, kommt es zu einem massiven Einfluss auf den Verlauf der Vortices. Alle Vortices, die nicht im Fallenzentrum liegen werden gebogen und winden sich um das Rotationszentrum, wie man an der Darstellung der Wellenfunktionen und Vortices in Abbildung 7.11 auf Seite 86 gut sehen kann.

Die Windungsrichtung, wenn man das System in Richtung des Teilchentransports betrachtet, ist entgegengesetzt zur Rotationsrichtung des Systems. Sind mehr Vortices im Zustand enthalten, wird jeder einzelne Vortex schwächer verwunden. Da die Stärke dieser Windung mit stärkeren Strömen außerdem zunächst linear ansteigt und schließlich nahe der terminierenden Bifurkation nahezu divergiert ist anzunehmen, dass die Windung direkt zum Teilchentransport beiträgt.

## Ausblick

In dieser Arbeit wurde ausführlich begründet, dass die  $\mathcal{PT}$ -symmetrische Doppelmulde auch im Fall kleiner Störungen von Falle und Gewinnanteilen eine erfolgsversprechende Realisierung darstellt. Vor allem die Existenz eines dynamischen Attraktors im Fall asymmetrischer Gewinn- und Verlustbeiträge würde eine experimentelle Verwirklichung deutlich stabilisieren. Es wäre daher besonders interessant zu betrachten, in wieweit sich die bemerkenswerten Ergebnisse von Vielteilchenrechnungen in einem solchen leicht asymmetrischen System wiederfinden lassen. Besonders zur Realisierung der Oszillation der Reinheit eines Kondensats [28] stellt diese Untersuchung eine wichtige Voraussetzung dar.

Aber nicht nur die asymmetrische Erweiterung der Doppelmulde verspricht neue Effekte, auch die Erweiterung zu drei Mulden, insbesondere der Symmetriebruch in der symmetrischen kreisförmigen Anordnung legt den Grundstein für neue Anwendungen. Zeitabhängige Analysen der Gross-Pitaevskii-Gleichung könnten beispielsweise aufklären, ob ein solches System einen geometrischen Transistor für kondensierte Bosonen darstellen kann.

Zuletzt steht eine endgültige Klärung des Zusammenhangs zwischen dem Teilchenstrom und der Vortexwindung aus. Zwei Ansätze können entsprechenden

Einblick in die Frage gewähren: Im Fall eines idealen Superfluids vereinfacht sich die Gross-Pitaevskii-Gleichung zu den Euler-Flussgleichungen. Für diesen Fall können analytische oder einfache numerische Rechnungen mit hoher Präzision ausgeführt werden, um zu überprüfen ob der Effekt auch in diesem Regime auftritt. Alternativ kann untersucht werden, ob die Verwindung auch in nicht-rotierenden Systemen mit nicht-zentralen Vortices auftritt. Damit ließe sich klären, ob die Verwindung eine Folge der nicht-isotropen Dichteverteilung um den Vortex darstellt oder tatsächlich durch die Rotation bedingt wird.

## Studienverlauf

---

- 10/2007– **Bachelor of Science: Physik**, *Universität Stuttgart*.  
09/2010 Gesamtnote: sehr gut mit Auszeichnung (1,1)  
10/2010– **Master of Science: Physik**, *Universität Stuttgart*.  
10/2012 Gesamtnote: sehr gut mit Auszeichnung (1,0)

## Berufliche Praxis

---

- seit 12/2012 **1. Institut für Theoretische Physik - Universität Stuttgart**, Wissenschaftlicher Mitarbeiter.

## Ausgewählte Veröffentlichungen (peer-reviewed)

---

- 2013 D. Dast, D. Haag, H. Cartarius, G. Wunner, R. Eichler, J. Main, *A Bose-Einstein condensate in a  $\mathcal{PT}$  symmetric double well*, *Fortschr. Phys.* **61**, 124
- 2013 D. Dast, D. Haag, H. Cartarius, J. Main, G. Wunner, *Eigenvalue structure of a Bose-Einstein condensate in a  $\mathcal{PT}$ -symmetric double well*, *J. Phys. A* **46**, 375301
- 2014 D. Haag, D. Dast, A. Löhle, H. Cartarius, J. Main, G. Wunner, *Nonlinear quantum dynamics in a  $\mathcal{PT}$ -symmetric double well*, *Phys. Rev. A* **89**, 023601
- 2014 D. Haag, H. Cartarius, and G. Wunner, *A Bose-Einstein condensate with  $\mathcal{PT}$ -symmetric double-delta function loss and gain in a harmonic trap: a test of rigorous estimates*, *Acta Polytechnica* **54**, 116
- 2015 D. Haag, D. Dast, H. Cartarius, and G. Wunner, *Finite element calculations of  $\mathcal{PT}$ -symmetric Bose-Einstein condensates*, *Int. J. Theor. Phys.* **54**, 4100
- 2015 D. Haag, D. Dast, H. Cartarius, G. Wunner,  *$\mathcal{PT}$ -symmetric currents of a Bose-Einstein condensate in a triple well*, *Phys. Rev. A* **92**, 053627



# Danksagung

Die Anfertigung dieser Dissertation, von der wissenschaftlichen Arbeit bis zum Niederschreiben, wurde von einigen Personen besonders unterstützt. Bei diesen möchte ich mich im folgenden bedanken.

Mein erster Dank gilt meinem Betreuer und Hauptberichter Herrn Prof. Dr. Günter Wunner. Der Freiraum, die eigene Arbeit stets selbst weiterzuentwickeln, die Unterstützung bei allen dringenden Fragen und die freundliche Aufnahme ins 1. Institut für Theoretische Physik haben mir ein großartiges Arbeitsumfeld geschaffen. Besonders hervorheben möchte ich dabei den Leiter meiner Arbeitsgruppe, Herrn PD. Dr. Holger Cartarius. Seit Beginn meiner Masterarbeit vor mehr als fünf Jahren war er für mich nicht nur als Ansprechpartner für alle wissenschaftlichen und technischen Fragestellungen eine großartige Hilfe, sein Organisationstalent waren außerdem ein Garant für den Erfolg aller Lehrveranstaltungen, an denen ich beteiligt war. Ich danke Herrn Prof. Dr. Johannes Roth für die freundliche Übernahme des Mitberichts und Herrn Prof. Dr. Tilman Pfau für die Übernahme des Prüfungsvorsitzes.

Allen Kollegen im Institut möchte ich für die wunderbare Balance zwischen Menschlichkeit und Professionalität danken; allen voran meinem Bürokollegen Dennis Dast für die Geduld für viele Stunden der Diskussion und die Möglichkeit, auch viele physikalische Fragestellungen zu bearbeiten, die nicht den Weg in diesen Abschlusstext gefunden haben. Für das Probelesen meiner Arbeit danke ich neben den bereits genannten Personen außerdem Jonathan Stysch, Jörg Main, Jan Schnabel, Robin Gutöhrlein und Philipp Lunt.

Zuletzt gehört mindestens ebenso viel Dank meinen Freunden und meiner Familie, die mich, allen voran meine wunderbare Frau Katrin, stets ermutigt, bestärkt und über alle Maßen unterstützt haben.

Danke!



### **Ehrenwörtliche Erklärung**

Ich erkläre, dass ich diese Dissertation, abgesehen von den ausdrücklich bezeichneten Hilfsmitteln, selbständig verfasst habe.

Stuttgart, den 16. Februar 2017

*Daniel Haag*